Improving the Performance of Cellulose Acetate Reverse Osmosis Membranes

Clare H. Worthley, BSc. Nanotechnology (Hons)

Thesis submitted to the School of Chemical and Physical Sciences
in the Faculty of Science and Engineering
Flinders University
in fulfilment of the requirements for the degree of

DOCTOR OF PHILOSOPHY
in
CHEMISTRY

Dr Stephen Clarke
Dr Milena Ginic-Markovic
Dr Kristina Constantopoulos

FLINDERS
UNIVERSITY
ADELAIDE
AUSTRALIA

2012
Adelaide, South Australia

Contents

Summary

Reverse osmosis membrane desalination technology has come a long way since the Loeb and Souririjan type membranes of the 1960s. Advances in production and engineering processes have overcome many inherent system limitations, however some remain. Truly biofouling-resistant membranes are yet to be realised, and membrane compaction remains an issue.

In this thesis methods for mitigating these two membrane limiting factors have been investigated; polymeric modification and nanoparticle inclusion.

In the first part of the project, a detailed study of the polymerisation of poly(2-hydroxyethyl methacrylate) via activators regenerated by electron transfer atom transfer radical polymerisation was undertaken. Conditions were chosen to be commercially attractive. The modified membranes were studied with fourier transform infrared spectroscopy (FTIR), x-ray photospectroscopy, nuclear magnetic resonance, and thermogravimetric analysis. Results showed that by varying the initial monomer volume and/or the polymerisation reaction time it was possible to create a series of modified membranes with a range of polymer graft densities, thus indicating the livingness of the polymerisation reaction.

In order to evaluate the ideal graft density, the properties of the modified membranes were further investigated. The polymer coating was clearly visible using scanning electron microscopy and an increase in surface roughness was observed with atomic force microscopy, in both cases confirming the increase in polymer graft density. Water contact angle studies explored the relationship between surface morphology and wettability, indicating conformational changes in the polymer. Hydrolysis had little effect on modified membrane filtration properties when soaked at pHs outside the recommended range for pristine cellulose acetate membrane (CAM).

Unique aquarium biofouling tests were performed, and showed a decrease in biofouling for the modified membranes. Stirred-cell experiments were used to evaluate the filtration properties of the modified membranes. From the results it was possible to determine optimum conditions for membrane modification to obtain a polymer graft density with maximum biofouling resistance and minimum loss of filtration properties.

In the second part of the project, aminopropylisobutyl polyhedral oligomeric silsesquioxane (POSS) was investigated as a nanocomposite additive. Since nanoparticle agglomeration and leaching were identified as issues in nanocomposite materials, an anchored nanoparticle was synthesised using isocyanate chemistry to attach POSS to cellulose acetate (CA). This anchored nanoparticle was compared to un-anchored POSS as an additive in CA membrane casting solutions at loadings of 0.5, 1.0 or 5.0 wt%. FTIR and energy dispersive X-ray microanalysis showed the anchored nanoparticle to have better dispersion in the resulting membranes. The nanocomposite membranes showed greater flux of water and salt than an unmodified CA control. Membrane compaction was mitigated at low nanoparticle loadings. Dynamic Mechanical Analysis (DMA) results suggest POSS has a plasticisation effect on the CA matrix.

Declaration

'I certify that this thesis does not incorporate without acknowledgement any material previously submitted for a degree or diploma in any university; and that to the best of my knowledge and belief it does not contain any material previously published or written by another person except where due reference is made in the text.'

....

(C.H.Worthley)

Acknowledgements

This project was a collaboration between Flinders University of South Australia and industry partners Windprospect, via Australian Research Council linkage grant no. LP0669119. I should begin by thanking these organisations for the opportunity.

In particular I would like to thank Bill and Andrew Dickson from Windprospect for their enthusiasm and confidence in this research.

From Flinders University I would like to thank first and foremost my supervising team for their expertise, encouragement and guidance on all matters: Dr Stephen Clarke, Dr Milena Ginic-Markovic, and Dr Kristina Constantopoulos. Also, members of the Materials and BioEnergy team and beyond for their practical advice and genuine friendship: Dr Elda Markovic, Dr Rachel Pillar, Dr Lucas Johnson, Dr Tom Barclay, and Dr Jess Lu.

Thanks for their technical expertise go to: Lyn Spencer and staff at Adelaide Microscopy for their help with SEM and EDAX, and Dr Rob Acres of the School of Chemical and Physical Sciences at Flinders University of South Australia for his assistance with XPS data acquisition and analysis.

Personal thanks for their love and support, always, to my parents and parents-in-law, and my husband, Nick, to whom I dedicate this thesis.

List of Figures

List of Tables

Abbreviations

AFM	Atomic force microscopy
AMPSA	2-acrylamido-2-methyl-1-propanesulfonic acid
APTES	3-aminopropyltriethoxysilane
ARGET	Activators regenerated by electron transfer
ATR	Attenuated total reflectance
ATRP	Atom transfer radical polymerisation
BiBBr	2-bromoisobutyryl bromide
BSA	Bovine serum albumin
CA	Cellulose acetate
CA-POSS	POSS-modified cellulose acetate
CAM(s)	Cellulose acetate membrane(s)
CAM-Br	Bromoinitiator-modified cellulose acetate
CAM-g-pHEMA	Celluloase acetate membrane grafted with pHEMA
$CDCl_3$	Deuterated chloroform
D_2O	Deuterated water
DMA	Dynamic mechanical analysis
DMAP	4-dimethylaminopyridine
DMF	Dimethyl formamide
DS	Degree of substitution
DTG	First derivative of the thermogravimetric curve
E.coli	Escherichia coli
EBiB	Ethyl 2-bromoisobutyryl bromide
EDAX	Energy dispersive X-ray microanalysis

EPS	Extracellular polymeric substances
FO	Forward osmosis
FTIR	Fourier transform infrared
HBr	Hydrobromic acid
HEMA	2-hydroxyethyl methacrylate
IMC	Initial monomer concentration
IMV	Initial monomer volume
KBr	Potassium bromide
Me6TREN	tris[2-(dimethylamino)ethyl]amine
MED	Multiple effect distillation
MeOH	Methanol
MF	Microfiltration
MMM	Mixed-matrix membrane
$MgSO_4$	Magnesium sulfate
MSF	Multi-stage flash distillation
MWCNT	Multi-walled carbon nanotube
NaCl	Sodium chloride
NaOH	Sodium hydroxide
NF	Nanofiltration
NMR	Nuclear magnetic resonance
OEG	Oligo(ethylene glycol)
OGMA	Polyglycidyl methacrylate
OH	Hydroxyl group
PC	Phosphorylcholine
PEG	Poly(ethylene glycol)
PEGMA	polyethylene glycol methacrylate
PES	Polyethersulfone

pHEMA	Poly(2-hydroxyethyl methacrylate)
PMA	Polymethacrylate
PMDETA	*N,N,N′,N′,N″*-pentamethyldiethylenetriamine
PMMA	Polymethyl methacrylate
POSS	Aminopropylisobutyl polyhedral oligomeric silsesquioxane
POSS-TDI	TDI-modified POSS
ppm	Parts per million
PRT	Polymerisation reaction time
PRTxxIMVx	pHEMA-modified CA membrane with PRT of xx minutes and IMV of x mL.
PVF	Poly(vinylidene fluoride)
qDMAEM	quaternized 2-(dimethylamino)ethyl methacrylate
RO	Reverse Osmosis
SEM	Scanning electron microscopy
SI	Surface initiated
SQRT	Square root
SR	Salt rejection
STDEV	Standard deviation
TDI	Toluene-2, 4-diisocyanate
TDS	Total dissolved solids
TEA	Triethylamine
TFC	Thin film composite
TGA	Thermogravimetric analysis
THF	Tetrahydrofuran
TiO_2	Titania
TPMA	Tris[(2-pyridyl)methyl]amine

UF	Ultrafiltration
UV	Ultraviolet
WCA	Water contact angle
wt%	Weight percent
XPS	X-ray photospectroscopy

1 Chapter One

Introduction

Preface

Desalination is an important area of research to combat a worldwide shortage of fresh water resources. In modern times membrane technology has emerged as a leader for efficient desalination, however there are still advances to be made.

This chapter provides a background into desalination, membranes and their limiting factors. It reviews the literature concerning overcoming these limitations and identifies gaps in the current knowledge. Lastly, the aims of this thesis and and its structure are outlined.

1.1 Background

1.1.1 Fresh water scarcity

Water is one of Earth's most abundant natural resources. Incredibly, less than 2% is available to us as fresh water in rivers, lakes and ground water aquifers, as shown in Figure 1.1. A further 1.74% is locked up in the polar ice caps. The remaining 96.5% is the salty water of the world's oceans [1].

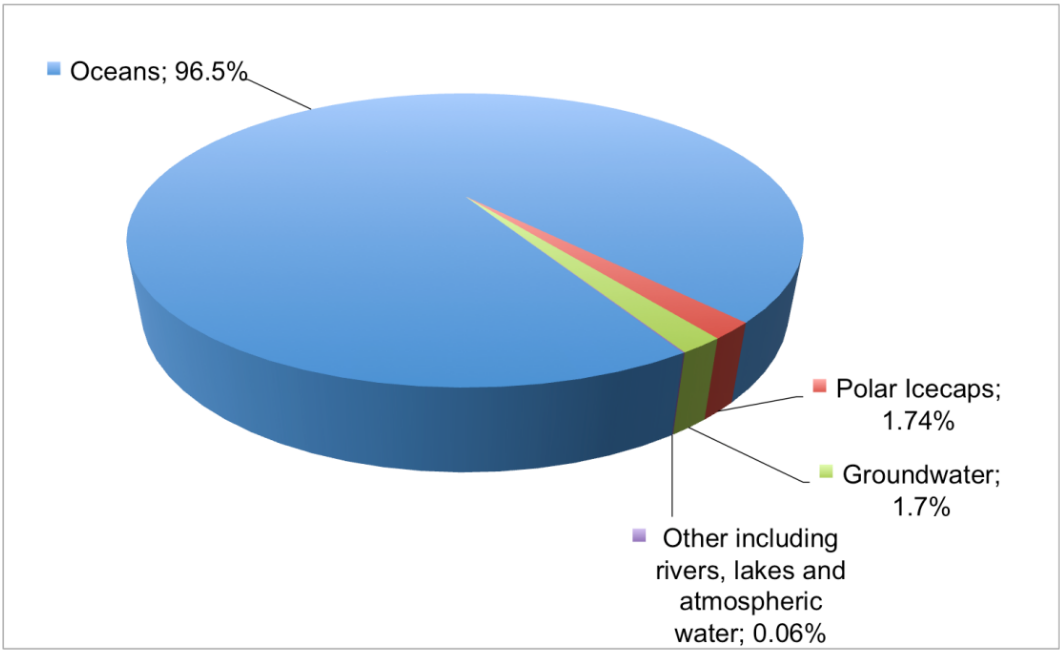

Figure 1.1. Relative amounts of Earth’s water resources [1].

Here in Australia many large urban population centres are currently experiencing water shortages. This is due to population growth leading to increased urban water demand and reduced inflow due to ongoing drought [2]. Water shortages mean it is becoming ever more important to utilise new sources of fresh water for the world’s population. One possible way to do this is through desalination of salty water.

1.1.2 Desalination

Desalination is the process of converting saline water to fresh water by the removal of salts. Desalination feedwaters are defined by their salinity in total dissolved solids (TDS). The salinity of seawater typically lies around 35,000 ppm TDS, [3] compared to 2,000 ppm TDS for brackish water and a maximum of 500 ppm TDS for potable water. Salinity level ranges for different feedwaters are shown in Table 1.1 [4].

Table 1.1. Feedwater characterisation by salt content [4].

	Minimum Salinity TDS (ppm)	Maximum Salinity TDS (ppm)
Seawater	15,000	50,000
Brackish Water	1,500	15,000
River Water	500	1,500
Pure Water	0	500

Desalination, however, is not a new idea. Sailors from ancient Greece produced drinking water aboard their ships by boiling seawater and condensing the steam on sponges [5]. The modern desalination industry had its beginnings in the 20th century and rapid growth occurred during the 1960's and 1970's into what is today a worldwide, multi-million dollar industry. In 2004, 20 milllion cubic metres of desalinated water were supplied each day around the world [6]. By 2016 this is projected to have increased to over 100 million m^3 a day [7].

Desalination methods are classified according to their separation technique. The two main types are thermal and membrane based. In Europe, almost all recently installed desalination plants use Reverse Osmosis (RO) membrane technology. Thermal processes use more energy but dominate in the Middle East due to the low cost of fossil fuel-based energy in this region [4].

1.1.3 Thermal Distillation

Thermal distillation removes salt by using a heat source and reduced pressures to cause evaporation and condensation of water. Two of the most common processes are multi-stage flash distillation (MSF) and multiple effect distillation (MED).

In MSF, feedwater enters the plant and is heated under high pressure. The heated seawater then passes into a low-pressure vessel, where it boils rapidly and "flashes" into steam. The steam is cooled and condenses into fresh water. The feed water component that has not been vaporised passes through several stages of progressively lower pressure, and continues to be partially vaporised and condensed at each stage [8]. The Shoaiba MSF Desalination Plant in Saudi Arabia is the world's largest desalination plant, with a capacity of 150 million m^3year^{-1} [9]. The energy consumption for MSF ranges from 10 to 25 $kWhm^{-3}$ [10].

In MED, the incoming feedwater is boiled in the first evaporator. Water boils at lower temperatures as pressure decreases, so the vapours from the first evaporator condense in the second and the heat of condensation serves to boil the seawater in the second evaporator. The evaporation-condensation cycle continues with each subsequent evaporator at lower pressure [11]. MED uses 4-25 $kWhm^{-3}$ [10].

1.1.4 Membrane-Based Desalination

Membrane processes are based on separation rather than distillation. A membrane is a semipermeable film that allows the selective passage of some substances but not others. Membranes are separated into groups based on the size of particles they filter, and can be described as either porous or non-porous.

1.1.4.1 Porous Membranes

Microfiltration (MF) membranes have the largest pore size (50-500 nm) and typically reject large particles and various microorganisms. Ultrafiltration (UF) membranes reject bacteria and soluble macromolecules such as proteins. UF has applications in the filtration of milk and whey, in protein fractionation, and renal function. Nanofiltration (NF) membranes are porous but have pore sizes on the order of 2 nanometres or less and fall between reverse osmosis and utlrafiltration membranes. NF separates sugars, organic molecules and multivalent salts, from water and monovalent salts. Membrane filtration processes, pore-sizes and typically filtered particles are shown in Table 1.2 [12].

Table 1.2. Membrane Filtration Spectrum [12].

Process	**Pore Diameter**	**Filtered Particles**
RO	Non-porous	- Monovalent ions
NF	≤ 2 nm	- Multivalent ions - Organic molecules
UF	2 - 50 nm	- Viruses - Proteins
MF	50 – 500 nm	- Bacteria - Suspended solids

1.1.4.2 Non-Porous Membranes

RO membranes allow the passage of water whilst rejecting salt and other dissolved solids. Before considering the process of reverse osmosis, it is helpful to describe natural, or forward, osmosis. Forward osmosis (FO) occurs when a semi-permeable membrane separates two aqueous solutions of different concentration. Water flows from the dilute side to the concentrate side until the concentrations reach equilibrium. The pressure required to stop the flow of water is known as the osmotic pressure. Since osmosis is driven by a difference in solute concentration, with water moving from low concentration to high concentration, water can be drawn across a membrane by a solution with higher solute concentration than the feed solution. This “draw solution” has several desirable characteristics [13]:

- high osmotic pressure (brought about by a solute with low molecular weight and that is highly soluble in water),
- ease of separation of the solute from the product water,
- re-cycleability

State-of-the-art applications include the use of ammonia and carbon dioxide to create highly concentrated draw solutions of ammonium salts [13]. When heated to around 60°C the salts decompose back into the constituent gases that can be easily separated and used to regenerate the draw solution. Another novel application is the use of magnetoferritin as a solute for draw solutions [9]. The advantage of using magnetoferretin is that it can be rapidly removed from product water using a magnetic field.

Forward osmosis has many advantages. FO operates with little or no applied pressure and therefore energy needs are dramatically reduced, i.e. energy needs are typically an order of magnitude less than energy needs required for RO [14]). In addition, less membrane support is required and fouling is potentially less with FO processes. Furthermore, the osmotic pressure can be higher than the applied pressures in RO, meaning higher water flux and higher percentage of water recovered. Although FO has many advantages, the fluxes observed using RO membranes for FO are typically too low. As such, FO membrane research is currently in its infancy and there is a need for novel membrane development.

The process of RO occurs when a pressure which is greater than the osmotic pressure is applied to the concentrated side, and hence the direction of natural osmosis is reversed, and water flows from the concentrated side to the dilute side [4]. Figure 1.2 shows the flow of water in RO as compared to FO, where $\Delta\pi$ is the osmotic pressure and ΔP is the applied pressure [15]. The water that passes through the membrane is now lower in salt concentration and is known as the "permeate". The water that is retained by the membrane is now more concentrated and is known as the "concentrate" or "retentate".

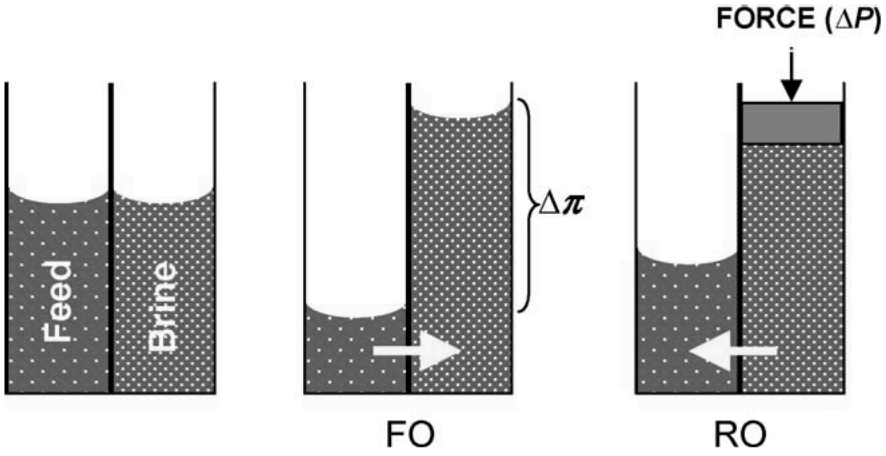

Figure 1.2. Forward Osmosis / Reverse Osmosis [15] .

RO membranes are essentially non-porous, and the movement of water through the membrane is via solution-diffusion, which will be discussed in Section 1.1.6 below.

1.1.5 Reverse Osmosis Desalination Plant Set-Up

Figure 1.3 shows the basic set-up of a RO desalination plant and a brief description of each stage follows. The important stages in terms of preventing membrane fouling are pre-treatment of the feedwater and membrane cleaning.

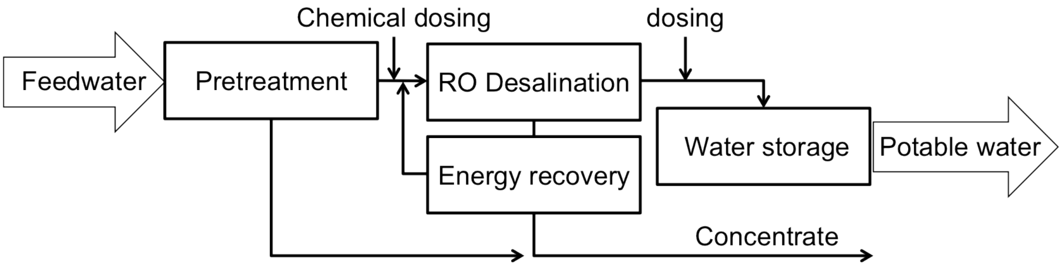

Figure 1.3. Schematic diagram showing the basic setup of a reverse osmosis desalination plant

(i) Feedwater abstraction - Feedwater is introduced to the system. In the case of seawater this can be via open seawater intake systems or coast and beach wells.

(ii) Pre-treatment - Currently, the most effective way to protect against fouling and minimise damage to the membrane, is with effective pre-treatment which typically includes several processes including: coagulation and fluocculation, physical filtration of particulate matter, pH adjustments, the addition of anti-scaling and anti-fouling chemicals, and chlorination (to prevent biological fouling) followed by dechlorination (to prevent oxidation of the membrane) [16].

(iii) Desalination - The feedwater is separated into pure water and brine via a semi-permeable membrane as discussed earlier. For feedwater containing 35,000 ppm of salt, membranes having a minimum rejection of 99.3% are required to produce drinking water in a single pass [17].

(iv) Energy Recovery - The concentrate leaves the desalination vessel under pressure. This pressure can be used to drive a turbine, thereby recovering a portion of the energy output for re-use.

(v) Post-treatment - Post-treatment involves a range of processes to make the water comply with potable water standards, including the removal of boron, pH adjustment and re-mineralisation to make the water palatable.

(vi) Membrane Cleaning - Membrane cleaning may be necessary when there is a significant (10-15%) decrease in flux, and a 10% increase in salt content of the permeate [18]. Cleaning methods fall into two categories: chemical and physical. Chemical methods are designed to loosen and dissolve foulants from the membrane. The chemicals used for cleaning depend on the type of foulants and the resistance of the membrane to the chemicals. Physical cleaning involves processes such as flushing with air, backflushing with permeate and sonication [19].

1.1.6 Critical RO Membrane Properties

Since reverse osmosis membranes are essentially non-porous, the transport of water is via solution-diffusion. The permeating species dissolves in the membrane and molecularly diffuses through it as a consequence of a concentration gradient [20]. Components are separated due to different solubilities and different diffusion rates in the membrane material. The following parameters will be indicative of the membrane performance.

1.1.6.1 Water flux

Water flux, J_i, is the superficial velocity of water through the membrane, and is defined as the amount of fluid transported across membrane per unit time per unit area. The solution-diffusion model is used to describe transport [17]:

$$J_i = L(\Delta P - \sigma \Delta \pi) \qquad \text{Eq. 1}$$

where, L is the intrinsic permeability of the membrane to water, ΔP is the transmembrane pressure difference (TMP), $\Delta \pi$ is the difference in osmotic pressure between the feed and the permeate solutions, and σ is the reflection coefficient.

Now, when $\Delta P < \Delta \pi$ water flows from the dilute to the concentrated solution (as in FO where $\Delta P = 0$), when $\Delta P = \Delta \pi$ no flow occurs, and when $\Delta P > \Delta \pi$ water flows from the concentrated to the dilute solution (as in RO).

The reflection coefficient σ represents salt-water coupling and can have values from 0 to 1. When $\sigma = 0$ the membrane shows no salt rejection, when $\sigma = 1$ the membrane shows total salt rejection. For RO membranes with high salt rejection σ approaches 1 and the equation can be simplified to:

$$J_i = L(\Delta P - \Delta \pi) \qquad \text{Eq. 2}$$

L is a constant, related to hydraulic permeability, describing the physical characteristics of the membrane:

$$L = \frac{DSV}{RTl} \qquad \text{Eq. 3}$$

where D is the water diffusivity in the membrane, S is the water solubility in the membrane, V is the molar volume of the water, R is the ideal gas constant, T is the ambient temperature, and l is the membrane thickness. The inverse relationship of flux (J_i) to membrane thickness (l) means that very thin membranes are required in order to achieve high permeability.

1.1.6.2 Salt Rejection

Salt flux, J_j is given by:

$$J_j = B(C_{feed} - C_{permeate}) \qquad \text{Eq. 4}$$

where B is the salt permeability constant, $C_{permeate}$ is the salt concentration in the permeate solution, and C_{feed} is the salt concentration in the feed solution. In many cases it is more appropriate to refer to salt rejection, R, which is a measure of the ability of the membrane to separate salt from the feed solution [21], and which is defined as follows [17]:

$$R = (1 - \frac{C_{permeate}}{C_{feed}})\ x\ 100\% \qquad \text{Eq. 5}$$

Because water flux increases with increasing pressure (Eq. 1) but salt flux is independent of pressure (Eq. 4) salt rejection increases with applied pressure [21].

The solution-diffusion model makes several assumptions, and therefore, modelling flux across a membrane is, in practice, quite complex. One assumption is that the pressure within the membrane is uniform at the applied pressure. Another assumption is that fluids on either side of the membrane are in equilibrium with the membrane material at the interface [21]. Factors affecting these assumptions include concentration polarisation, membrane compaction and fouling. These factors will be elaborated upon in Section 1.1.8.

1.1.7 Membrane Materials

Aromatic polyamides and cellulose acetate are two of the main polymeric materials used in the fabrication of commercially available RO membranes.

1.1.7.1 Polyamide Composites

Polyamide Thin Film Composite (TFC) membranes are considered the state-of-the-art membranes fabricated by most manufacturers for use in seawater desalination. TFCs are made of three layers (Figure 1.5). A woven or non-woven polyester fabric is typically used as a backing layer for a porous, highly permeable support layer such as polysulfone. The final layer of the TFC consists of a thin, cross-linked aromatic polyamide film (Figure 1.4).

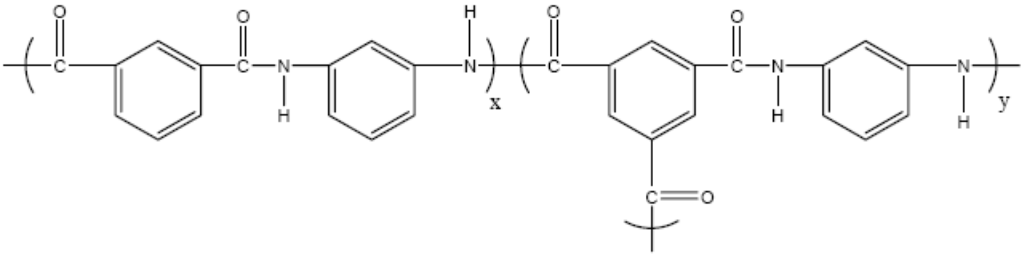

Figure 1.4. Chemical structure of polyamide repeat unit [17].

Polyamide is formed via interfacial polymerisation [17]. Cadotte [22] first used this technique to create polyamide TFCs. In interfacial polymerisation, two immiscible solvents are used and polymerisation takes place at the interface until a thin film poses a diffusion barrier and the reaction is terminated [4]. For example, polyamide TFC membranes are prepared using a polysulfone support membrane and contacting the surface with an aqueous *m*-phenylenediamine solution followed by contacting the surface with trimesoyl chloride; polyamide then forms at the interface of the two immiscible solutions.

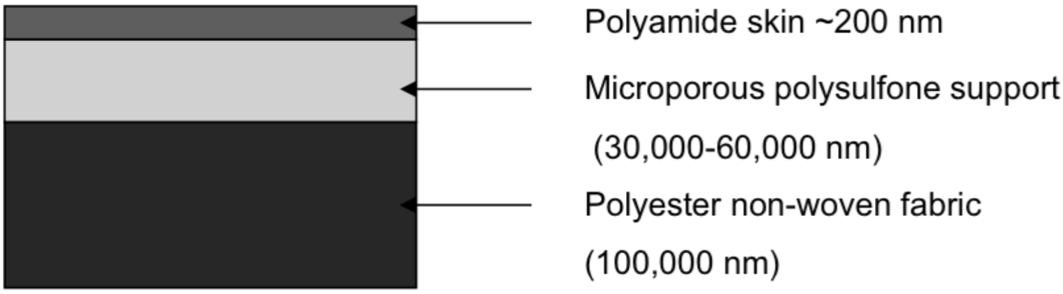

Figure 1.5. Representation of a cross-section of a TFC polyamide membrane showing the thickness of different layers.

TFCs have a wide tolerance to temperature and pH, coupled with high salt rejection and water flux. Polyamide TFCs have poor mechanical properties under high pressure and undergo membrane compaction. In addition, the polyamide layer is sensitive to much lower levels of chlorine compared to other more chlorine-resistant membranes. It is understood that the polyamide undergoes degradation by ring chlorination [23]. The polyamide layer suffers from high surface roughness, which makes polyamide TFCs prone to biofouling [4].

1.1.7.2 Cellulose acetate (CA)

Cellulose is a rigid molecule found in plant materials, and can therefore be considered a renewable resource. Its rigidity gives CA membranes their strength. Each glucose unit in the cellulose backbone contains three hydroxyl groups that can undergo acetyl substitution (Figure 1.6).

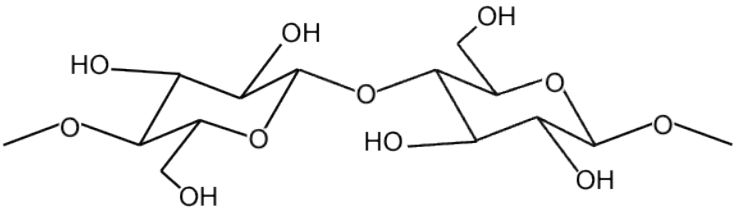

Figure 1.6. Chemical structure of the cellulose repeat unit.

CA is formed when cellulose reacts with acetic anhydride to form acylated cellulose and acetic acid (Figure 1.7). The term cellulose acetate actually describes a variety of acetylated cellulose polymers, including cellulose diacetate and cellulose triacetate [24].

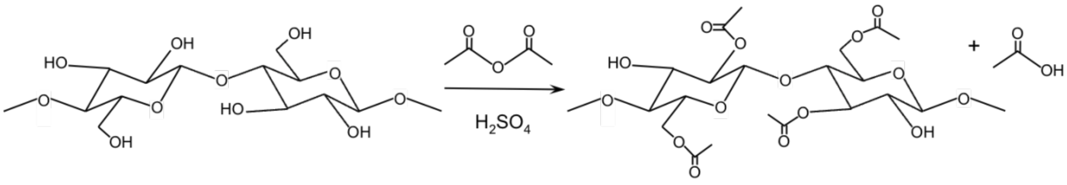

Figure 1.7. Formation of cellulose acetate from cellulose and acetic anhydride

The ratio of acetyl to hydroxyl groups determines the physical characteristics of the polymer. For example, acetyl groups are more hydrophobic than hydroxyl groups, and therefore, the degree of acetylation determines the hydrophilicity of CA membranes. Also the degree of acetylation is inversely proportional to the permeability of the membrane to water and salt. In other words, a high degree of acetylation leads to high salt rejection and low flux, a low degree of acetylation leads to low salt rejection and high flux. McCray *et al.* [25] attributed this to decreased crystallinity of the polymer with decreased acetyl content, meaning that more free water was present in the membrane and could transport more salt. Commercially available CA membranes usually have an acetylation degree of around 2.7.

CA membranes were first investigated for their salt rejecting properties by Reid *et al.* [26] but the observed water fluxes were too low to be practical for desalination [20]. In 1960, Loeb and Sourirajan [27] developed the first high flux, asymmetric, CA membrane with good salt rejection properties. Their membrane showed up to 100 times higher flux than any symmetric membranes known at the time [4].

CA membranes (CAMs) have an asymmetric structure, typical of RO membranes, consisting of a thin (typically less than 0.8 nm [19]), dense, salt rejecting layer and a porous support layer. CAMs are formed by a process known as phase inversion, which occurs when a previously homogenous polymer solution is immersed in a non-solvent [28]. The polymer rich phase precipitates to form the membrane. The surface polymerises quickly and forms a continuous and very smooth structure known as a surface layer. Once the surface layer is formed, mixing of the solvent and the coagulant becomes slower, and solvent-nonsolvent exchange leads to phase separation, and results in the porous sponge-like structure of the support layer. It is a requirement of the phase inversion method that the solvent must be miscible with both water and the swelling agent used, and must leach out of the nascent membrane prior to the swelling agent, otherwise an impermeable membrane is formed [29].

When Loeb and Souririjan made the first successful, integrally skinned desalination membrane they cold-cast onto glass from a quaternary formulation of 22.2 wt% cellulose acetate, 66.7 wt% acetone, 10.0 wt% water and 1.1 wt% magnesium perchlorate [27]. It was the addition of the magnesium perchlorate, which acted as a pore former/swelling agent that gave the vast improvements in water flux compared to previous methods. Several subsequent techniques have used other inorganic electrolytes similar to magnesium perchlorate to for CAMs [30]. Manjikian *et al.* [29] then made an improvement to the method by substituting both the water and the magnesium perchlorate with formamide, and replacing the cold cast procedure with a room temperature casting procedure to form membranes. A solution of 25 wt% CA, 30 wt% formamide, and 45 wt%

acetone was used in their ternary formulation. Later, Kesting and Menefee [30] studied the effects of varying the concentration of formamide in acetone solutions of CA. They found that more formamide lead to more swelling and therefore thicker membranes. The minimum amount of formamide to achieve permeability was approximately 20wt%. Other variables affecting membrane casting include evaporation time between casting and submersion, and temperature of the annealing bath [31].

Although CAMs exhibits high water flux and salt rejection, they suffer from several disadvantages. A comparison of the properties of TFC and CA membranes is shown in Table 1.3. CA is susceptible to hydrolysis under acidic and alkaline pH conditions, limiting the operating pH of CAMs to between 4 and 8. The rate of hydrolysis also increases with temperature [17], and therefore CA is limited to an operating temperature below 30 °C. CA can also be degraded by oxidation due to chlorine and other oxidising agents in the feedwater. Furthermore, CAMs are known to undergo a period of flux decline caused by membrane compaction under high operating pressures [32].

Table 1.3. Comparison of TFC and CA membrane material properties.

	TFC	**CA**
Ease of manufacture	Average	Excellent
Salt Rejection	Excellent	Good
Water Flux	Excellent	Good
pH Range	Broad	Limited
Temperature Range	Broad	Limited
Mechanical Strength	Poor	Poor
Chlorine Resistance	Poor	Good
Biofouling Resistance	Poor	Average

Although other membranes have been developed, CAMs are still widely used for desalination and other RO applications [25] such as the removal of viruses from waste water [33], the concentration of food products such as grape juice for winemaking [34], and the desalination of oil-contaminated water and industrial wastewater [35].

1.1.8 RO Membrane Limiting Factors

RO membrane systems currently represent the fastest growing segment of the seawater desalination market [36], however, overcoming natural osmotic pressure with significant flow rate is energy intensive [37]. The theoretical minimum energy required to remove salt from water is independent of the method employed and is directly related to the osmotic pressure and the volume of desalinated water. Average seawater has an osmotic pressure of around 27 bar, which equates to just over 0.75 $kWhm^{-3}$ and varies according to the water salinity [38]. As shown in Figure 1.8 [39], the specific energy of RO has dropped from 10 $kWhm^{-3}$ to below 4 $kWhm^{-3}$ in the last 20 years and is now approaching the theoretical minimum of 0.7 $kWhm^{-3}$ [40]. Much of the current research is aimed at further increasing the energy efficiency of the RO desalination process. The two most important factors are the energy cost and the membrane replacement cost [41]. Important membrane factors that are limiting the approach to the theoretical minimum energy for RO, and leading to more frequent membrane replacement include such factors as concentration polarisation, membrane compaction, deterioration and fouling.

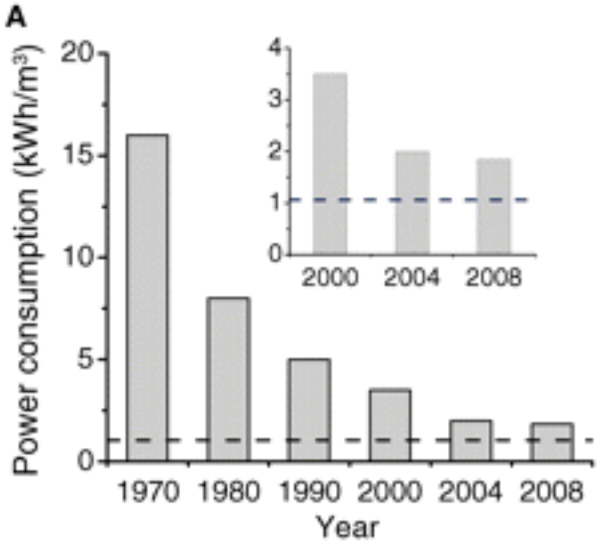

Figure 1.8. Power consumption of RO processes from 1970 to 2008 [39].

1.1.8.1 Concentration Polarisation

As a consequence of the passage of water through the membrane, solutes are carried to, and accumulate at, the membrane surface [4, 42]. The increased salt concentration directly at the membrane causes an increase in local osmotic pressure, resulting in decreased water flux and decreased salt rejection.

Concentration polarisation (J_w) is represented as follows:

$$\frac{C_m - C_p}{C_f - C_p} = e^{(\frac{Jw}{k})} \qquad \text{Eq. 6}$$

Where C_m is the concentration at the membrane surface, C_p is the permeate bulk solution concentration, C_p is the feed bulk concentration and k is the mass transfer coefficient. Concentration polarisation is mitigated in practice by utilizing stirring when performing dead-end filtration or by operating in cross-flow conditions where the flow of water is tangentially over the membrane surface. These measures increase the shear rate and encourage the transport of the solutes back into bulk solution [43].

1.1.8.2 Membrane Compaction

High applied pressure is fundamental to RO membrane processes. It affects flux both positively, by providing the main driving force for transport, and negatively, because of the phenomenon of compaction.

As part of their intrinsic asymmetric structure, CA RO membranes comprise a porous mechanical support layer. High feed pressures cause physical compaction of this layer, which damages the membranes internally. The compaction behaviour of a membrane depends on the support layer structure and porosity, and mechanical strength [44]. For example, Persson *et al.* [45] showed that a sponge-like structure is less affected by compaction than a structure with macrovoids. Compaction occurs because under high operating pressures reorganization of the membrane polymer structure can occur. This results in lowered pore volume, increased hydraulic resistance and reduced flux. Membrane compaction is irreversible, and therefore remains an important cause of higher long-term operating costs [46].

1.1.8.3 Membrane Deterioration

Membrane deterioration is irreversible by cleaning. Chemical degradation of the CAM occurs via two main pathways, oxidation and hydrolysis. CA can suffer scission of the polymer backbone (Figure 1.9) caused by chlorine and other oxidising agents present in the feedwater or added during pre-treatment. This reduces the mechanical strength and increases permeate flux.

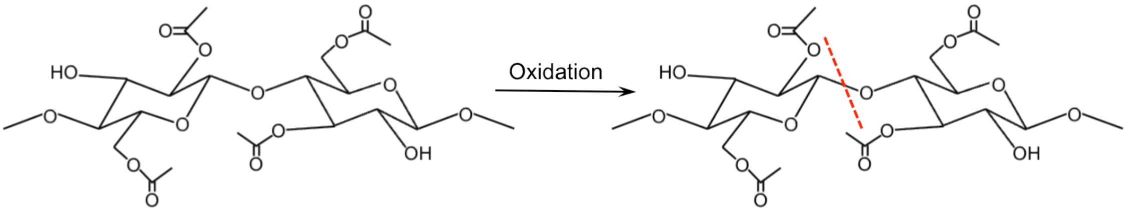

Figure 1.9. Oxidation of cellulose acetate.

CA can also undergo hydrolysis which involves the removal of acetyl groups from the polymer backbone. (Figure 1.10). This leads to changes in the performance of the membrane because the concentration of acetyl groups in the polymer influences the water flux and salt rejection of the membrane [47]. The hydrolysis reaction is strongly dependant on pH and is faster under acidic or alkaline conditions [4]. CAMS are said to have an operating range between pH 4 and pH 8. The narrow pH range of CAMs is a problem because the pH of seawater is between 7.5 and 8.5 [48], and base is often added in pre-treatment to aid in the removal of boron [49]. Chemical membrane deterioration is mitigated in practice by careful selection and maintenance of operation conditions.

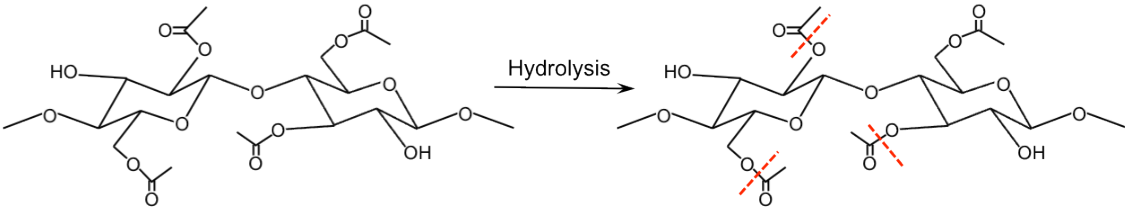

Figure 1.10. Hydrolysis of cellulose acetate.

1.1.8.4 Membrane Fouling

Fouling is caused by undesired secondary interactions (adsorption or adhesion) between the foulant and the membrane, and can occur via three main pathways:

1) Suspended Solids - Suspended or colloidal solids include particles such as clay or silica, which accumulate on the membrane surface. When the particles

are very small a coagulating agent is often added during pre-treatment to allow the filtration of suspended solids from feedwater.

2) Dissolved Solids - Total dissolved solids (TDS) such as salt ions are soluble in feed water, and can accumulate at the membrane surface due to concentration polarisation. The accumulated substances can become so concentrated that they form a precipitate layer on the membrane known as scaling. Scaling is somewhat reversible by chemical cleaning. In seawater, calcium carbonate and calcium sulphate are the most common scaling salts [50]. Other salts which can cause scaling in seawater desalination are barium sulfate, strontium sulfate, calcium fluoride and silica [51]. Dissolved solids can also include natural organic matter (NOM) [16].
3) Biological Matter - Biofouling on membranes can be described as an irreversible deposition and accumulation of bioorganic matter onto the surface of the membranes. This type of fouling is caused by the attachment of microorganisms in the feedwater, such as bacteria, fungi and algae, and NOM such as proteins, to the membrane surface and the subsequent growth of colonies on the surface [52]. The microorganisms and their secretions of extracellular polymeric substances (EPS) form a biofilm that is stabilized by weak physico-chemical interactions including hydrophobic and/or electrostatic interactions, hydrogen-bonding and van der Waal's interactions [53]. Predominantly, three phases of biofilm development are known to occur, i.e., (i) induction phase, the initial adhesion of proteins and other biological matter to the membrane surface via weak physicochemical interactions; (ii) logarithmic growth phase, when growth of bacterial colonies on the membrane surface occurs at a much faster rate than the attachment of new cells; and, (iii) plateau phase, in which attachment/growth and death/detachment of bacteria are in equilibrium (Figure 1.11) [54] [55].

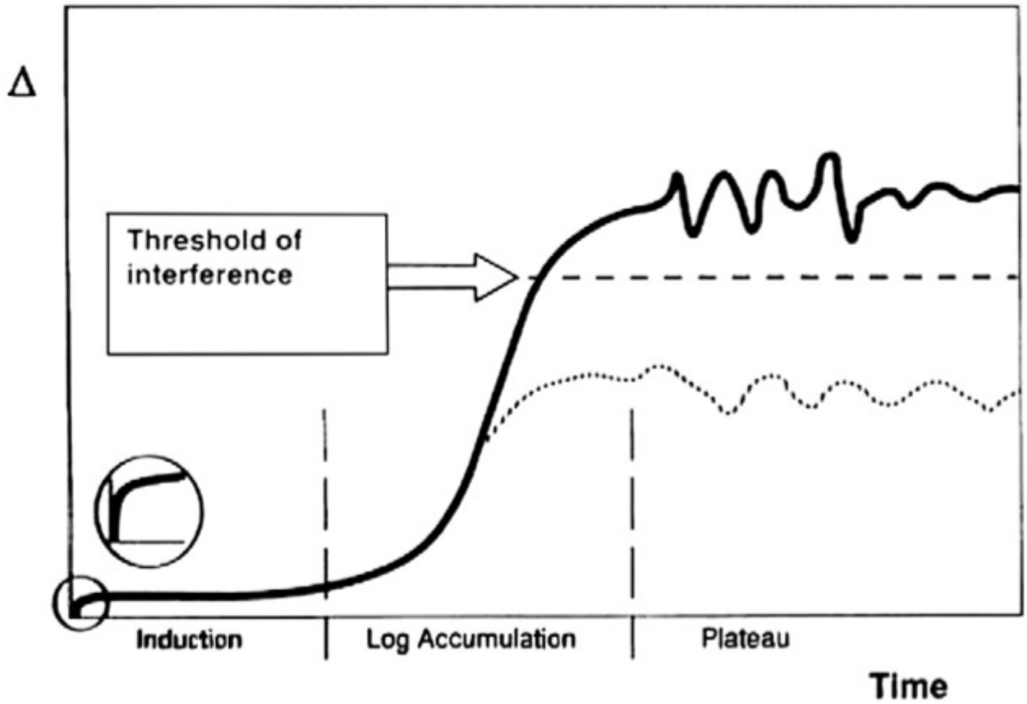

Figure 1.11. The three phases of biofouling. Δ represents the accumulation of biofilm with respect to time [55] .

Once the biofilm reaches the plateau phase it increases the fluid friction resistance and the overall hydraulic resistance of the membrane [52], which in turn leads to a reduction in water flux, requiring higher pressures to maintain flow, and demanding increased energy usage. Therefore, ideal membrane surfaces should act to mitigate biofilm formation at the induction phase, in order to minimize their biofouling potential below the threshold of interference.

In practice, water is often disinfected with chemicals such as chlorine during pre-treatment to prevent fouling by living organisms, however this can lead to degradation of the membrane as discussed in Section 1.1.8.3 above.

The concept of critical flux, a flux below which no irreversible fouling occurs, was first described by Howell *et al.* [56]. However, recent research by Tay and Song [57] suggests that fouling still occurs but is undetectable by measuring flux decline in the early stages.

1.1.8.5 Biofouling Tests

Typical tests for biofouling resistance often consist of dead-end filtration of a model protein system such as fibrinogen or bovine serum albumin (BSA), followed by analysis of the surface to determine the amount of protein attachment. Since bacterial attachment is be preceded by protein attachment, levels of biofouling are inferred. As with all model systems, there are inherent limitations to the technique. For example, Ang and Elimelech [58] found a synergistic fouling effect when RO membranes are fouled by both BSA and alginate, as compared to fouling by BSA or alginate alone. Membrane fouling is a complex process and is also affected by pH, ionic strength and temperature [59].

Truly biofouling-resistant membranes are yet to be realized. In order to solve the problem of biofouling three different approaches are applied: (1) mechanical detachment of biofoulers, (2) killing and inactivation of organisms, and (3) the surface modification of substrate materials with low-fouling coatings [60].

1.1.8.6 Mechanical Detachment of Biofoulants

Common methods of physically dislodging foulants include forward and backflushing permeate water in alternate directions across the face of the membrane, or backflushing permeate water from the permeate side to the feed side [61]. In some cases chemicals such as phosphate, citric acid and ionic compounds are used to disrupt the interactions between the foulant and the membrane surface prior to mechanical detachment [62].

1.1.8.7 Organism Killing and Inactivation

This approach involves dosing the feed with biocides or the use of UV irradiation to kill biofouling microorganisms. Interesting recent developments combine this approach with membrane surface modification, using bacteriocidal particles on the membrane surface to kill any bacteria which approach the surface [63]. Examples of bacteriocidal particles used in the literature include silver [64, 65] and TiO_2 [66, 67]. In most cases simply killing the bacteria is insufficient since dead biomass will remain on the membrane surface.

1.1.8.8 Membrane Surface Modification

In this approach the membrane is chemically altered to achieve surface properties which are less susceptible to biofouling. Kochkodan *et al.* [68] photochemically modified polyethersulfone (PES) and poly(vinylidene fluoride) (PVF) ultrafiltration membranes with 2-acrylamido-2-methyl-1-propanesulfonic acid (AMPSA), quaternized 2-(dimethylamino)ethyl methacrylate (qDMAEM), and poly(2-hydroxyethyl methacrylate) (pHEMA). They showed that pHEMA coatings were best able to resist fouling by *E.coli*, thus demonstrating that **hydrophilicity, chemical neutrality and low surface roughness** are the most important properties for resisting biofouling. Similarly, Song *et al.* [69] modified polysulfone membranes with HEMA via UV-irradiation in order to improve hydrophilicity. The resulting membrane had higher flux and less fouling by oily wastewater than the original membrane. Poly(ethylene glycol) (PEG) and oligo(ethylene glycol) (OEG) coatings have been shown to improve resistance to nonspecific protein adsorption [70], where steric exclusion effects and hydration are considered as critical factors for PEG or OEG polymers in resisting protein adsorption. However these polymers are not stable and are easily auto-oxidized in the presence of oxygen or transition metal ions [70]. Similarly, phosphorylcholine (PC)-based polymers have been shown to decrease biopolymer adsorption [71], but these polymers are fragile; the phosphoester groups being readily hydrolysable [72-74].

Covalent attachment of the coating to the membrane is desirable so that the coating cannot be degraded or washed away over time. For example layer-by-layer processes use ionic or self–assembly processes to form coatings, however they are known to disassemble under conditions where the bonds are unstable [75]. Surface initiated, controlled/living radical polymerisation is a versatile and powerful technique, which has been used for the surface modification of various substrates such as gold [76], silicon wafers [76], carbon nanotubes [77] and polymer membranes [78, 79]. The most extensively used modification method involves a covalent graft polymerisation method, which occurs in two forms: 'grafting to' and 'grafting from'. For membrane coatings, however, the 'grafting from' approach is preferable because it enables a higher graft density than the 'grafting to' approach, while still preserving control over the polymer architecture and coating thickness [80].

1.1.8.9 Nanocomposite Membranes

Organic membranes containing inorganic fillers have been used in the literature to enhance antifouling and mechanical properties. The aim of so-called mixed matrix or composite membranes is to combine the materials in such a way that the benefits of each are obtained. For example, organic membranes are cheap and easy to manufacture, but have poor mechanical strength, while inorganic materials are sometimes expensive but show good mechanical and thermal properties. CAMs have traditionally been reinforced with mineral fillers. In the 1970s Goosens *et al.* [32] [81] used several types of mineral fillers (silicum and aluminium oxides and montmorrilonites) incorporated into CA casting solutions in order to improve compaction resistance. In 1983 Finken *et al.* [82] used montmorrilonite at concentrations of up to 2000ppm to cast membranes with enhanced mechanical stability and stabilized long-term flux. Recently, there has been a trend toward nanoparticle fillers, forming membranes known as nanocomposites. The advantage of using nanoparticles is their high surface area leading to more interactions and efficient interfacial stress transfer therefore very low loadings are needed (typically <5 wt%) [83]. In the literature commonly used nanofillers include silica, silver nanoparticles [38] , carbon nanotubes [84], zeolites [46], and perhaps the most commonly used nanofiller titanium oxide (TiO_2) [38]. Nanocomposties containing these nanofillers have been used to aid mechanical and thermal stability, biofouling resistance, increased flux and targeted degradation.

Zeolites are sometimes known as molecular sieves. They are crystalline aluminosilicate materials with well-defined pore structures that have intercrystalline microporous channels of 0.4nm for Type-A zeolites, and 0.56nm for MFI-type zeolites (Figure 1.12) [85]. It has been calculated that zeolites could achieve 100% ion rejection because the channel size is smaller than the hydrated ions. Water permeation is also affected by the Si/Al ratio, which determines hydrophilicity and other characteristics [86].

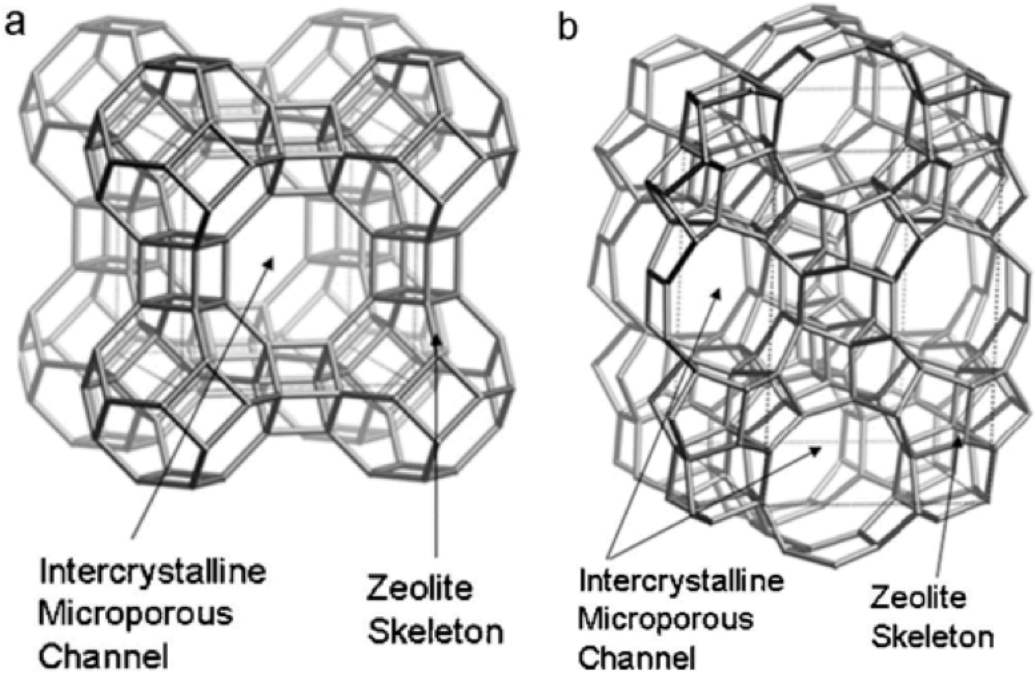

Figure 1.12. Zeolite structures (a) A-type (b) MFI-type [85].

Initial experiments used MFI-type zeolites on an alumina substrate, but the flux and salt rejection were too low for practical use [87]. Enchanced water flux and ion rejection were achieved with high Al content MFI-type zeolite membranes [86]. Jeong *et al.* [88] made nanocomposite membranes with type-A zeolites dispersed in polysulfone. Water permeability was nearly double and solute rejection equivalent to polysulfone membranes. Penderagst *et al.* [46] cast polysulfone membranes containing amorphous non-porous silica or type-A zeolite nanoparticles. The nanocomposite membranes tended to have higher initial flux and less flux decline caused by membrane compaction.

Li *et al.* [67] prepared dispersed TiO_2 nanoparticles in PES casting solutions to prepare microporous PES-TiO_2 composite membranes via phase-inversion. They observed increased hydrophilicity, permeation and mechanical strength at 4 wt% loading. Higher loadings resulted in aggregation of the nanoparticles. Wu *et al.* [89] also made PES-TiO_2 nanocomposites via phase-inversion, but found 0.5 wt% to be the optimal loading. Yang *et al.* [90] prepared nanocomposites of TiO_2 in polysulfone. They found water permeability, hydrophilicity, mechanical strength and anti-fouling properties were improved at a loading of 2 wt%, however, above this loading nanoparticle aggregation caused a decline in nanocomposite membrane performance.

Zodrow *et al.* [65] incorporated silver nanoparticles into polysulfonate UF membranes and achieved antimicrobial properties toward several bacteria. However, leaching of the nanoparticles was an issue. Taurozzi *et al.* [91] investigated the effect of silver nanoparticle incorporation route into polysulfonate membranes. They found that in situ reduction of silver led to formation of homogeneously distributed and smaller nanoparticles. Their membranes also showed anti-biofouling activity upon the release of the silver nanoparticlers from the membrane.

CNT nanocomposite membranes have been shown to increase water flux by an order of magnitude, relative to other nanoporous materials [92]. Since flow of water is through the central pore of the nanotube, CNTs must be aligned in the membrane (Figure 1.13 [93]). Synthesis of aligned arrays is complex [83, 91, 92]. Ion rejection is believed to occur via a combination of static interactions and size exclusion.

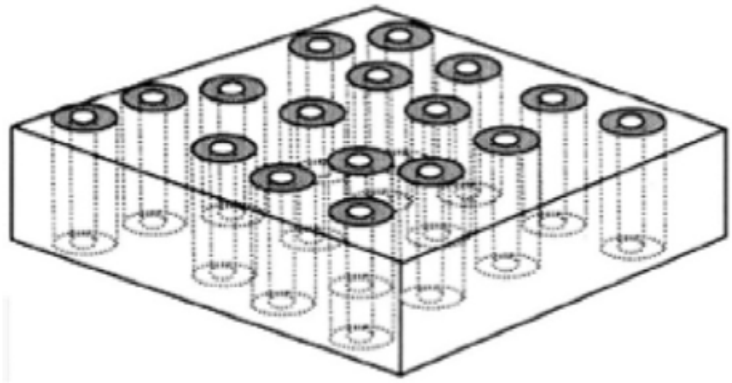

Figure 1.13. Schematic of the ideal aligned CNT nanocomposite membrane [93].

Composite strength is affected by filler particle size, loading and adhesion between the particles and the polymer matrix. Even dispersion of the nanoparticles is essential in order to have desirable particle/matrix interactions [93, 94]. Therefore, agglomeration and leaching are major concerns for nanocomposite materials. When nanoparticles form agglomerates they can have a deleterious effect on the membrane properties. Furthermore, leaching of some nanoparticles has been reported to have serious health concerns [94]. One solution to agglomeration and leaching is to anchor the nanoparticles in the polymer matrix. This has been done by functionalising the nanoparticle with a group that has favourable interactions with the polymer matrix. For example, Li *et al.* [84] made nanocomposite CA membranes with multiwalled carbon nanotubes (MWCNTs) either neat or acid treated. The acid treated MWCNTs showed more uniform dispersion than the neat, this was attributed to the interaction between the carboxyl groups and the ester groups of CA resulting in good interfacial adhesion. Choi *et al.* [95] also used acid treatment of MWCNTs to achieve better dispersion in polysulfone casting solutions. Razmjou *et al.* [96] modified TiO_2 nanoparticles using 3-aminopropyltriethoxysilane (APTES) as a silane coupling agent, and incorporated the modified nanoparticle in PES UF membranes. The results showed good dispersion of the modified nanoparticles due to less agglomeration.

1.2 Aims Of This Thesis

A review of the literature reveals obstacles to the reduction of costs for CA RO membranes by lowering energy requirements and increasing membrane lifetime. Of the major obstacles, concentration polarisation is combated using engineering solutions, and chemical degradation of the membrane can be avoided by selecting the correct operational conditions. However, substantial gains are still to be made in the areas of biofouling and membrane compaction.

In relation to the former, it is well known that the desirable properties for biofouling resistance are hydrophilicity, smoothness and charge neutrality. Polymers present an attractive option for membrane modification, due to their ability to form covalent bonds with the membrane surface. The literature also reveals that current biofouling resistance tests often rely on model systems that are far removed from real world operating conditions. It is therefore desirable to test membranes in a true seawater environment.

In relation to the latter, the field of nanocomposites holds promise for combating membrane compaction, however aggregation and leaching of nanoparticles remain problems. An opportunity exists to overcome this obstacle by anchoring the nanoparticles in the polymeric matrix.

Given this context, the aims of this thesis are to develop CA RO membranes with reduced biofouling, increased energy efficiency and extended lifetime by:

1. Surface modification of CA RO membrane using commercially attractive radical polymerisation techniques;
2. Optimisation of reaction conditions to achieve a range of polymer graft-densities;

3. Biofouling resistance tests that more closely imitate actual fouling conditions;
4. Characterisation of the modified membranes to determine ideal outcome: prevention of biofouling of the membrane whilst maintaining water flux and salt rejection properties;
5. Synthesis of CA-anchored nanoparticles;
6. Inclusion of anchored and unanchored nanoparticles in the CA matrix at different weight % to determine the effect of anchoring the nanoparticles on their dispersion in the membrane matrix;
7. Investigation of the effect of nanoparticle inclusion on the filtration properties and mechanical strength of the membranes.

1.3 Thesis Outline

Chapter Two details the materials and synthetic and analytical methods employed throughout this research.

Chapter Three focuses on Aims 1 and 2. It contains a detailed look at the modification of the CA membrane surface, including the rationale behind the choices of monomer, solvents and reagents, and looks at the effect of varying polymerisation reaction time and initial monomer concentration.

This work is further expanded in Chapter Four, which includes further characterisation of the modified membranes, including resistance to biofouling, and flux and salt rejection data, addressing Aims 3 and 4.

Aims 5, 6 and 7 are covered in Chapter Five. It discusses the synthesis of the anchored nanoparticles, and the effect of their inclusion in the CA matrix on membrane mechanical strength as well as filtration properties.

Chapter Six summarises the findings from this research, and discusses future recommendations arising from the work.

References

1. V. Babkin; R. Klige, 1.2 the Hydrosphere. In *World Water Resources at the Beginning of the Twenty-First Century*, Shiklomanov, I.; Rodda, J., Eds. Cambridge University Press: Cambridge, United Kingdom, 2003; pp 1-10.
2. D. Knights; I. MacGill; R. Passey *The Sustainability of Desalination Plants in Australia: Is Renewable Energy the Answer?*; UNSW: 2006.
3. A. Villfafila; I. Mujtaba. Fresh Water by Reverse Osmosis Based Desalination: Simulation and Optimisation, Desalination 155 (2003) 1-13.
4. C. Fritzmann; J. Lowenberg; T. Wintgens; T. Melin. State-of-the-Art of Reverse Osmosis Desalination, Desalination 216 (2007) 1-76.
5. S. Kalogirou. Seawater Desalination Using Renewable Energy Sources, Progress in Energy and Combustion Science 31 (2005) 242-281.
6. T. Shibata. Cellulose Acetate in Separation Technology, Macromolecules 39 (2006) 8609-8615.
7. Q. Schiermeier. Purification with a Pinch of Salt, Nature 452 (2008) 260-261.
8. H. Krishna *Introduction to Desalination Technologies*; Texas Water Development Board: 1989.
9. T. Cath; A. Childress; M. Elimelech. Forward Osmosis: Principles, Applications and Recent Developments, Journal of Membrane Science 281 (2006) 70-87.
10. J. Blank; G. Tusel; S. Nisanc. The Real Cost of Desalted Water and How to Reduce It Further, Desalination 205 (2007) 298-311.
11. K. Robinson; M. Khan; M. de Paz Banez; X. Wang; S. Armes. Controlled Polymerization of 2-Hydroxyethyl Methacrylate by ATRP at Ambient Temperature, Macromolecules 34 (2001) 3155-3158.
12. M. Ulbricht. Advanced Functional Polymer Membranes, Polymer 47 (2006) 2217-2262.
13. J. McCuthcheon; R. McGinnis; M. Elimelech. Desalination by Ammonia-Carbon Dioxide Forward Osmosis: Influence of Draw and Feed Solution

Concentrations on Process Performance, Journal of Membrane Science 278 (2006) 114-123.

14. R. McGinnis; M. Elimelech. Energy Requirements of Ammonia-Carbon Dioxide Forward Osmosis Desalination, Desalination 207 (2007) 370-382.
15. T. Cath; A. Childress; M. Elimelech. Forward Osmosis: Principles, Applications, and Recent Developments, Journal of Membrane Science 281 (2006) 70-87.
16. N. Voutchkov. Considerations for Selection of Seawater Pretreatment System, Desalination 261 (2010) 354-364.
17. A. Sagle; B. Freeman *Fundamentals of Membranes for Water Treatment*.
18. J. Qiu; Y. Zhang; Y. Shen; Y. Zhang; H. Zhang; J. Liu. Hydrophilic Modification of Microporous Polysulfone Membrane via Surface-Initiated Atom Transfer Radical Polymerization of Acrylamide, Applied Surface Science 256 (2010) 3274-3280.
19. E. Chian; J. Chen; P. Sheng; Y. Ting; L. Wang, Reverse Osmosis Technology for Desalination. 2007.
20. D. Paul. Reformultion of the Solution-Diffusion Theory of Reverse Osmosis, Journal of Membrane Science 241 (2004) 371-386.
21. J. Wijmans; R. Baker. The Solution-Diffusion Model: A Review, Journal of Membrane Science 107 (1995) 1-21.
22. J. Cadotte. Interfacially Synthesized Reverse Osmosis Membrane. Patent no. 4,277,344, 1981.
23. S. Alvonitis; W. Hanbury; T. Hodgekiss. Chlorine Degradation of Aromatic Polyamides, Desalination 85 (1992) 321-334.
24. A. Carlmark ; E. Malmstrom. ATRP Grafting from Cellulose Fibres to Create Block Co-Polymer Grafts, Biomacromolecules 4 (2003) 1740-1745.
25. S. McCray; V. Vilker; K. Nobe. Reverse Osmosis Cellulose Acetate Membranes II. Dependance of Transport Properties on Acteyl Content, Journal of Membrane Science 59 (1991) 317-330.

26. C. Reid; Breton. Water and Ion Flow across Cellosic Membranes, Journal of Applied Polymer Science 1 (1959) 133-143.
27. S. Loeb; S. Sourirajan *Seawater Demineralisation by Means of a Semipermeable Membrane*; University of California, Department of Engineering: Los Angeles, 1960.
28. S. Nunes; K. Peinemann, *Membrane Technology in the Chemical Industry*. 2nd ed.; Wiley-VCH.
29. S. Manjikian; S. Loeb; J. McCutchan In *Improvement in Fabrication Techniques for Reverse Osmosis Desalination Membranes*, The First International Symposium on Water Desalination, 1965; US Dept. of Interior, Office of Saline Water (Washington DC): 1965; pp 159-173.
30. R. Kesting; A. Menefee. Role of Formamide in Preparation of Cellulose Acetate Membranes, Kolloid-Zeitschrift & Zeitschrift fur Polymere 230 (1969) 341-346.
31. I. Pinnau, Membrane Separations | Membrane Preparation. In *Encyclopedia of Separation Science*, Wilson, I. D., Ed. Academic Press: Oxford, 2000; pp 1755-1764.
32. I. Goossens; A. Van Haute. The Influence of Mineral Fillers on the Menbrane Properties of High Flux Asymmetric Cellulose Acetate Reverse Osmosis Membranes, Desalination 18 (1976) 203-214.
33. R. Okey; P. Stavenger. Reverse Osmosis Applications in Industiral Waste Water Treatment, Membrane Process Ind. Symp. (1966) 127-156.
34. Y. Liu; Y. Sin. Application of Reverse Osmosis in Wine Brewing, Niangjiu 32 (2005) 99-100.
35. M. Cheryan; N. Rajagopalan. Membrane Processing of Oily Streams. Wastewater Treatment and Waste Reduction, Journal of Membrane Science 151 (1998) 13-28.
36. K. Chinu; A. Johir; V. S.; H. Shon; J. Kandasamy. Assessment of Pretreatment to Microfiltration for Desalination in Terms of Fouling Index and Molecular

Weight Distribution, Desalination 250 (2010) 644-647.

37. J. Holt In Innovative technical solutions for water management in Australia, Australian Academy of Science, 2006; Australian Academy of Science, 2006.
38. K. Kim; B. Van der Bruggen. The Use of Nanoparticles in Polymeric and Ceramic Membrane Structures: Review of Manufacturing Procedures and Performance Improvement for Water Treatment, Environmental Pollution 158 (2010) 2335-2349.
39. M. Elimelech; W. Phillip. The Future of Seawater Desalination: Energy, Technology, and the Environment, Science 333 (2011) 712-717.
40. M. Shannon; P. Bohn; M. Elimelech; J. Georgiadis; B. Marinas; A. Mayes. Science and Technology for Water Purification in the Coming Decades, Nature 452 (2008) 301-310.
41. S. Avlonitis; K. Kuroumbas; N. Vlachakis. Energy Consumption and Membrane Replacement Cost for Seawater RO Desalination Plants, Desalination 157 (2003) 151-158.
42. M. Amiri; M. Samiei. Enhancing Permeate Flux in a RO Plant by Controlling Membrane Fouling, Desalination 207 (2007) 361-369.
43. R. Bian; K. Yamamoto; Y. Watanabe. The Effect of Shear Rate on Controlling the Concentration Polarization and Membrane Fouling, Desalination 131 (2000) 225-236.
44. K. Ebert; D. Fritsch; J. Koll; C. Tjahjawiguna. Influence of Inorganic Fillers on the Compaction Behaviour of Porous Polymer Based Membranes, Journal of Membrane Science 233 (2004) 71-78.
45. K. Persson; V. Gekas; G. Tragardh. Study of Membran Compaction and its Influence on Ultrafiltration Water Permeability, Journal of Membrane Science 100 (1995) 155-162.
46. M. Pendergast; J. Nygaard; A. Ghosh; E. Hoek. Using Nanocomposite Materials Technology to Understand and Control Reverse Osmosis Membrane Compaction, Desalination 261 (2010) 255-263.

47. S.B. McCray; J. Glater, Effects of Hydrolysis on Cellulose Acetate Reverse Osmosis Transport Coefficients. In *Reverse Osmosis and Ultrafiltration*, American Chemical Society: 1985; Vol. 281, pp 141-151.
48. E. Prenesti; E. Ferrara; S. Berto; P. Fisicaro; P.G. Daniele. Development of a Reference Solution for the pH of Seawater, Analytical and Bioanalytical Chemistry 388 (2007) 1877-1883.
49. B. Andrews; B. Dave; P. Lopez-Serrano; S.-P. Tsai; R. Frank; M. Wilf; E. Koutsakos. Effective Scale Control for Seawater RO Operating with High Feed Water Ph and Temperature, Desalination 220 (2008) 295-304.
50. R. Nijboer; B. Holst; S. Poedts; J. Goedbloed; Y. Iwasa; L. Haigun; M. Al-Shammiri; M. Al-Dawas. Maximum Recovery from Seawater Reverse Osmosis Plants in Kuwait, Desalination 110 (1997) 37-48.
51. A. Rahardianto; J. Gao; C. Gabelich; M. Williams; Y. Cohen. High Recovery Membrane Desalting of Low-Salinity Brackish Water: Integration of Accelerated Precipitation Softening with Membrane RO, Journal of Membrane Science 289 (2007) 123-137.
52. H. Flemming. Reverse Osmosis Membrane Biofouling, Experimental Thermal and Fluid Science 14 (1997) 382-391.
53. M. Pasmore; P. Todd; S. Smith; D. Baker; J. Silverstein; D. Coons; C. Bowman. Effects of Untlrafiltration Membrane Surface Properties on Pseudonmonas Aeruginosa Biofilm Initiation for the Purpose of Reducing Biofouling, Journal of Membrane Science 194 (2001) 15-32.
54. H.-C. Flemming. Reverse Osmosis Membrane Biofouling, Exp. Therm Fluid Sci. 14 (1997) 382-391.
55. A. Matin; Z. Khan; S. Zaidi; M. Boyce. Biofouling in Reverse Osmosis Membranes for Seawater Desalination: Phenomena and Prevention, Desalination 281 (2011) 1-16.
56. R. Field; D. Wu; J. Howell; B. Gupta. Critical Flux Concept for Microfiltration Fouling, Journal of Membrane Science 100 (1995) 259-272.

57. K. Tay; L. Song. A More Effective Method for Fouling Characterisation in a Full-Scale Reverse Osmosis Process, Desalination 177 (2005) 95-107.
58. W. Ang; M. Elimelech. Protein (BSA) Fouling of Reverse Osmosis Membranes: Implications for Wastewater Reclamation, Journal of Membrane Science 296 (2007) 83-92.
59. H. Mo; K. Tay; H. Ng. Fouling of Reverse Osmosis Membrane by Protein (BSA): Effects of pH, Calcium, Magnesium, Ionic Strength and Temperature, Journal of Membrane Science 315 (2008) 28-35.
60. T. Vladkova, Surface Modification Approach to Control Biofouling. In *Marine and Industrial Biofouling*, Flemming, H.; Murthy, P.; Venkatesan, R.; Cooksey, K., Eds. Springer: 2008; pp 135-164.
61. J. Arnal; B. Garcia-Fayos; M. Sancho, Membrane Cleaning. In *Expanding Issues in Desalination*, Ning, R., Ed. InTech: 2011; pp 63-84.
62. H. Flemming; G. Schaule; T. Griebe; J. Schmitt; A. Tamachkiarowa. Biofouling - the Achilles Heel of Membrane Processes, Desalination 113 (1997) 215-225.
63. H. Flemming, Microbial Biofouling: Unsolved Problems, Insufficient Approaches, and Possible Solutions. In *Biofilm Highlights*, H., F.; Wingender, J.; Szewzyk, U., Eds. Springer: 2011; Vol. 5, pp 81-110.
64. H. Yang; J. Lin; C. Huang. Application of Nanosilver Surface Modification to Ro Membrane and Spacer for Mitigating Biofouling in Seawater Desalination, Water Research 43 (2009) 3777-3786.
65. K. Zodrow; L. Brunet; S. Mahendra; D. Li; A. Zhang; Q. Li; P. Alvarez. Polysulfone Ultrafiltration Membranes Impregnated with Silver Nanoparticles Show Improved Biofouling Resistance and Virus Removal, Water Research 43 (2009) 715-723.
66. S. Kwak; S. Kim. Hybrid Organic/Inorganic Reverse Osmosis (RO) Membrane for Bactericidal Anti-Fouling. 1. Preparation and Characterization of TiO_2 Nanoparticle Self-Assembled Aromatic Polyamide Thin-Film-Composite

(TFC) Membrane, Environmental Science and Technology 35 (2001) 2388-2394.

67. J. Li; Z. Xu; H. YAng; L. Yu; M. Liu. Effect of TiO_2 Nanoparticles on the Surface Morphology and Performance of Microporous PES Membrane, Applied Surface Science 255 (2009) 4725-4732.
68. V. Kochkodan; N. Hilal; V. Goncharuk; L. Al-Khatib; T. Levadna. Effect of the Surface Modification of Polymer Membranes on Their Microbiological Fouling, Colloid Journal 68 (2006) 267-273.
69. K. Song; K. Lee. Treatment of Oily Wastewater Using Membrane with 2-Hydroxyethyl Methacrylate-Modified Surface, Korean Journal of Chemical Engineering 24 (2007) 116-120.
70. E. Ostuni; R. Chapman; R. Homlin; S. Takayama; G. Whitesides. A Survey of Structure-Property Relationships of Surfaces That Resist the Adsorption of Protein, Langmuir 17 (2001) 5605-5620.
71. S.-H. Ye; C.A. Johnson; J.R. Woolley; S. T.A.; L.J. Gamble; W.R. Wagner. Covalent Surface Modification of a Titanium Alloy with a Phosphorylcholine-Containing Copolymer for Reduced Thrombogenicity in Cardiovascular Devices, Journal of Biomedical Materials Research Part A 91A (2009) 18-28.
72. A.L. Lewis; P.D. Hughes; L.C. Kirkwood; S.W. Leppard; R.P. Redman; L.A. Tolhurst; P.W. Stratford. Synthesis and Characterisation of Phosphorylcholine-Based Polymers Useful for Coating Blood Filtration Devices, Biomaterials 21 (2000) 1847-1859.
73. E.F. Murphy; J.R. Lu. Characterisation of Protein Adsorption at the Phosphorylcholine Incorporated Polymer-Water Interface, Macromolecules 33 (2000) 4545-4554.
74. Y. Iwasaki; K. Ishihara. Phosphorylcholine-Containing Polymers for Biomedical Applications, Analytical and Bioanalytical Chemistry 381 (2005) 534-546.
75. D. Bergbreiter; K. Liao. Covalent Layer-by-Layer Assembly - an Effective,

Forgiving Way to Construct Functional Robust Ultrathin Films and Nanocomposites, Soft Matter 5 (2009) 23-28.

76. Z. Bao; M.L. Breuning; G.L. Baker. Control of the Density of Polymer Brushes Prepared by Surface-Initiated Atom Transfer Radical Polymerization, Macromolecules 39 (2006) 5251-5258.
77. Y.-L. Liu; W.-H. Chen. Modification of Multiwall Carbon Nanotubes with Initiators and Macroinitiators of Atom Transfer Radical Polymerization, Macromolecules 40 (2007) 8881-8886.
78. J. Lindqvist; E. Malmstrom. Surface Modification of Natural Substrates By Atom Transfer Radical Polymerisation, Journal of Applied Polymer Science 100 (2006) 4155-4162.
79. N. Singh; Z. Chen; N. Tower; S. Wichramasinghe; N. Soice. Modification of Regenerated Cellulose Ultrafiltration Membranes by Surface Initiated Atom Transfer Radical Polymerisation, Journal of Membrane Science (2008)
80. K.L. Beers; S.G. Gaynor; K. Matyjaszewski. The Synthesis of Densely Grafted Copolymers by Atom Transfer Radical Polymerization, Macromolecules 31 (1998) 9413-9415.
81. I. Goosens; A. Van Haute. The Use of Direct Osmosis Tests as Complementary Experiments to Determine the Water and Salt Permeabilities of Reinforced Cellulose Acetate Membranes Desalination 26 (1978) 299-308.
82. H. Finken. Bentonite-Stabilized CDA/CTA Membranes: I. Improved Long-Term Transport Properties, Desalination 48 (1983) 207-221.
83. L. Hamming; R. Qiao; P. Messersmith; B. L. Effects of Dispersion and Interfacial Modification on the Macroscale Properties of TiO_2 Polymer–Matrix Nanocomposites, Composites Science and Technology 69 (2009) 1880-1886.
84. M. Li; I.-H. Kim; Y. Jeong. Cellulose Acetate/Multiwalled Carbon Nanotube Nanocomposites with Improved Mechanical, Thermal, and Electrical Properties, Journal of Applied Polymer Science 118 (2010) 2475-2481.
85. K. Lee; T. Arnot; D. Mattia. A Review of Reverse Osmosis Membrane

Materials for Desalination—Development to Date and Future Potential, Journal of Membrane Science 370 (2011) 1-22.

86. L. Li; N. Liu; B. McPherson; R. Lee. Enhanced Water Permeation of Reverse Osmosis through MFI-Type ZeoliteMembranes with High Aluminum Contents, Industrial & Engineering Chemistry Research 46 (2007) 1584-1589.
87. L. Li; J. Dong; T. Nenoff; R. Lee. Desalination by Reverse Osmosis Using MFI Zeolite Membranes, Journal of Membrane Science 243 (2004) 401-404.
88. B.-H. Jeong; E. Hoek; Y. Yan; A. Subramani; X. Huang; G. Hurwitz; A. Ghosh; A. Jawor. Interfacial Polymerisation of Thin Film Nanocomposites: A New Concept for Reverse Osmosis Membranes, Journal of Membrane Science - Rapid Communication 294 (2007) 1-7.
89. G. Wu; S. Gan; L. Cui; Y. Xu. Preparation and Characterization of PES/TiO_2 Composite Membranes, Applied Surface Science 254 (2008) 7080-7086.
90. Y. Yang; H. Zhang; P. Wang; Q. Zheng; J. Li. The Influence of Nano-Sized TiO_2 Fillers on the Morphologies and Properties of PSF UF Membrane, Journal of Membrane Science 288 (2007) 231-238.
91. J. Taurozzi; H. Arul; V. Bosak; A. Burban; T. Voice; M. Bruening; V. Tarabara. Effect of Filler Incorporation Route on the Properties of Polysulfone– Silver Nanocomposite Membranes of Different Porosities, Journal of Membrane Science 325 (2008) 58-68.
92. J. Holt; H. Park; Y. Wang; M. Staderman; A. Artyukhin; C. Grigoropoulos; A. Noy; O. Bakajin. Fast Mass Transport through Sub–2-Nanometer Carbon Nanotubes, Science 312 (2006)
93. A. Ismail; P. Goh; S. Sanip; M. Aziz. Transport and Separation Properties of Carbon Nanotube-Mixed Matrix Membrane, Separation and Purification Technology 70 (2009) 12-26.
94. C. Lam; J. James; R. McCluskey; S. Arepalli; R. Hunter. A Review of Carbon Nanotube Toxicity and Assessment of Potential Occupational and Environmental Health Risks, Critical Reviews in Toxicology 36 (2006) 189-

217.

95. J. Choi; J. Jegal; W. Kim. Fabrication and Characterization of Multi-Walled Carbon Nanotubes/Polymer Blend Membranes, Journal of Membrane Science 284 (2006) 406-415.

96. A. Razmjou; J. Mansouri; V. Chen. The Effects of Mechanical and Chemical Modification of TiO_2 Nanoparticles on the Surface Chemistry, Structure and Fouling Performance of PES Ultrafiltration Membranes, Journal of Membrane Science 378 (2011) 73-84.

2 Chapter Two

Materials and Methods

Preface

This chapter contains details on the materials and methods employed during the experimental work undertaken for this thesis. It is presented in four sections.

- The first section lists the sources for general solvents and laboratory reagents used throughout this work.
- The second section describes techniques for the preparation of samples and methods of characterisation used throughout this work.
- The third section describes the methods for materials synthesized during this work. Materials specific to each synthesis are listed with the relevant method.
- The fourth section includes synthetic and error calculations.

Details pertaining to particular aspects of this work are provided in the corresponding chapters.

2.1 Material Sources - General solvents and reagents

Unless otherwise stated, all reagents and solvents were used as received.

Acetone was purchased from Univar Australia.

Dichloromethane (anhydrous, 99.8%) was supplied by Sigma-Aldrich.

Diethyl ether was purchased from Merck.

Ethanol was purchased from Merck.

Formamide was obtained from Fluka.

n-Hexane (96%) was purchased from Scharlau.

Isopropanol (99.5%) was obtained from Optigen.

Methanol was purchased from Merck.

$MgSO_4$ (97+%) was purchased from Aldrich. Prior to use it was dried overnight at 110 °C.

Sodium hydroxide (NaOH, 98%) was purchased from Sigma-Aldrich.

Toluene (98%) was purchased from Sigma-Aldrich.

2.2 Materials Synthesis

Characterisation of synthesised materials is discussed in the relevant chapter.

2.2.1 Synthesis of Tris[(2-pyridyl)methyl]amine (TPMA)

Materials

2-picolyl chloride hydrochloride (98%) was purchased from Aldrich.

2-(aminomethyl) pyridine (99%) was purchased from Aldrich.

Method

Tris[(2-pyridyl)methyl]amine (TPMA) was prepared by methods described by Tyeklar *et al.* [1] Namely, 2-picolyl chloride hydrochloride (4.85g, 2.9 x10^{-2}mol) in 25mL of deionised water was stirred at 0°C using an ice bath. To this solution was added 5.3M NaOH (5.62mL) the reaction mixture turned bright red. To this mixture was added a solution of 2-(aminomethyl) pyridine (1.6g, 1.48 x10^{-2}mol) in dichloromethane (25mL). The reaction mixture was then allowed to warm to room temperature. Over the next 48 hours an additional 5.63mL of 5.3M NaOH was added. The crude mixture was then washed with 15% NaOH (2 x 12.5mL aliquots) and the organic phase was collected and dried over $MgSO_4$ overnight. The solution was passed through a filter and dichloromethane was removed under vacuum. The retained solid was extracted 3 times with boiling diethyl ether to yield yellow crystals. The TPMA was purified by recrystallisation from diethyl ether to give a white crystalline solid.

2.2.2 Synthesis of bromo-initiator modified CAMs

Materials

Commercially available Sepa CF CA (cellulose acetate) RO CE membranes were purchased from GE Osmonics. Prior to use, the membranes were cut into 5.0 cm x 5.0 cm coupons, and then sonicated in diethyl ether for 10 minutes.

4-dimethylaminopyridine (DMAP. 99.0%) was purchased from Fluka.

Triethylamine (TEA. 99.5%)) was obtained from Aldrich.

2-Bromoisobutyryl bromide (BiBBr) was purchased from Aldrich and distilled prior to use.

Method

A standard solution was made containing DMAP (2.7 x10^{-3}g) catalyst in diethyl ether (0.100 L). The CA membrane coupon was added to a 25mL vial containing 20.0 x10^{-3}L of the stock solution, with stirring at 0°C in an ice bath, under nitrogen. TEA (0.23 x10^{-3}L, 1.65 x10^{-6}mol) and ATRP initiator BiBBr (0.19 x10^{-3}L, 1.50 x10^{-6}mol) were injected simultaneously. The reaction mixture was stirred for 5 minutes at 0°C, then allowed to warm to room temperature, and stirred for a further 3 hours [2]. The modified membrane was thoroughly washed using the following procedure: washed with diethyl ether; sonicated in diethyl ether for 20 minutes; shaken in a methanol/diethyl ether mixture for 5 minutes; sonicated in methanol for 10 minutes; sonicated in methanol / water (1:1 v/v) for 10 minutes; sonicated in deionised water for 1 hour. The bromo-initiator modified membranes were stored in methanol/water (1:1 v/v) in the refrigerator overnight, and used the next day to avoid oxidation.

2.2.3 HEMA purification

Materials

2- Hydroxyethyl methacrylate (HEMA, 97%) was purchased from Aldrich.

Aluminium oxide (activated, basic) was purchased from Sigma-Aldrich.

Method

HEMA was purified using a method described by Carlmark and Malmstrom [3]. Briefly, the HEMA monomer was dissolved in water and washed with ten equivalents of hexane, then the organic layer was extracted with NaCl and dried over $MgSO_4$ before being passed over a column of basic alumina.

2.2.4 Surface grafting of 2-hydroxyethyl methacrylate polymers from CA membrane using SI-ARGET ATRP

Materials

Copper (II) chloride was obtained from Aldrich.

TPMA was synthesized as described in 2.2.1.

2- Hydroxyethyl methacrylate (HEMA, 97%) was purchased from Aldrich and purified before use. See 2.2.3 for purification method.

Ethyl 2-bromoisobutyryl bromide (EBiB, 98%) was purchased from sigma-Aldrich.

L-ascorbic acid (99%) were obtained from Aldrich.

Method

A stock solution was prepared containing copper (II) chloride (0.79 x10^{-3}g) and TPMA (6.50 x10^{-3}g)) in water/methanol (1:1 v/v, 3 x10^{-3} L). The monomer HEMA (5.365g, 3.219g 2.146g or 1.073g) was added to 3.0 x10^{-3}L of the stock solution in a 25 mL vial. To this was added either EBiB (0.06 x10^{-3}L), for polymerisation in solution, or the functionalized membrane for surface-initiated polymerisation. The solution was purged under nitrogen, then L-ascorbic acid (7.2 x10^{-3}g) dissolved in water/methanol (1:1 v/v, 1.0 x10^{-3}L) was injected, and the solution was stirred for the desired amount of time. After surface-initiated polymerisation the membrane was washed thoroughly and sonicated in water 5 times, changing the water between each sonication. The pHEMA-grafted membranes were stored in water/methanol (1:1 v/v) in the refrigerator to prevent biofouling. Trace amounts of copper were not removed from the final product.

2.2.5 Cell-Fixing Solutions

Materials

Glutaraldehyde Solution (25% in water) was purchased from Fluka.

Paraformaldehyde was purchased from Riedel-deHaen.

Phosphate buffered saline tablets were purchased from Sigma.

Method

Phosphate buffered saline was made according to the manufacturer's instructions: one tablet was dissolved in 200mL of demineralised water. To prepare the fixative solution, paraformaldehyde (4.00g) was dissolved in phosphate buffered saline (60.0mL) at 60°C. Sucrose (4.0g) was then added and the solution allowed to cool to room temperature. Glutaraldehyde solution (25% solution in water, 2.0mL) was added and the final volume adjusted to 100mL using phosphate buffered saline.

2.2.6 Synthesis of cellulose acetate-grafted POSS

Materials

Aminopropylisobutyl polyhedral oligomeric silsesquioxane (POSS) was purchased from Hybrid plastics.

Toluene-2, 4-diisocyanate (TDI, 95%) was purchased from Aldrich.

Dibutyltin dilaurate (95%) was purchased from Aldrich.

1-methyl-2-(pyrrolidinone) (99%) was purchased from Sigma.

Cellulose acetate (39.8 wt%, avg. m_n 30,000) was obtained from Sigma-Aldrich, and dried overnight at 110°C before use.

Method

Aminopropylisobutyl POSS (1g, 1.434 mmol) and toluene-2,4-diisocyanate (0.1999 g, 1.434 mmol) were placed in a 100 mL two-necked flask equipped with a magnetic stirrer, reflux condenser and N_2 purge. 20 mL of toluene was added to dissolve POSS and the reaction mixture was heated to 80°C for 15 min. Dibutyltin dilaurate (0.1 mL) catalyst was added and the reaction progress was monitored by FTIR spectroscopy. To 6 mL (0.442 mmol) of the reaction mixture then cellulose acetate polymer (13.27 g, MW 30000, 0.442 mmol) dried overnight at 110°C, then dissolved in 1-methyl-2-(pyrrolidinone) was added and the reaction mixture was heated to 50°C.

2.2.7 Membrane Casting

Materials

Cellulose acetate (39.8 wt%, avg. m_n 30,000) was purchased from Sigma-Aldrich, and dried overnight at 110°C before use.

Aminopropylisobutyl polyhedral oligomeric silsesquioxane (POSS) was purchased from Hybrid plastics.

CA-POSS was synthesized using the method described in 2.2.6.

Method

Solutions were made by slowly adding cellulose acetate (25 wt %) to acetone (45 wt %, 11.5 mL) and formamide (30 wt %, 5.3 mL) with stirring [4]. If a nanofiller was used (POSS or CA-POSS), it was dissolved in the acetone prior to the addition of cellulose acetate and formamide. Due to the low solubility, the solutions were left covered, in the fridge overnight to allow complete dissolution.

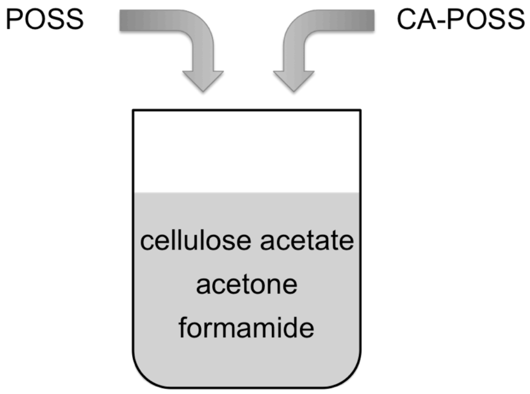

Figure 2.1. Casting solutions for cellulose acetate membranes with nanofiller.

A line of solution (approx. 1 cm thick) was poured onto a glass plate at room temperature, then drawn out into film with doctors blade set at a thickness of 0.25 mm, as shown in Figure 2.2. The membrane was allowed to air-dry for 90 seconds before the entire plate was immersed in a 0°C ice/water bath for 90 minutes. It was then immersed into a water bath at 90°C for 10 minutes.

Figure 2.2. Set up for membrane casting with doctor's blade and glass plate.

The membrane was stored in water until use in stirred-cell, or, if the membrane wa*s* being dried for characterisation, water was exchanged with iso-propanol, then n-hexane before drying [5].

2.3 Instrumental analysis and characterisation procedures

2.3.1 Delamination of CA from polyester backing

For some analytical techniques it was necessary to delaminate the cellulose acetate membrane layer from the polyester support layer. Delamination was achieved by simply peeling the CA away from the substrate using tweezers. In some cases where the delamination was difficult the polyester side was stuck to a bench-top surface with double sided tape to facilitate peeling.

2.3.2 Nuclear Magnetic Resonance (NMR)

Deuterated chloroform ($CDCl_3$) and deuterated water (D_2O) were obtained from Cambridge Isotope Laboratories and used without purification.

^{1}H data was recorded on a Bruker 400MHz using $CDCl_3$. The solvent peaks were used as an internal standard. For membranes, a piece approximately 0.5 cm x 0.5 cm was delaminated from the polyester backing before being dissolved in 1mL of $CDCl_3$. When checking for exchangeable protons in CAM-Br, the spectrum was acquired, then a drop of D_2O was added to the NMR sample tube and shaken, and the spectrum was re-run.

2.3.3 Fourier Transform InfraRed Analysis (FTIR)

Attenuated total reflectance (ATR) technique employed. Nicolet Nexus 8700 FT-IR Spectrophotometer (Thermo Electron Corporation) fitted with a ‘Smart Orbit’ ATR accessory containing a diamond crystal internal reflection element. Experimental parameters are outlined in Table 2.1. Membrane samples were placed active-face down on the ATR crystal, and held in place by a clamp. A background was run before each sample set. Automatic baseline correction and scale normalization were performed for each set of data.

Table 2.1. Summary of spectral collection parameters used in ATR-FTIR experiments.

Parameter	**Description**
Spectral Range	500-4000 cm^{-1}
Number of scans	64
Resolution	4 cm^{-1}
Detector	DTGS TEC
Beamsplitter	KBr
Mirror Velocity	0.6329 cm s^{-1}

2.3.4 X-ray PhotoSpectroscopy (XPS)

XPS measurements were performed with an ultrahigh vacuum instrument built by SPECS GmbH. The instrument is equipped with a source for metastable helium atoms and UV light, with a dual X-ray source for Al Kα and Mg Kα and with an ion source for rare gas ions with kinetic energy of 1 to 5 keV.

Samples were prepared by adhering a 1 cm x 1 cm piece to a sample stub with double sided tape. Stubs were then pumped down and stored in a desiccator over night prior to analysis. High-resolution XPS spectra were obtained to identify elements and their chemical state in the surface and near surface region of the samples.

Analysis was performed using Mg Kα X-rays (1253.6 eV) operating at 100W. The analyser is a SPECS Phoibos HSA3000, and the pass energy used for high resolution scans was 20 eV for Br 3d and 10 eV C 1s, with a 0.05 eV energy step, 200 ms dwell time for Br 3d and 100 ms dwell time for C 1s. Survey scans were collected with a pass energy of 40 eV and a 0.5 eV step, 100 ms dwell time.

2.3.5 ThermoGravimetric Analysis (TGA)

Data was collected using a TGA 2950 ThermoGravimetric Analyser from TA Instruments. Platinum pans with aluminium inserts were employed. Membranes were delaminated from their polyester backing to minimize the number of peaks and avoid peak overlap. Sample heated from room temperature to 600°C at a rate of 10°C/min under 50mL/min high purity N_2. The instrumental temperature calibration was performed using the Curie temperatures of nickel and alumel standard reference materials (TA Instruments). Data was analysed using TA Universal Analysis software.

2.3.6 Graft Density

To find the pHEMA graft density, the area of the membrane sample was measured with electronic calipers before analysis by TGA. The weight change of pristine CAM was subtracted from the weight change of CAM-g-pHEMA in the region of 275°C to 600°C, to give the mass per area of pHEMA.

2.3.7 Scanning Electron Microscopy (SEM) and Energy Dispersive X-ray Microanalysis (EDAX)

Samples were delaminated and mounted face-up onto SEM stubs with double-sided carbon tape. For morphology investigations, samples were snapped after immersion in liquid nitrogen, to obtain a sharp edge. Some samples were brittle enough to snap without first immersing in liquid nitrogen. After snapping, samples were mounted side-on by sandwiching between two brass plates before sputter coating. To reduce charging effects samples were sputter-coated with platinum (5.0 nm) using a Quorumtech K757X Sputter coater, using the film thickness monitor. Samples were imaged using either a FEI Phenom SEM with a 5kV accelerating voltage and a high sensitivity backscatter electron detector, or a Quanta450 SEM fitted with an SSD detector for x-ray detection. In this technique the electron beam was focussed onto a small part of the sample and the x-rays generated from the illuminated part of the sample were collected. When looking at different areaas on the membrane, the beam was focussed to a similar size. Elemental analysis was performed using Genesis software, and a comparison of the peak height for Si, relative to C was made.

2.3.8 Atomic Force Microscopy (AFM)

AFM samples were prepared by delaminating the cellulose acetate layer (CA and CAM) from the polyester backing, followed by attachment of square samples (approx. 1 cm^2) to an AFM stub with carbon tape. AFM images were obtained in tapping mode in air with a Multimode Atomic Force Microscope, equipped with a Nanoscope IV Scanning Probe, at ambient temperature. The surface roughness measurements (R_a - arithmetic mean roughness; R_q – root mean square) were calculated from the AFM images using the 5.31r1 software program.

2.3.9 Water Contact Angle (WCA)

WCA measurements were carried out in air with a water droplet (static sessile drop method), and analysed using ImageJ software. Delaminated membranes were attached face-up to a glass slide with double-sided tape and placed on a horizontal platform. A MilliQ water droplet was placed on the membrane surface and an image captured by camera. The internal angle of both sides of the water droplet was determined for at least 6 droplets per sample, and the mean value calculated.

2.3.10 Water Uptake Experiments

Water uptake was measured using a method described by Nagai *et al.* [6] Two 1 cm x 1 cm pieces of membrane per sample were weighed, and then immersed in demineralised water overnight. Samples were then removed from water, briefly pressed between filter paper to remove excess water and weighed within 5 seconds to reduce experimental error. The samples were returned to the water, and the process repeated until two weights were recorded within 1.0 mg. Water uptake was calculated as a percentage of the weight of the sample by the equation:

$$Water\ Uptake = \left(\frac{W_{wet} - W_{dry}}{W_{dry}} \right) x\ 100\% \qquad \text{Eq. 7}$$

Where W_{wet} is the mean weight of the wet membrane, and W_{dry} is the weight of the membrane before water soaking.

Water uptake was reported relative to the water uptake percentage of pristine CAM.

2.3.11 Stirred-Cell

Sodium chloride solution (2000 ppm) was made by dissolving 2.00g of NaCl in 2.00L of MilliQ water in a volumetric flask. A circular membrane disc approximately 5 cm in diameter was cut from the membrane. Analysis of the membrane water permeability and salt rejection were conducted using a Sterlitech HP4750 unit (shown in Figure 2.3, [7]) with magnetic stirrer under pressure (specific pressures are given in the relevant chapters).

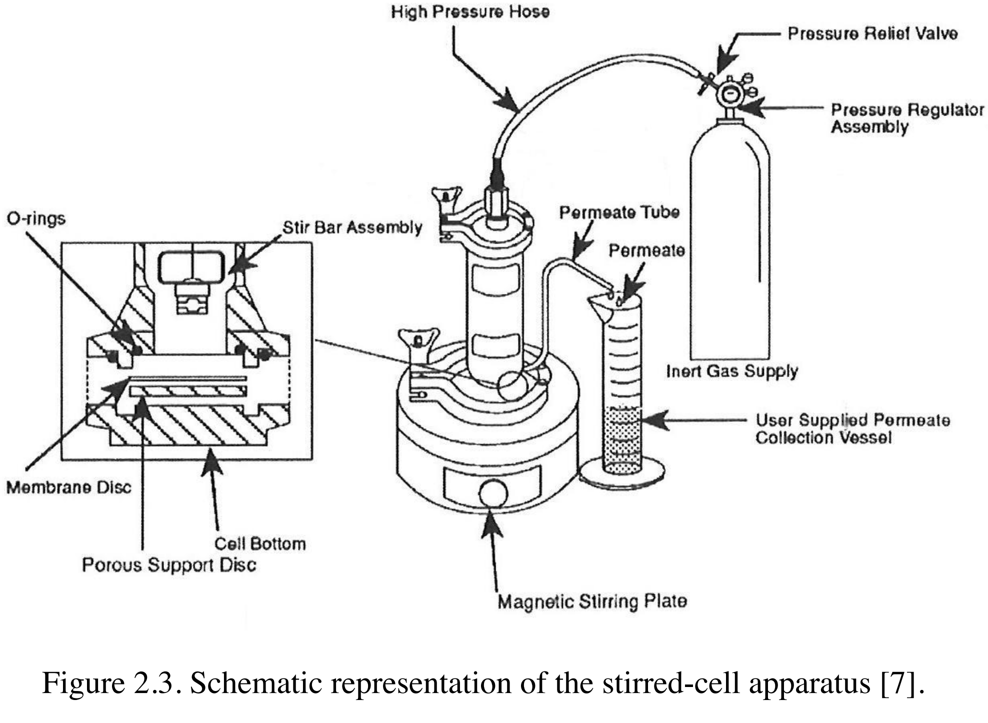

Figure 2.3. Schematic representation of the stirred-cell apparatus [7].

In this technique water was forced through the membrane under pressure perpendicular to the membrane surface. Water that passed through the membrane was collected via the permeate tube for measurements. Pure water tests were conducted with MilliQ water (resistivity = 18 MΩ cm) and salt rejection tests with 2000 ppm NaCl solution. Permeate was collected and weighed to determine flux. Conductivity of the feed solution, concentrate and permeate were measured and converted to concentration (mg/L) using the calibration curve prepared by Dr Lucas Johnson, shown in Figure 2.4.

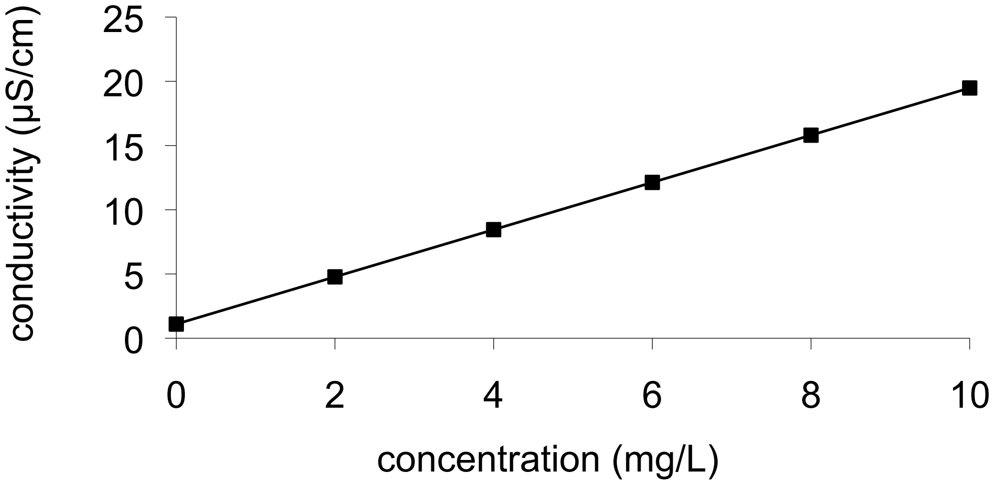

Figure 2.4. Calibration curve for the conversion of NaCl conductivity to concentration

Salt rejection was determined via the equation:

$$R = \left(1 - \frac{C_{permeate}}{C_{feed}}\right) x\ 100\% \qquad \text{Eq. 5}$$

Where Cperm is the permeate concentration and Cavg is the average of the concentrate and feed concentrations [8].

2.3.12 Dynamic Mechanical Analysis (DMA)

DMA was conducted using TA Instruments Q800 apparatus with a tension film clamp attachment (Figure 2.5, [9]) and operating in multifrequency – strain mode. In this technique the membrane was held between a fixed clamp and a moveable clamp at a designated preload force. A sinusoidal stress was applied and the modulus determined over the range of temperatures.

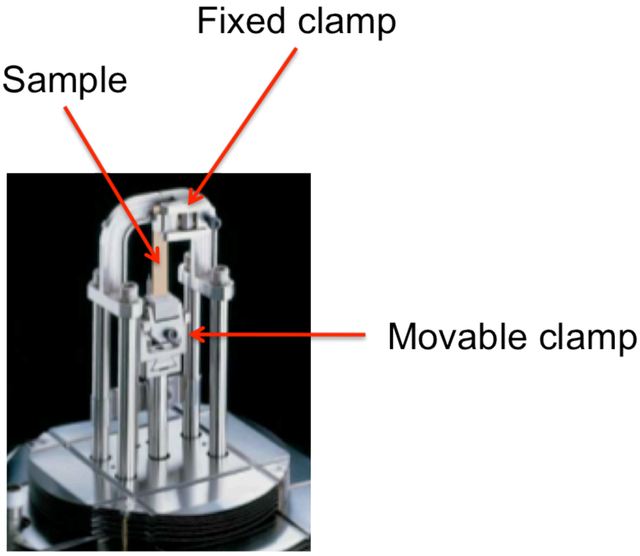

Figure 2.5. Tension film clamp for the DMA apparatus [9].

Samples were thouroughly air-dried prior to analysis. Sample size was measured with electronic calipers and was approximately 6 x10^{-3} m by 10 x10^{-3} m. Samples were equilibrated at -20 °C, then ramped to 220 °C at 2.00 °C/minute. Software analysis was performed using TA Universal Analysis software. Samples were tested in triplicate and selected results presented.

2.3.13 Static Aquarium Tests

Biofouling testing was carried out using natural seawater collected from the Gulf off the South Australian coast at the site of the city of Adelaide’s desalination plant. After pHEMA grafting each membrane was placed inside a plastic container with a screw-top lid that was previously perforated with 10-12 holes in the sides, this kept the membrane suspended and allowed for the flow of water through the container. The containers were then placed in the open-topped, natural seawater aquarium, which had a salinity of 20,000 ppm (temperature 16°C, pH 8.2) and water cycling at a flow rate of 360 L/hr. The aquarium was fitted with a seawater recirculation system attached to a biofilter and protein skimmer. Pristine CA membrane samples were also included as controls, and were treated the same way as the modified membranes. Samples were left in the aquarium for at least three weeks. A schematic representation of the seawater aquarium and cell fixing are shown in Figure 2.6.

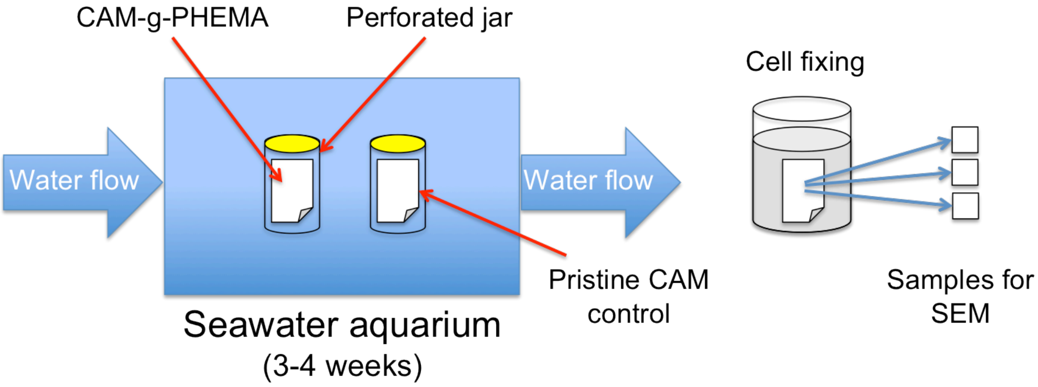

Figure 2.6. Schematic representation of the seawater aquarium setup and cell fixing.

2.3.13.1 Cell fixing

The method of cell-fixing was modified from Pieracci *et al*. [10] After removal from the aquarium, membranes were gently rinsed with phosphate buffered saline to remove any unbound organic matter. To fix the samples for SEM analysis, three replicate 1 cm x1 cm samples were cut from each membrane, and soaked overnight in a solution containing paraformaldehyde (4%) and glutaraldehyde (0.5%) in phosphate buffered saline (synthesis described in section 2.2.5). The next day samples were rinsed and soaked for at least 20 minutes in a series of solutions of ethanol in water (50%, 70%, 85%, 95% and 100%) sequentially to dry. The samples were then dried between filter paper overnight before preparation for SEM.

2.3.13.2 Cell counting

For biofouling tests, SEM images were taken at 1200x magnification (100 μm horizontal field width) at three random areas on the sample. Within each of these, three images were taken at 10000x magnification (10 μm horizontal field width) for the identification and counting of bacterial cells. Figure 2.7 shows a schematic of this regime.

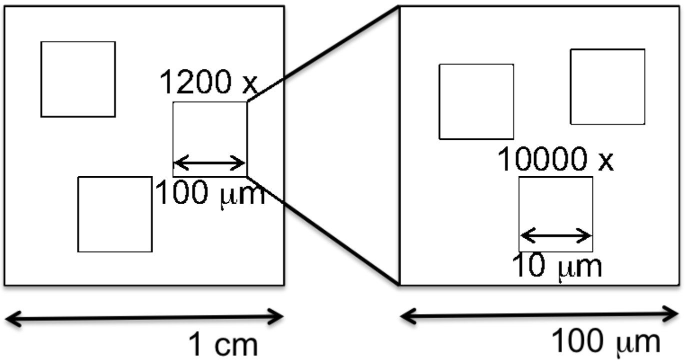

Figure 2.7. Schematic representation of the areas imaged for bacterial cell counting.

2.3.14 pH Resistance Tests

Materials

Citric acid, (99.5%), sodium phosphate (dibasic) (98.5%, Na_2HPO_4), and sodium carbonate (99.0%Na_2CO_3) were purchased from Sigma Aldrich.

Sodium bicarbonate (99.7%$NaHCO_3$) was purchased from Fluka.

Method (modified from Vos, [9] and Fujiwara [11, 12])

pH buffer solutions were made as shown in Table 2.2, and topped up to 200 mL with demineralised water. Modified or unmodified membranes (5 cm x 5 cm) were soaked for 24 hours in the buffer solutions. They were then rinsed thoroughly with demineralised water, and tested for performance using stirred-cell to determine which conditions had a detrimental effect on membrane performance. Results were compared to a control membrane which had not been soaked overnight.

Table 2.2. pH buffer solutions.

r.t. pH	vol. (L)	acid/base	c (mol/L)	mw (g/mol)	moles	mass (g)
2.2	0.1	citric acid	0.4	210.14	0.04	8.41
	0.1	Na_2HPO_4	0.075	141.96	0.0075	1.06
9.0	0.1	$NaHCO_3$	0.238	84.01	0.0238	2.00
	0.1	Na_2CO_3	0.1	124.00	0.01	1.24

2.3.15 Membrane Hydrolysis

A cleaned CA membrane was immersed in 0.5M NaOH and stirred at room temperature for 4 hours. After the reaction the membrane was washed thouroughly with demineralised water and stored dry.

2.4 Calculations

2.4.1 POSS Content of Nanocomposites

The calculations of the POSS content in the composite membranes were based on the concentration of hydroxyl groups (OH) in cellulose acetate. This was found from the acetyl content of the cellulose acetate as specified by the manufacturer and using the following equation [13]:

$$DS = 162 \times \%A / [4300 - (42 \times \%A)] \qquad \text{Eq. 8}$$

where: DS = degree of substitution,

$162 = M_{cellulose}$

%A = Acetyl content (39.8%)

$4300 = M_{acetyl\ group} \times 100$

$42 = M_{acetyl\ group - H}$

This calculation gives an average of 2.45 acetyl groups per ring, and therefore an average of 0.55 OH groups per ring.

Since the cellulose acetate average molecular weight was 30,000, there were approximately 113 repeat units per chain, and approximately 62 OH groups available for substitution by POSS. The purpose of modifying the cellulose acetate with POSS was to facilitate the dispersion of POSS in a CA membrane; therefore we did not wish to substitute all of the OH groups, since hydrogen-bonding interactions would facilitate dispersion. A POSS:OH ratio of 1:24 was chosen, to give an average of approximately 2.58 POSS molecules per cellulose acetate chain.

The cast membranes are named according to their wt% of POSS only. For example, CA-POSS 5wt% has 41.4 wt% CA-POSS additive, but since the ratio of POSS to CA was 2.58, the proportion made up by POSS was only 5wt%. Additive ratios were calculated to give either equivalent mol% or wt% of additive (whether CA-POSS or POSS). For example, CA-POSS 5wt% had 41.4 mol% POSS, this is comparable to POSS 1wt%, which had 34.30 mol% POSS.

Calculations of the mass, mol% and wt% of CA-POSS and POSS additives and CA are shown in Table 2.3.

Table 2.3. Calculations of the mass, mol% and wt% of CA-POSS and POSS additives and CA in cast membranes.

Additive	weight (g)	CA-POSS (mol%)	POSS (mol%)	CA-POSS (wt%)	POSS (wt%)	CA (g)
none	-	-	-	-	-	5.0000
CA-POSS	0.41	19.44	7.52	8.2	1	4.59
CA-POSS	2.07	98.16	37.97	41.4	5	2.93
CA-POSS	0.041	1.94	0.75	0.82	0.1	4.959
CA-POSS	0.207	9.82	3.80	4.14	0.5	4.793
POSS	0.05	-	34.30	-	1	4.95
POSS	0.25	-	171.51	-	5	4.75
POSS	0.005	-	3.43	-	0.1	4.995
POSS	0.025	-	17.15	-	0.5	4.975

2.4.2 Biofouling Resistance Calculations

SEM images were inspected visually, and a count was made of the number of bacteria cells per area. Only bacteria that were completely within the frame of the image were counted. The mean was calculated for a minimum of 27 images – three images for each of three areas on each of three replicate samples. The standard error of the mean was calculated by dividing the standard deviation of the mean by the square root of n.

2.4.3 Error Analysis

Error calculations were carried out using Microsoft Excel. Outliers were deemed to be greater than twice the standard deviation. The standard error of the mean was calculated using the formula:

=(STDEV(range))/(SQRT(COUNT(range)))

where STDEV is the standard deviation, and SQRT is square root.

References

1. Z. Tyeklar; R. Jacobson; N. Wei; N. Murthy; J. Zubieta; K. Karlin. Reversible Reaction of Dioxygen (and Carbon Monoxide) with a Copper(I) Complex. X-Ray Structures of Relevant Mononuclear Cu(I) Precursor Adducts and the Trans-(.Mu.-1,2-Peroxo)Dicopper(II) Product, Journal of the American Chemical Society 115 (1993) 2677-2689.
2. A. Carlmark; E. Malmstrom. Atom Transfer Radical Polymerisation from Cellulose Fibers at Ambient Temperature, Journal of the American Chemical Society 124 (2002) 900-901.
3. A. Carlmark ; E. Malmstrom. ATRP Grafting from Cellulose Fibres to Create Block Co-Polmer Grafts, Biomacromolecules 4 (2003) 1740-1745.
4. S. Manjikian; S. Loeb; J. McCutchan In *Improvement in Fabrication Techniques for Reverse Osmosis Desalination Membranes*, The First International Symposium on Water Desalination, 1965; US Dept. of Interior, Office of Saline Water (Washington DC): 1965; pp 159-173.
5. I. Pinnau, Membrane Separations | Membrane Preparation. In *Encyclopedia of Separation Science*, Wilson, I. D., Ed. Academic Press: Oxford, 2000; pp 1755-1764.
6. K. Nagai; S. Tanaka; Y. Hirata; T. Nakagawa; M.E. Arnold; B.D. Freeman; D. Leroux; D.E. Betts; J.M. DeSimone; F.a. DiGiano. Solubility and Diffusivity of Sodium Chloride in Phase-Separated Block Copolymers of Poly(2-Dimethylaminoethyl Methacrylate), Poly(1,1 0 - Dihydroperfluorooctyl Methacrylate) and Poly(1,1,2,2-Tetrahydroperfluorooctyl Acrylate), Polymer 42 (2001) 9941-9948.
7. Sterlitech TM HP4750 Stirred Cell Instruction Manual. Sterlitech TM: Vol. V.2-1.
8. C. Bartels; R. Franks; S. Rybar; M. Schierach; M. Wilf. The Effect of Feed Ionic Strength on Salt Passage through Reverse Osmosis Membranes, Desalination 184 (2005) 185-195.

9. TA Instruments Thermal Analysis DMA Q800. TA Instruments: 2010.
10. J. Pieracci; J. Crivello; G. Belfort. Photochemical Modification of 10 KDa Polyethersulfone Ultrafiltration Membranes for Reduction of Biofouling, Journal of Membrane Science 156 (1999) 223-240.
11. K. Vos; F. Burris; R. Riley. Kinetic Study of the Hydrolysis of Cellulose Acetate in the pH Range of 2-10, Journal of Applied Polymer Science 10 (1966) 825-832.
12. N. Fujiwara; H. Matsuyama. Optimization of the Intermittent Chlorine Injection (ICI) Method for Seawater Desalination RO Plants, Desalination 229 (2008) 231-244.
13. M. Elomaa; T. Asplund; P. Soininen; R. Laatikainen; S. Peltonen; S. Hyvarinen; A. Urtti. Determination of the Degree of Substitution of Acetylated Starch by Hydrolysis, 1H NMR and TGA/IR, Carbohydrate Polymers 57 (2004) 261-267.

3 Chapter Three

Synthesis of pHEMA-Modified Cellulose Acetate Membranes

Preface

To improve biofouling resistance, cellulose acetate reverse osmosis (RO) membranes (CAMs) were modified by reacting surface hydroxyl groups with an atom transfer radical polymerisation (ATRP) initiator, 2-bromoisobutyryl bromide, followed by polymeric grafting of 2-hydroxyethyl methacrylate (pHEMA) using ARGET (activators regenerated by electron transfer) ATRP. This chapter examines, in detail, the reactions involved in grafting pHEMA from the surface of CAMs. It includes discussions on the choices of polymerisation technique, solvent, catalyst and reducing agent. Several analytical techniques were employed to confirm initiator attachment to the surface, and polymer growth thereafter. Monomer volume and polymerisation reaction time were varied, and the relationships with the amount of polymer detected were investigated. The result of the work in this chapter was the synthesis of a series of modified membranes with varying polymer graft densities, suitable for testing as antifouling membranes.

Work presented in this chapter has been published in the Journal of Membrane Science, 385–386 (2011) 30–39.

3.1 Introduction

Asymmetric cellulose acetate membranes (CAMs) are commonly used in the reverse osmosis (RO) desalination of brackish waters. The advantage of using CAMs for this process is that they have favorable chemical and materials properties. CAMs are reproducible, biodegradable, biocompatible, and are relatively low cost because they derive from naturally occurring cellulose [1]. Furthermore, they are relatively stable and chlorine tolerant, they have a neutral surface charge, and due to available surface hydroxyl groups they can be readily derivatized [1]. The aim of this section was to modify CA RO membranes in order to impart them with biofouling resistance potential. As discussed in Chapter One, the desirable surface properties to inhibit biofouling are hydrophilicity, low surface roughness, and neutral charge. In the literature, modification with poly 2-hydroxyethyl methacrylate (pHEMA) has been used as a method of increasing hydrophilicity [2, 3].

The HEMA monomer (Figure 3.1) is charge-neutral and contains a pendant hydroxyl functional group that renders it hydrophilic. It is the formation of hydrogen bonds between this group and water molecules that creates the ability to resist biofouling via a tightly bound hydration layer [4]. Belfer *et al.* [5] propose that it is the energy involved in breaking these hydrogen bonds, as well as chain crowding effects, that keep large and hydrophobic molecules from approaching the membrane surface.

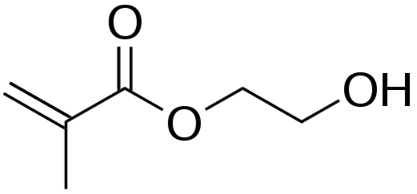

Figure 3.1. Structure of the 2-hydroxyethyl methacrylate monomer.

The surface roughness of the resulting polymer is affected by its polydispersity, and depends on the polymerisation technique employed. Atom Transfer Radical

Polymerisation (ATRP) is a living polymerisation technique that allows the covalent attachment of low polydispersity polymer chains to the membrane surface. ATRP was developed simultaneously in 1995 by Krzysztof Matyjaszewski and Mitsuo Sawamoto [6, 7]. In ATRP a transition metal complex such as copper in the lower oxidation state (complexed with a ligand) (Cu^I-X/Ligand) acts as a catalyst. An initiator (often a halide, R-X) with a transferable atom or group, undergoes a one electron redox reaction with the catalyst, forming the metal complex in the higher oxidation state with a coordinated halide ligand (Cu^{II}-X_2/Ligand) and a propagating radical (R*) at a rate of activation (k_a). The radical propagates with a rate (k_p), adding monomer (M), and is rapidly and reversibly deactivated (k_{da}) by reacting with the oxidized transition metal halide complex to reform the lower oxidation state transition metal catalyst. A schematic representation of ATRP is shown in Figure 3.2 [8]. Deactivation of a growing chain stops its activity until it is activated again, allowing it to propagate further, it does not terminate the chain. This allows the ATRP process to be described as 'living polymerisation'.

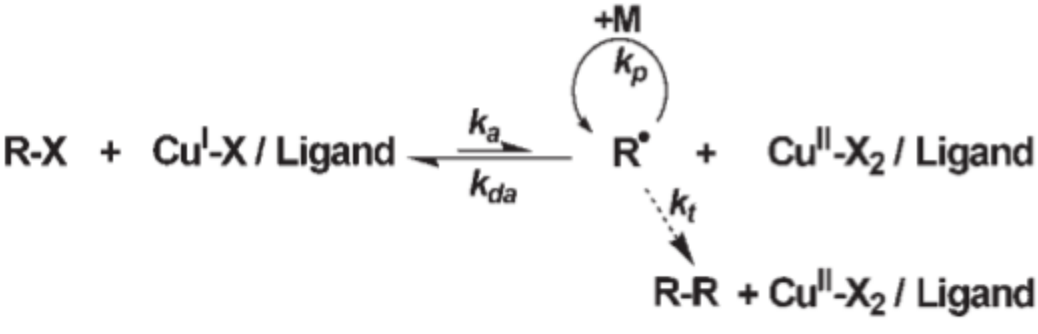

Figure 3.2. Proposed mechanism of ATRP [8].

Polymers with predetermined molecular weights can be synthesised by repeating this sequence until the desired level of monomer consumption is reached. ATRP is well suited for grafting from surfaces such as cellulose acetate since free hydroxyl groups at the substrate surface can be easily converted to ATRP initiators, and subsequently used to initiate the growth of polymer brushes [9]. Covalent surface attachment of a number of different monomers via ATRP has been achieved by several groups [9, 10]. In 2003, Carlmark and Malmström [9] first demonstrated the controlled growth of polymethacrylate/pHEMA brushes from cellulose filter paper by modifying hydroxyl groups on the surface with initaitor 2-bromoisobutyrl bromide and then performing ATRP. They also demonstrated the grafting of methacrylate and styrene onto several different cellulosic substrates in 2006 [11]. Singh *et al.* [12] modified the surface of a cellulose ultrafiltration membrane with polyethylene glycol methacrylate (PEGMA) using the same initiating system, giving control over membrane pore size. Recently, Lindqvist *et al.* [10] created pH and temperature responsive cellulose surfaces via surface-initiated ATRP of *N*-isopropylacrylamide and 4-vinylpyridine. However, the disadvantage of using ATRP in a manufacturing process is that it requires inert conditions and a large amount of copper catalyst, which is difficult to remove from the final product [13].

In this study it was desirable to use a polymerisation technique that would be more suited to the manufacturing environment. The Activators ReGenerated by Electron Transfer (ARGET) ATRP polymerisation technique, developed in 2006 by the Matyjaszewski group [13], was selected for this work because it has many advantages over the traditional ATRP technique.

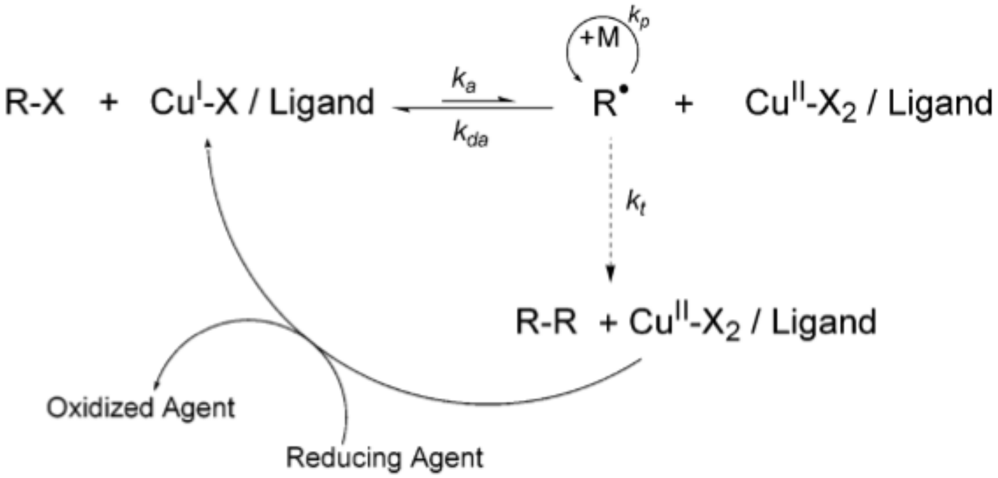

Figure 3.3. Proposed mechanism of ARGET ATRP [14].

In ARGET ATRP (Figure 3.3) [14] an excess of reducing agent is employed to continuously regenerate Cu(I) (the activator) *in situ* from Cu(II) generated during termination. Hence, with ARGET ATRP only a very small amount of copper catalyst (typically ppm) is required for the reaction; oxidatively stable Cu(II) can be used to regenerate Cu(I), which simplifies the experimental procedure; and importantly, the reaction can be carried out in the presence of limited amounts of air because the reducing agent also acts to scavenge oxygen from the reaction vessel. Other radical polymerisation processes must be carried out in deoxygenated systems because oxygen in the system can react with radicals and cause chain termination. In ARGET ATRP, the reducing agent preferentially reacts with oxygen before reacting with Cu(II). This tolerance to the presence of oxygen means that ARGET ATRP can be applied to grafting from large surfaces that are difficult to place in deoxygenated systems, and also gives rise to an induction period during oxygen consumption before polymerisation is initiated.

In 2009, Hansson *et al*. demonstrated the use of ARGET ATRP to modify cellulose with styrene, polymethyl methacrylate (PMMA) and polyglycidyl methacrylate (PGMA) [15]. Thus demonstrating the value of ARGET ATRP as a method for membrane modification.

In this study, a pHEMA coating was polymerized from the CAM surface by first reacting the CA hydroxyl groups with an ATRP initiator, 2-bromoisobutyryl bromide (BiBBr), followed by the polymeric growth of pHEMA using ARGET ATRP. Reaction conditions were varied in order to achieve membranes with a range of graft densities, suitable for biofouling resistance tests.

3.2 Results and discussion

Commercially available Sepa CF CA (Cellulose Acetate) RO CE Membranes are asymmetric CA coated on a polyester support layer substrate. They are typically used for RO of brackish water.

Prior to chemical reactions, it was necessary to clean the membrane in order to achieve a fresh cellulose acetate surface. This was evident from the TGA curve of the as-received membrane (Figure 3.4), which showed a degradation step between 300 and 400 °C, representing the cellulose acetate itself, as well as a weight loss event between 75 °C and 200 °C, and one at 500 °C to 550 °C, these two presumably representing some chemical added by the manufacturer in order to protect the pristine membrane until use. Since this additive is an unknown chemical and may affect the surface chemistry of the membranes, it was desirable to remove it before membrane modification. Pristine membranes were either soaked in water overnight, or sonicated in diethyl ether for 10 minutes, before being dried and analysed by TGA.

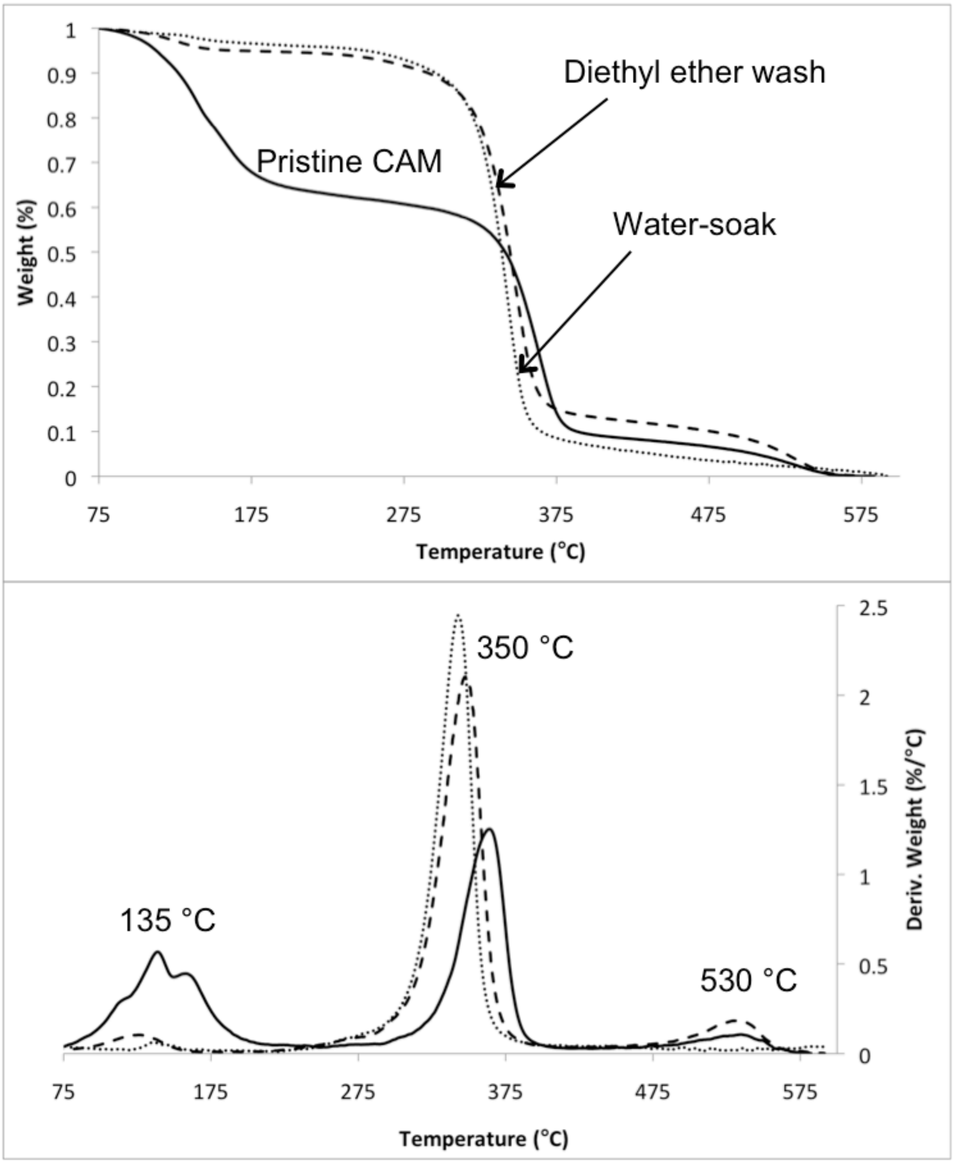

Figure 3.4. TGA and DTG curve overlays of pristine CAM, and CAM cleaned with water or diethyl ether.

Both cleaning methods reduced the size of the additive peaks relative to the cellulose acetate peak (Figure 3.4). In the case of the water soak the high temperature weight loss is no longer present and the low temperature weight loss has been reduced to a small peak around 100 °C, which is likely the loss of water.

Therefore, in subsequent experiments, "pristine CAM" refers to an as-received membrane that has been soaked in water overnight.

3.2.1 Synthesis of bromo-initiator modified CA membranes

The surface-initiated ARGET ATRP from the CAM was performed by a two-step process as shown in Figure 3.5 (modified from Carlmark and Malmstrom [16]).

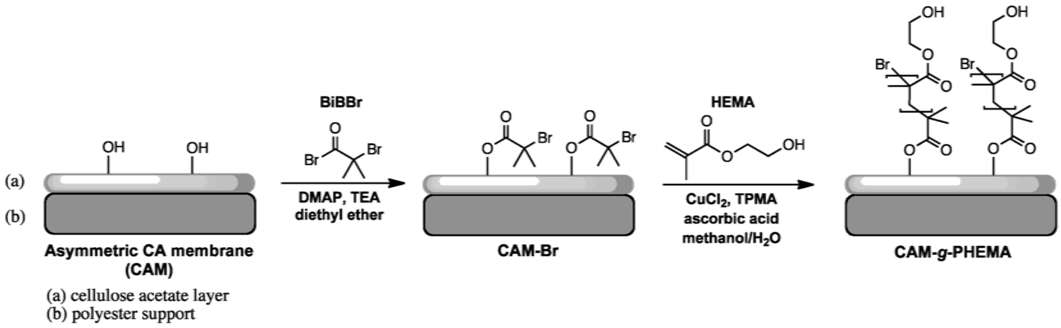

Figure 3.5. Reaction scheme for surface modification of CAM.

The first step in the membrane modification was the conversion of CAM hydroxyl groups to initiator. Membranes pieces were cut into 5 cm x 5 cm squares and positioned following the curve of the 25mL glass reaction vial, such that the active face of the membrane faced in toward the solution, but the membrane was out of the path of the magnetic stirrer. Several solvents were investigated, however dimethyl formamide (DMF), chloroform, acetone and tetrahydrofuran (THF) all had a disastrous effect on the membrane, dissolving the CA or delaminating it from the polyester substrate. Only diethyl ether, methanol, ethanol and water were found to be suitable solvents that did not damage the membranes.

For the initiation reaction, known ATRP initiator bromoisobutyryl bromide (BiBBr) was allowed to react with the hydroxyl groups of the CAM in the presence of DMAP and TEA in diethyl ether at 0 ºC, and then stirred at room temperature for 3 hours. It is well known that the CAMs need to be kept between pH 4 and 8 to avoid hydrolysis. The TEA is necessary to neutralize the HBr generated by the reaction of BiBBr with the OH groups of the cellulose acetate, and avoid low pH conditions. However, when TEA and BiBBr were added sequentially, the pH of the solution was measured to be between 8.5 and 9.0. This exceeds the manufacturer's recommended "safe" pH range. Therefore, TEA and BiBBr were injected simultaneously, resulting in a pH of 5.5, and avoiding extreme pH conditions. Membranes were washed thoroughly before analysis to remove excess salt and reactants.

3.2.1.1 ATR-FTIR Analysis

ATR-FTIR measurements were performed to characterise the surfaces of pristine CAM and CAM-Br. Figure 3.6 shows their corresponding absorbance spectra. In the FTIR spectrum of pristine CAM characteristic cellulosic peaks can be seen (-OH stretching at 3484cm^{-1}, asymmetric and symmetric C-H stretching at 2944cm^{-1} and 2886cm^{-1} respectively, C=O stretching at 1730cm^{-1}, carboxylate C-O stretch at 1215cm^{-1}, asymmetric stretching of the C-O-C bridge at 1161cm^{-1}, and stretching of pyranose ring C-O-C at 1028cm^{-1}) [17].

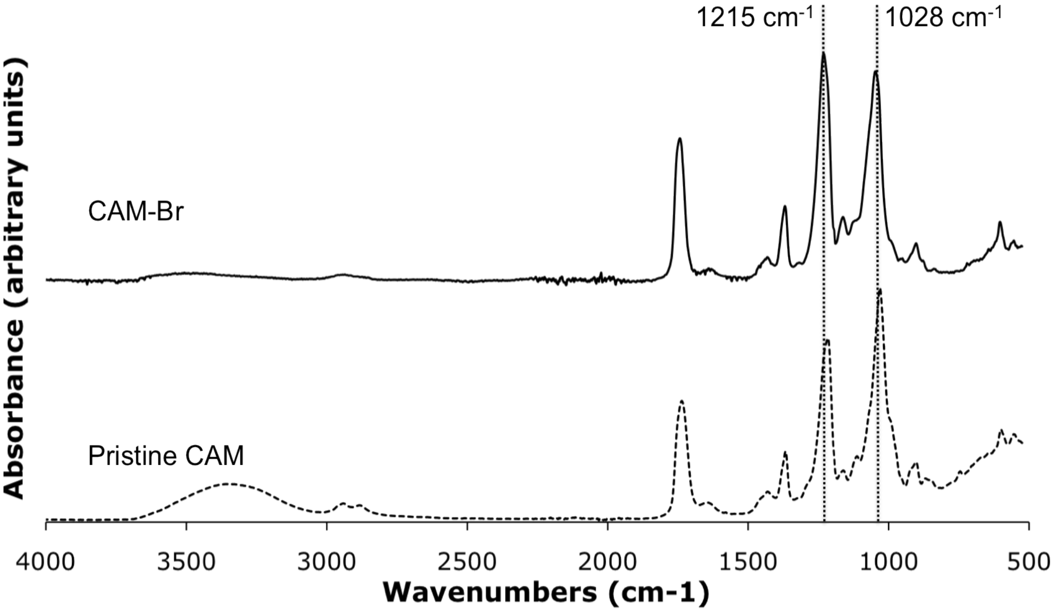

Figure 3.6. ATR-FTIR comparing the carboxylate (1215 cm^{-1}) to pyranose ring (1028 cm^{-1}) peak ratios for CAM-Br and pristine CAM.

Characteristic peaks in the spectra of CAM-Br are almost unchanged when compared to pristine CAM. However, the broad peak at 3484 cm^{-1} associated with the hydroxyl groups in pristine CAM, disappears almost completely. In addition, the CAM-Br spectrum shows an increase in carboxylate C-O stretch at 1215cm^{-1} relative to the C-O-C pyranose ring stretch at 1028cm^{-1} (Figure 3.6). This corresponds to the conversion of surface -OH groups to carbonyl groups of the newly formed bromoesters, confirming the covalent attachment of the initiator. Shen and Huang [18] attached BiBBr to cellulose diacetate in solution, before grafting with poly(methyl methacrylate) (PMMA). They also noted a decline in the -OH stretch upon initiator attachment.

Table 3.1. The ratio of carboxylate to pyranose ring FTIR peak intensities with increasing initiator attachment reaction time until 60 minutes, after which no further increase is observed.

Reaction Time (minutes)	Peak Ratio 1215/1028
0	0.79
5	1.07
10	1.07
30	1.06
60	1.16
120	1.15
210	1.17
360	1.11

In addition, FTIR was used to follow the progress of the reaction by recording the ratio of the carboxylate peak (1215cm^{-1}) height to the pyranose peak (1028cm^{-1}) height (Table 3.1) with respect to time. The ratio of peaks changes rapidly then tails off after a period of initiator modification time longer than 60 minutes, indicating that the reaction occurs in a short amount of time and then the amount of initiator on the membrane surface plateaus. Carlmark and Malmstrom [9] used the same initiating system on cellulose fibres for the ATRP of poly methacrylate (PMA). Contrary to current results, they were unable to detect initiator using FTIR, and attributed this to the very thin nature of the bromo-ester layer. Therefore, they used XPS to assess the bromo content of the initiator-modified cellulose and reported no increase in the amount of initiator after 6 hours reaction time. In the case of cellulose acetate, which has fewer OH groups for substitution with the initiator, the threshold appears to occur at even lower reaction times. Three hours was judged to be more than sufficient for the reaction to reach equilibrium.

3.2.1.2 ^{1}H NMR Analysis

To further confirm the attachment of BiBBr to the membrane surface, ^{1}H NMR was performed. Figure 3.7 displays the spectra for CAM-Br in $CDCl_3$. The peaks in the chemical shift region (d) = 3.5−5.1 ppm are due to the methylene and hydrogen protons on the cellulose backbone, while the methyl protons in the acetyl groups appeared at d = 1.9-2.2 ppm. The peak at d = 1.67 ppm is not present in the ^{1}H NMR spectrum of pristine CAM. Shen and Huang [18] assigned this peak to the methyl protons in the ester group ($-(CH_3)_2Br$) confirming the substitution of the hydroxyl groups on the CAM with 2-bromoisobutyryl groups. However, the broadness of the peak suggests that it may in fact be due to an exchangeable proton, as in an –OH group. If this were the case, the peak should disappear on the addition of D_2O. In fact the peak only diminished, suggesting overlap of the two peaks, and rendering the ^{1}H NMR inconclusive in determining the covalent attachment of BiBBr.

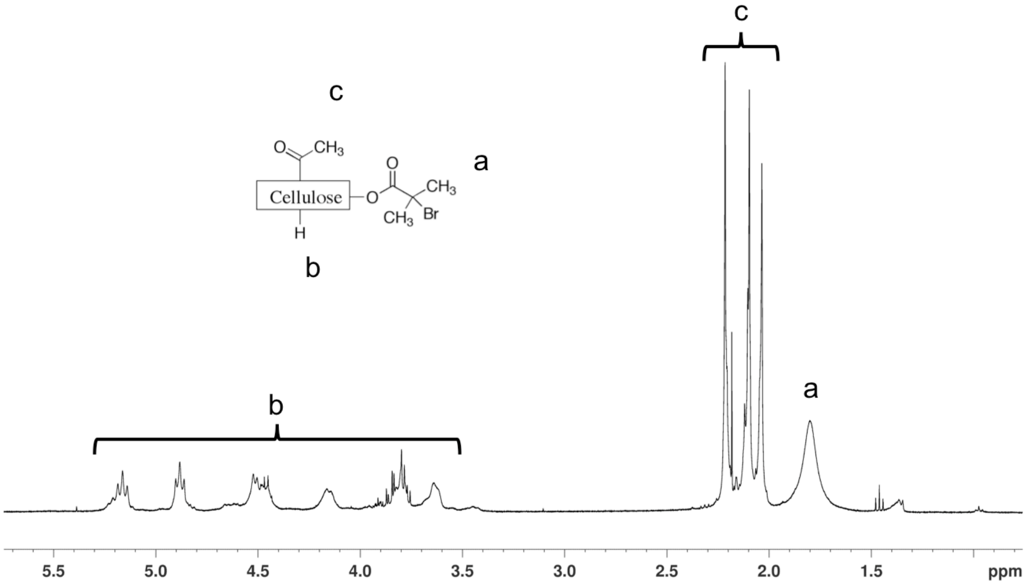

Figure 3.7. ^{1}H-NMR of CAM-Br.

3.2.1.3 XPS Analysis

Another technique which is commonly used to demonstrate the attachment of the bromo-initiator is XPS [19-21], which shows the absence of Br on pristine CAM prior to modification, and the presence on CAM-Br.

Figure 3.8 shows the survey spectrum of CAM-Br. Peaks can be seen at 529 eV corresponding to the oxygen 1s peak, and at 285 eV corresponding to the carbon 1s peak. A very small peak is just visible at 70 eV corresponding to the bromine 3d peak. The presence of this peak is confirmed by a high-resolution scan in the bromine 3d region, as shown in the inset of Figure 3.8. This shows that bromine (and hence the bromo-initiator) is present in CAM-Br.

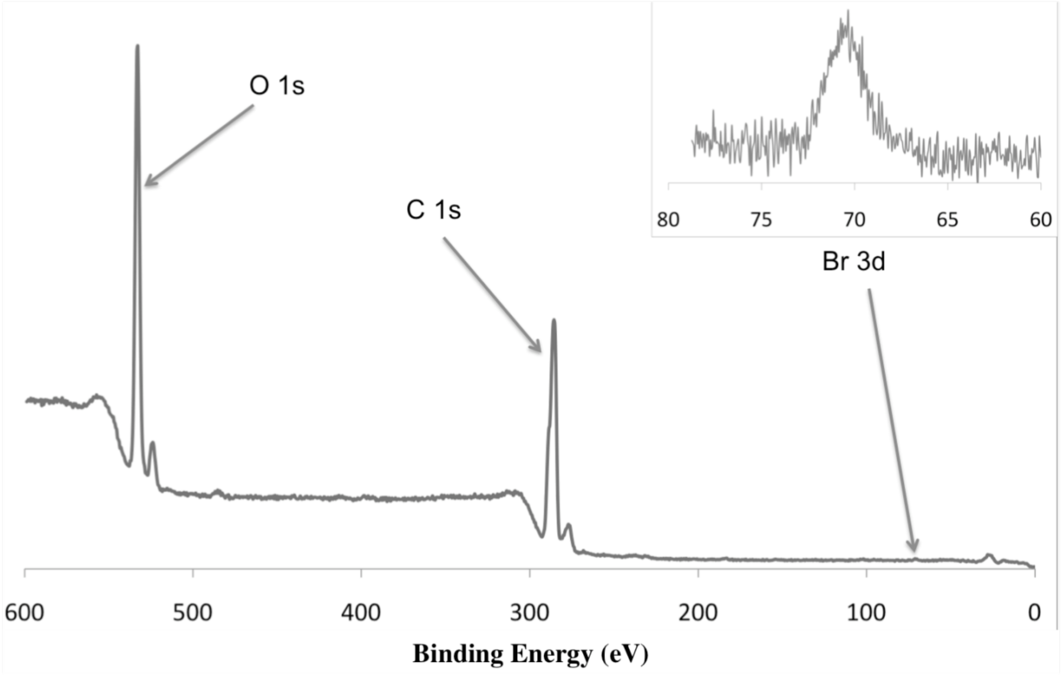

Figure 3.8. XPS survey spectrum of CAM-Br, with inset showing high resolution Br3d scan.

Table 3.2. Elemental surface composition of CAM and CAM-Br from XPS.

Sample	Element (atom %)			
	C (total)	O	Br	C (O=C-O)
CAM	68.42	31.58	0.00	22.7
CAM-Br	68.45	31.29	0.26	24.7

Table 3.2 shows the elemental surface composition of CAM and CAM-Br. After the initiation reaction there is 0.26% bromine present. This is lower than the 0.82% measured by Liu *et al*. [21] when attaching BiBBr to a cellulose surface, however this is to be expected because some of the –OH groups present in cellulose have been substituted by acetate groups in cellulose acetate, meaning that there are fewer sites for BiBBr attachment. It is also possible that some initiator attachment has occurred at a depth greater than 10 nm, beyond the detection of XPS.

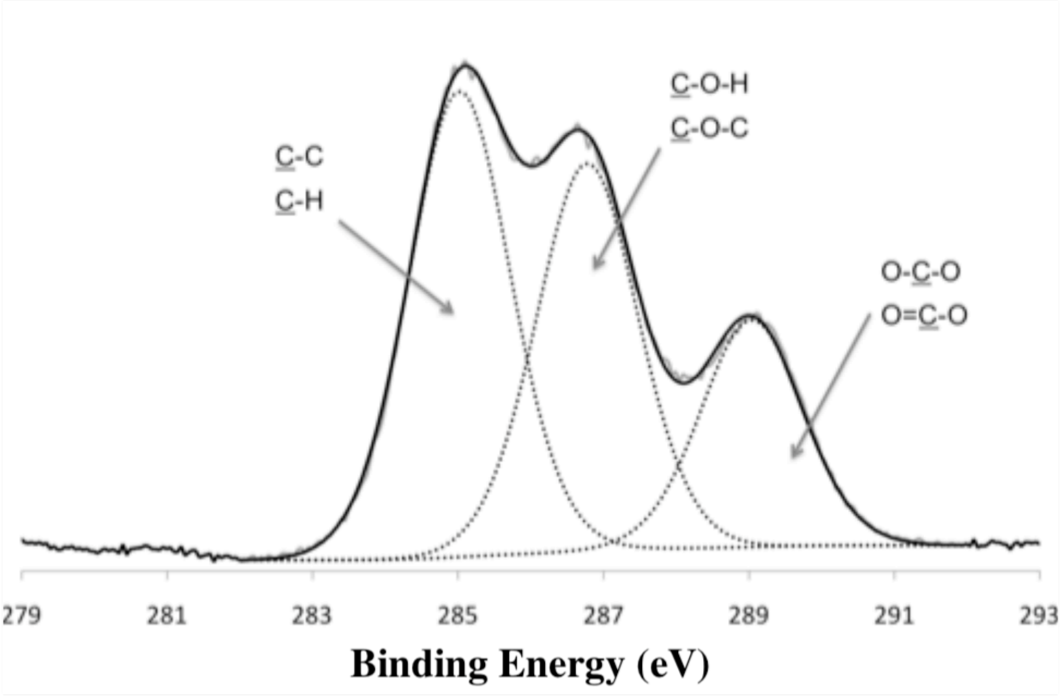

Figure 3.9. High resolution C1s scan of CAM-Br

A high-resolution scan in the C1s region was performed in an attempt to prove that the initiator was covalently attached to the CAM surface. Curve-fitting was used to resolve the spectrum, shown in Figure 3.9, into three peaks with binding energies of 284.6, 286.3 and 288.6 eV attributed to $\underline{C}$-H/$\underline{C}$-C, $\underline{C}$-O-H/$\underline{C}$-O-C and O-$\underline{C}$-O/O=$\underline{C}$-O respectively [22]. The presence of the O=C-O peak at 288.6 eV was previously used as proof of covalent attachment of BiBBr to a cellulose surface [21], however, since the O=C-O linkage is also present in cellulose acetate, in this case only the atom % increase in the O=C-O peak can be used. As shown in Table 3.2, an increase of 2% (from 22.7% to 24.7%) after initiator grafting indicates the initiator is indeed covalently bound to the CAM surface via an ester linkage.

All evidence of initiator attachment is, of course, best supported by successful growth of polymers from the membrane.

3.2.2 Polymer Grafting

The second step in the two-step reaction was the growth of the pHEMA chains from the initiation sites on CAM-Br. Polymer grafting was carried out under ARGET ATRP conditions in the presence of TPMA as the ligand, ascorbic acid as the reducing agent, and copper chloride as the catalyst.

Paterson *et al.* [23] have recently reported the bulk polymerisation of pHEMA via ARGET ATRP. However, their focus was on producing low molecular weight, water-soluble pHEMA for use as a degradable scaffold material in tissue engineering. Their best results were obtained using hydrazine as the reducing agent, and methanol as the solvent, as both provide greater control and hence lower molecular weight polymers.

However, an important consideration for this project is attractiveness as an industrial process. To this end, a relatively simple, quick, and environmentally friendly process is sought. ARGET ATRP was chosen because it employs only small amounts of copper catalyst.

ATRP of HEMA is typically carried out in water or aqueous methanol (50 vol %). Water has been found to have an accelerating effect on the reaction, leading to high yields and high molecular weight in under one hour [24]. It has also been found that performing the reaction in methanol or aqueous methanol gives better control over the reaction, and that the reaction is markedly slower in methanol than in aqueous methanol [25]. These observations have been attributed to the unusually high activity of the Cu(I) catalyst in water. In this study, the polymerisation was carried out at room temperature in aqueous methanol (50 vol %) because the use of less methanol is industrially and environmentally more desirable.

Another reason ARGET ATRP is industrially attractive is that the system can tolerate small amounts of oxygen. Although the reaction is carried out under nitrogen, rigorous deoxygenation is not necessary. Since the reducing agent (ascorbic acid) is used in excess it is able to first scavenge any oxygen present in the system (i.e. an induction period), and only once the residual oxygen is consumed can the reducing agent go on to reduce the Cu(II) to Cu(I) and initiate polymerisation.

Another advantage of using ARGET ATRP, and one that differentiates this approach from other antifouling coatings which are just physisorbed to the surface, is that the coating is covalently attached to the surface of the membrane, and therefore should be stable for the lifetime of the membrane.

TPMA was chosen as the ligand because it has been shown to be superior in terms of temperature and pH stability to other common ligands Me6TREN and PMDETA [13]. Also for environmental reasons, ascorbic acid (vitamin C) was chosen as the reducing agent. Although hydrazine has been shown to give greater control for the ARGET ATRP of HEMA [23], ascorbic acid is less environmentally harmful, and the faster polymerisation achieved is more industrially attractive. Hansson *et al.* [15] reported that the stronger reducing agent, ascorbic acid, did not give rise to an induction period. Furthermore, a thorough washing regime including sonication in several solvents means that any unreacted chemicals are readily removed.

A sacrificial initiator is often used as a way to control the polymerisation reaction by lowering the initial monomer-to-initiator ratio and increasing the overall initiator concentration, thereby allowing some radical coupling in solution to build up the concentration of deactivator [26] since ATRP relies on a dynamic equilibrium between active and dormant species. Another reason for the use of sacrificial initiator is for the purpose of analysis of the polymer molecular weight and polydispersity, which can be difficult for bound polymer [27]. One must assume that bulk polymerisation occurs at the same rate as surface polymersation, indeed good conformity is suggested in the literature [28].

However, in this case it was found that the polymer formed in the bulk was attaching to the membrane surface, even when no bromo-initiator was present. While solutions without EBiB were clear for the duration of the reaction, solutions with EBiB were cloudy and membranes were often sticky. Therefore it was decided to discontinue use of the sacrificial initiator. As a consequence the system contained a low concentration of initiator, which was manifested as a large jump in the amount of polymer at short polymerisation reaction times (PRTs) [28].

Polymerisation reactions were initially carried out with constant initial monomer concentration (IMC) of 2.06 molL^{-1}, but varying (PRTs) of 30 minutes, and 1, 3 and 6 hours. As will be explained in the following pages, this was later revised to 15, 30, 45 and 60 minutes. Also, a second series of reactions was carried out with constant PRT of 30 minutes, but varying the IMC to 0.52, 1.03, 1.55 and 2.58 molL^{-1}, corresponding to initial monomer volumes (IMV) of 1, 2, 3 and 5 mL. The aim of this was to investigate the livingness of the system, as well as to create a series of membranes with different amounts of polyHEMA coverage, in order to be able to study the effect on membrane properties such and biofouling and filtration properties.

3.2.2.1 Thermal Analysis

Thermogravimetric Analysis was performed in order to determine the proportion of pHEMA on membranes that had been polymerized for different amounts of time.

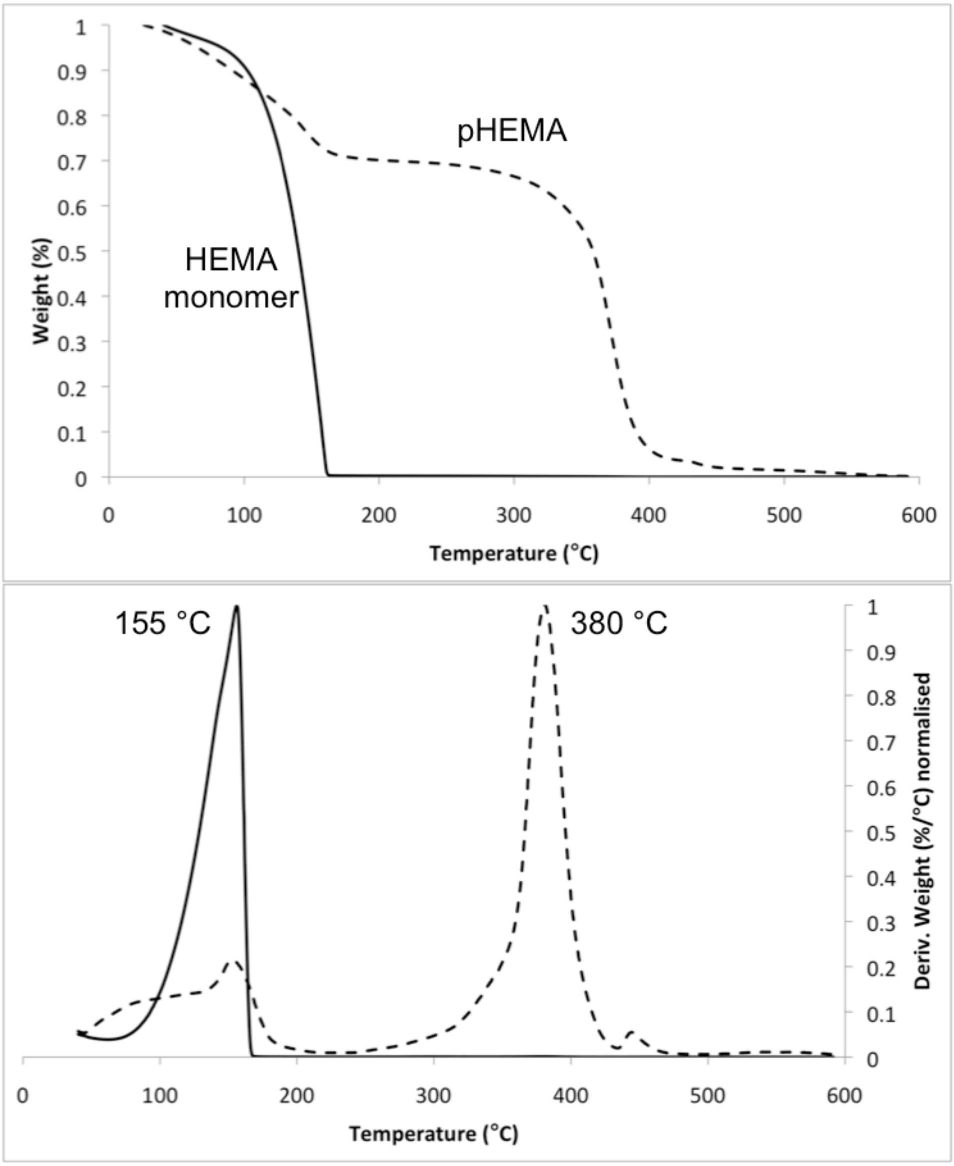

Figure 3.10. TGA and DTG curve overlays of the HEMA monomer and homopolymer.

Figure 3.10 depicts TGA and DTG (first derivative) thermograms (under nitrogen atmosphere) of the HEMA monomer and homopolymer. Over the temperature range of room temperature to 600 °C, the HEMA monomer fully decomposed exhibiting one weight loss peaking around 155 °C. The pHEMA homopolymer showed two degradation steps, the mass loss below 200 °C is the loss of solvents and residual monomer, whereas the polymer itself fully degrades between 250 and 450 °C.

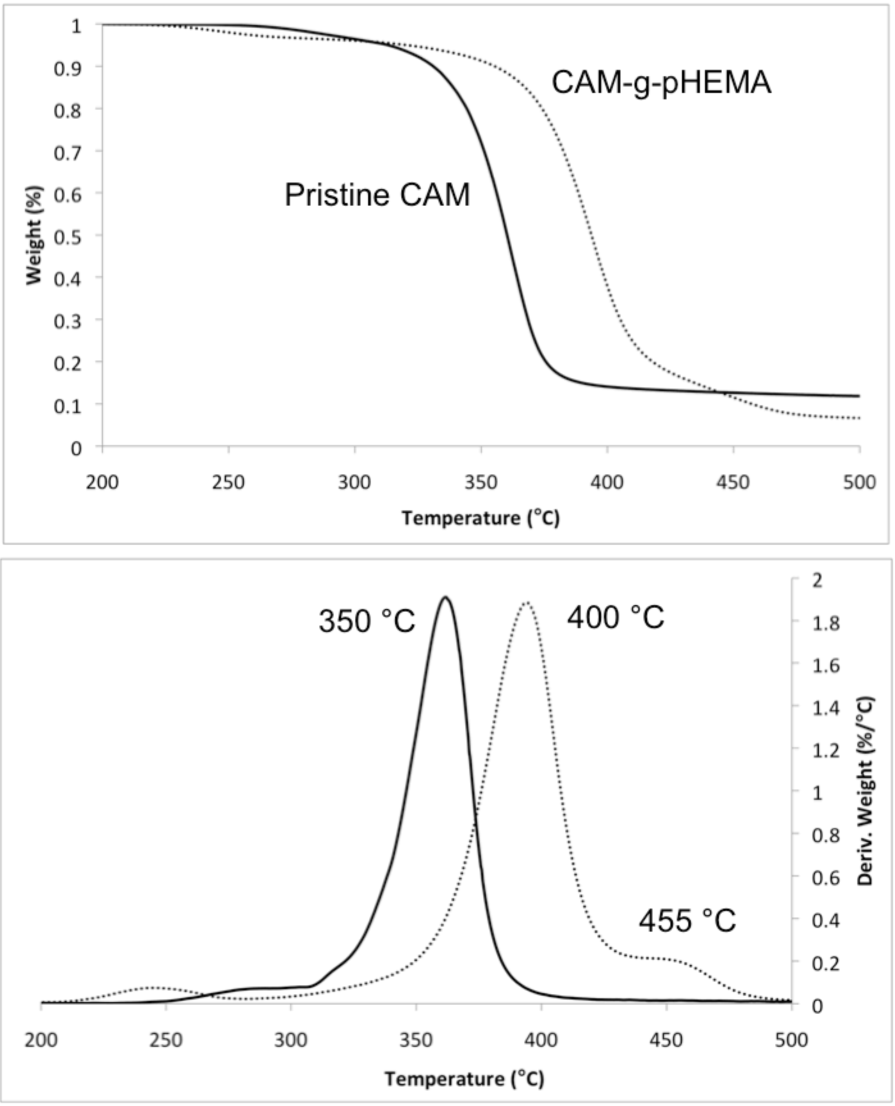

Figure 3.11. TGA and DTG curve overlays of pristine CAM and CAM-g-pHEMA.

Figure 3.11 shows the TGA and DTG thermograms of pristine delaminated CAM and delaminated CAM-g-PHEMA, PRT 30 minutes. Pristine CAM degrades in a single step between 300 and 400 °C. In comparison, the CAM-g-PHEMA sample displayed a three-step degradation with the first weight loss of around 240 °C (4 wt%); some researchers [29] have attributed this peak to bound water, however, others suggest that volatiles have all been removed before 200°C. This has not been investigated further in the current study. The second weight loss from 350 to 425 °C (80 wt%) represents the degradation of CAM, and the third weight loss, from 425 to 475 °C (8 wt%) represents covalently attached pHEMA. The shift in the DTG cellulose acetate peak maximum from approximately 350 °C for pristine CAM to approximately 400 °C for CAM-g-pHEMA represents significantly improved thermal (oxidative) stability of the composite, and reflects the conversion of secondary OH groups to esters in the membrane.

Figure 3.12 shows an overlay of TGA and DTG curves for membranes that had been polymerized for 30 minutes, 1, 3 and 6 hours. With increasing PRT there is an increase in the mass loss at ~420 °C, corresponding to an increase in pHEMA coverage of the membrane surface. The weight percentages of pHEMA are 6, 21, 41 and 67%, respectively.

At PRTs greater than 3 hours (i.e. when the percentage of pHEMA rises above 50%) the membranes are swollen, delaminated and wrinkled in appearance. It is well known that pHEMA is a hydrogel, and therefore swells in water. The polyester backing, however, does not swell in water and this causes membranes with a high amount of pHEMA to buckle and delaminate from the backing.

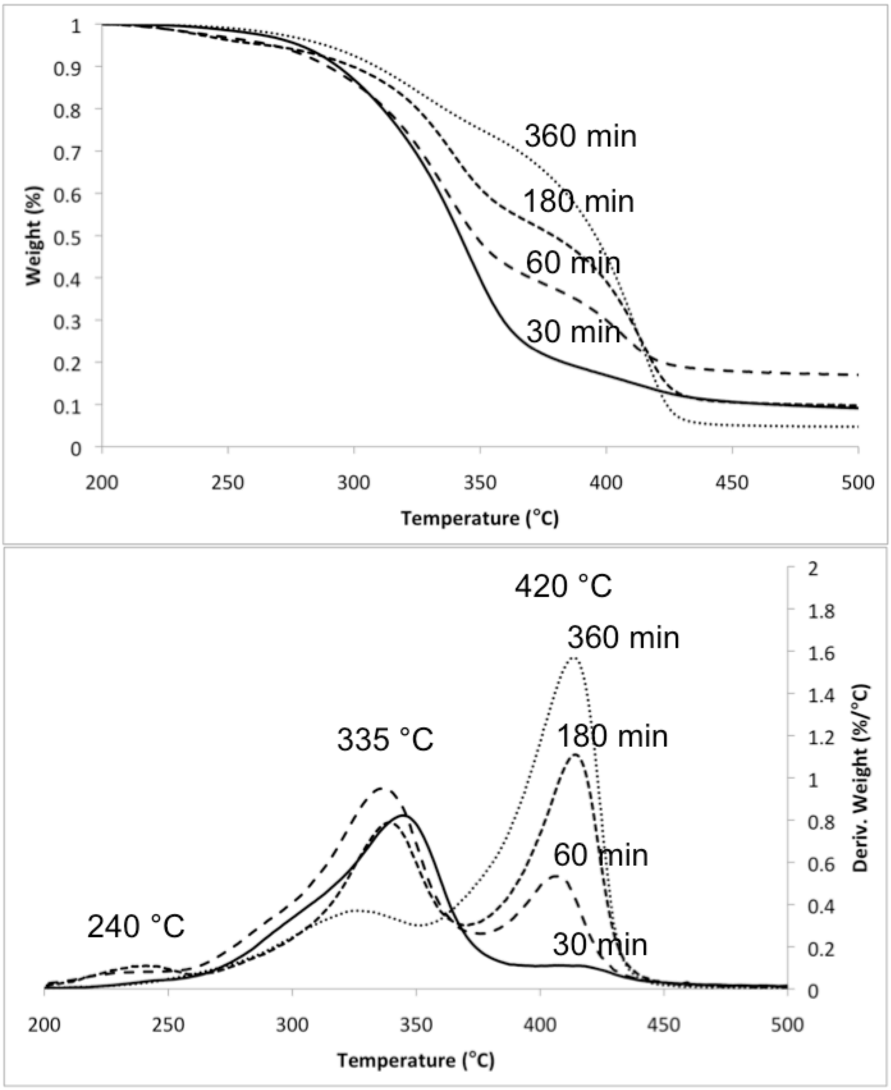

Figure 3.12. TGA and DTG curve overlay of membranes with varying PRTs. The increasing peak at approximately 420 °C corresponds to increasing pHEMA on the membrane surface with increasing reaction time.

Since the aim of this research is to create a desalination membrane, the desired polymer coating must be thin enough to allow the passage of water. Therefore, the shorter PRTs of 15, 30, 45 and 60 minutes, resulting in polymer weight percentages lower than 20%, were used for further tests.

3.2.2.2 Reaction Kinetics

In order to investigate the livingness of the reaction when varying PRT, a series of membranes were modified by keeping the IMC and initiator-modification time constant at 2.58 molL^{-1} and 3 hours, respectively, and varying the PRT between 15 and 60 minutes. The modified membranes were characterized by TGA, the mass change after polymer grafting was taken from the results, and ln([M_0]/[M]) was calculated.

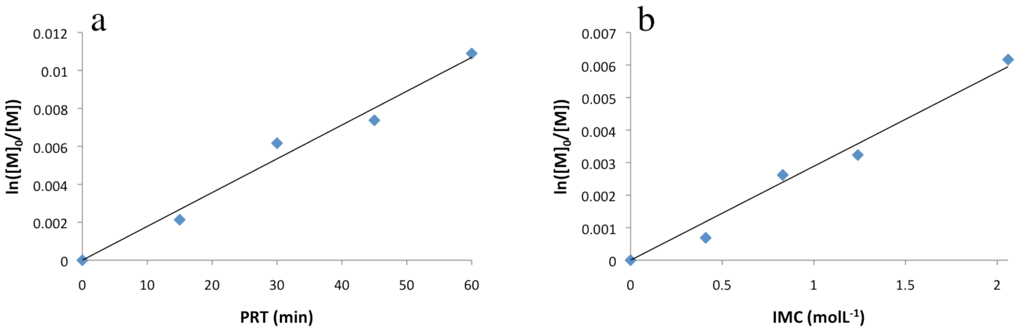

Figure 3.13. Kinetic plot for the ARGET ATRP of HEMA with (a) varying PRT, and (b) varying IMC.

Figure 3.13 (a) shows the kinetic plot over the range of PRTs. The straight-line relationship between PRT and ln([M]$_0$/[M] indicates a controlled polymerisation with first order kinetics over this time range. It is interesting to note that the polymerisation is controlled despite the absence of sacrificial initiator in the system. It is generally accepted that the addition of either sacrificial initiator, or deactivator is required in order to avoid rapid polymerisation and termination due to the concentration of deactivator being too low to trap propagating radicals [9, 30]**.** At the short PRTs employed the so-called "persistent radical effect" is not observed.

Note also that polymer is detected by TGA even at low PRT. This indicates that the induction time caused by the reducing agent first scavenging any oxygen present in the system before reducing the Cu(II) to Cu(I) and activating the reaction is very short. This agrees with the results of Hansson *et al.* [15] who saw no induction period when using ascorbic acid as the reducing agent for the ARGET ATRP of PMMA and PGMA.

Since 2.58 $molL^{-1}$ is a large excess of monomer, and a thin, even polymer coating is desired, lower IMCs of 0.52, 1.03, 1.55 $molL^{-1}$ were also investigated, while keeping PRT constant at 30 minutes. A first order, living polymerisation was also observed when varying the IMC with constant PRT, as evidenced by the straight line relationship between $\ln([M]_0/[M]$ and IMC (Figure 3.13 (b)).

3.2.2.3 Graft Density

Graft density is a measure of surface coverage in terms of polymer mass per area. It was calculated by subtracting the TGA weight loss of pristine CAM from the weight loss of CAM-g-pHEMA in the region of 275 °C to 600 °C, for a membrane of known area.

Figure 3.14 shows the combined range of graft densities observed for the CAM-g-pHEMA membranes created by varying the PRT and the IMC. Graft density increases with increasing PRT and IMC, as predicted from the reaction kinetics. It ranges from 0.15 $\mu g/cm^2$ for 30 minutes PRT and 0.52 $molL^{-1}$ IMC, to 2.33 $\mu g/cm^2$ for 60 minutes PRT and 2.58 $molL^{-1}$ IMC.

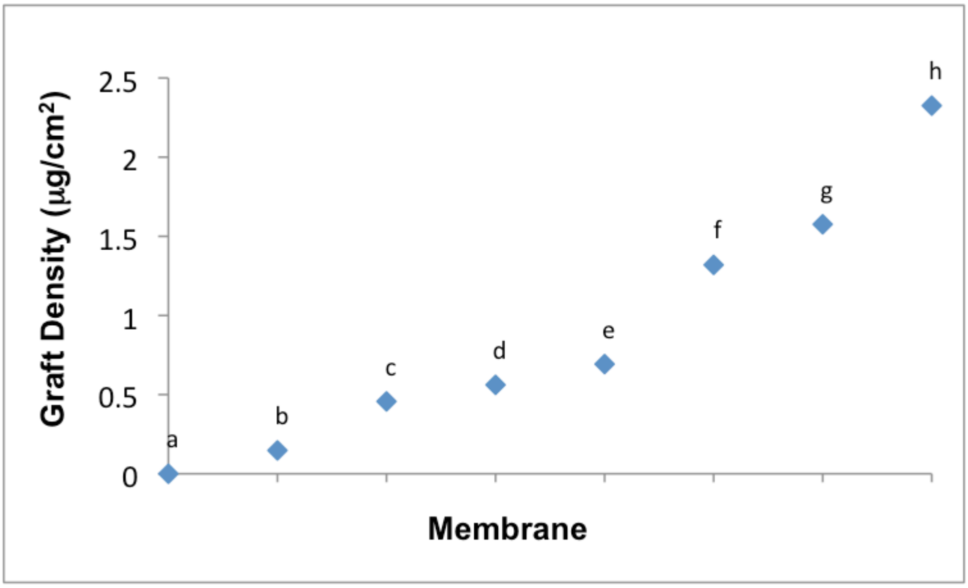

Figure 3.14. Graft density for all CAM-g-pHEMA. Pristine CAM is shown at zero graft density (membrane a).

Graft densities of between 0 and 5 μg/cm^2 were previously reported for surface-grafted poly(methacrylic acid) via UV-induced free-radical graft polymerisation [31], and for pHEMA grafted to nylon via ATRP [32].

Hereafter, CAM-g-pHEMA data will be presented in order of graft density, with membranes labeled (x) PRT(min) IMV(mL), as presented in Table 3.3:

Table 3.3. Key for pristine CAM and CAM-g-pHEMA membrane labels and reaction conditions.

Membrane	**Graft Density (μg/cm^2)**	**PRT (min)**	**IMV (mL)**	**IMC (molL^{-1})**
(a) pristine CAM	0	0	0	0
(b) PRT30IMV1	0.15	30	1	0.52
(c) PRT15IMV5	0.46	15	5	2.58
(d) PRT30IMV2	0.56	30	2	1.03
(e) PRT30IMV3	0.69	30	3	1.55
(f) PRT30IMV5	1.17	30	5	2.58
(g) PRT45IMV5	1.35	45	5	2.58
(h) PRT60IMV5	2.33	60	5	2.58

3.2.2.4 ATR-FTIR Analysis

Figure 3.15 shows the absorbance spectra of (a) pristine CAM, CAM-g-PHEMA with increasing graft density ((d) PRT30IMV2, (e) PRT30IMV3, (f) PRT30IMV5 and (h) PRT60IMV5), and pHEMA in the range of 800 to 1500 cm^{-1}. Some membrane spectra are omitted for clarity. Not shown within the range of the FTIR spectrum presented are characteristic pHEMA peaks at 3378 cm^{-1} (-OH stretching), 2994 cm^{-1} and 2952 cm^{-1} (asymmetric and symmetric C-H stretching). Other characteristic pHEMA peaks at 1278 cm^{-1} (C-O stretch), asymmetric and symmetric stretching of the C-O-C bridge at 1161cm^{-1} and 1072 cm^{-1} can be clearly seen.

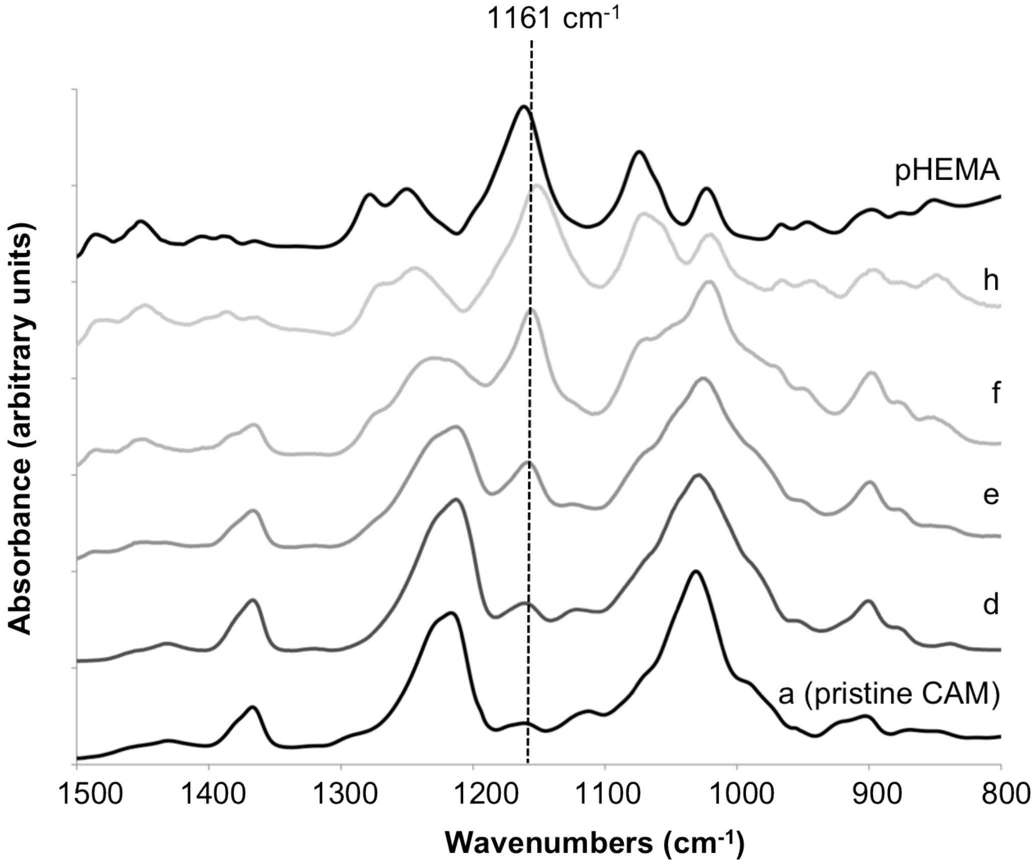

Figure 3.15. ATR-FTIR in the range 800-1500 cm-1 for pristine CAM, CAM-g-pHEMA with increasing graft density, and pHEMA.

After polymerisation, the ATR-FTIR of CAM-g-PHEMA (d) PRT30IMV2 retains much of the character of pristine CAM. However, several peaks are also evident which are due to pHEMA on the membrane surface, and CAM-g-pHEMA ((e) PRT30IMV3, (f) PRT30IMV5, and (h) PRT60IMV5) resemble pHEMA even more closely. For example, the asymmetric stretch of the C-O-C bridge at 1161 cm^{-1} is very weak in pristine CAM, in CAM-g-PHEMA (h) this peak is the strongest peak, resembling that seen for pHEMA. Also, in the region of the C-O stretch (1230-1280 cm^{-1}), the modified membranes show characteristics of both spectra, with a large peak at 1215cm^{-1}, contributed by pristine CAM, and a peak at 1278cm^{-1} contributed by pHEMA. Assignments of some important bands are shown in Table 3.4. The close resemblance of the spectrum of CAM-g-pHEMA (h) PRT60IMV5 to pHEMA, suggests that the graft layer is approaching the penetration depth of ATR-FTIR.

Table 3.4. Spectral band assignments comparing pristine CAM, CAM-g-pHEMA and pHEMA.

Peak Assignment	Pristine CAM	CAM-g-pHEMA	pHEMA
ν (OH)	3484 cm^{-1}	3354 cm^{-1}	3378 cm^{-1}
ν $(CH)_a$, ν (CH)	2944, 2886 cm^{-1}	2994, 2946, 2884 cm^{-1}	2994, 2952 cm^{-1}
ν (C-O)	1215 cm^{-1}	1215, 1278 cm^{-1}	1278 cm^{-1}
ν $(C\text{-}O\text{-}C)_a$, bridge	1161 cm^{-1}	1161 cm^{-1}	1161 cm^{-1}
ν (C-O-C), bridge	-	1074 cm^{-1}	1072 cm^{-1}
ν (C-O-C), ring	1028 cm^{-1}	1026 cm^{-1}	-
γ (-C-O-)	-	747 cm^{-1}	748 cm^{-1}

The ATR-FTIR results are consistent with graft density data presented above (i.e. higher graft density corresponds to higher peak intensity at characteristic wavenumbers for pHEMA).

3.3 Conclusion

A detailed study of the two-step modification of CA membrane surfaces with pHEMA has been undertaken. In the first step, the membrane OH groups were substituted with known ATRP initiator BiBBr, as confirmed by FTIR, XPS and NMR. TEA and BiBBr needed to be injected simultaneously to maintain pH, and reaction times beyond 3 hours gave no further product.

In the second part of the reaction pHEMA chains were successfully grafted from the surface of commercially available cellulose acetate reverse osmosis membranes using surface-initiated ARGET ATRP. The polymerisation conditions were designed to create an industrially attractive process, by using ppm levels of copper catalyst, half the amount of methanol solvent, and environmentally friendly reducing agent ascorbic acid. Sacrificial initiator was not employed since it lead to excess polymer adhering to the membrane surface, even in the absence of initiator. A new TGA DTG peak was observed at 410 °C for modified membranes, corresponding to pHEMA degradation. Reaction kinetics and FTIR confirmed the livingness of the reaction, showing increasing polymer graft density with increasing reaction times and monomer concentration. This was the first time pHEMA had been grafted from cellulose acetate using ARGET ATRP.

The outcome of this body of work was the synthesis of a series of membranes with different graft densities, ranging from 0 to 2.33 $\mu g/cm^2$, and suitable for testing for properties including hydrophilicity, surface roughness and biofouling resistance. The properties of the modified membranes are presented in Chapter Four, along with their separation performance.

References

1. X.-S. Fan; Z.-T. Liu; Z.-W. Liu; J. Lu. Cellulose Acetate Membrane Synthesis from Biomass of Ramie, Journal of Applied Polymer Science 117 (2010) 588-595.
2. J. Koehler; M. Ulbricht; G. Belfort. Intermolecular Forces between a Protein and a Hydrophilic Modified Polysulfone Film with Relevance to Filtration, Langmuir 16 (2000) 10419-10427.
3. H. Yamagishi; J. Crivello; G. Belfort. Evalutation of Photochemically Modified Poly(Arylsulfone) Ultrafiltration Membranes, Journal of Membrane Science 105 (1995) 249-259.
4. C. Zhao; L. Li; Q. Wand; Q. Yu; J. Zheng. Effect of Film Thickness on the Anitfouling Performance of Poly(Hydroxy-Functional Methacrylates) Grafted Surfaces, Langmuir 27 (2011) 4906-4913.
5. S. Belfer; R. Fainshtain; Y. Purison; J. Gilron; M. Nystrom; M. Manttari. Modification of Nf Membrane Properties by in Situ Redox Initiated Graft Polymerisation with Hydrophilic Monomers, Journal of Membrane Science 239 (2004) 55-64.
6. J. Wang; K. Matyjaszewski. Controlled/"Living" Radical Polymerisation. Atom Transfer Radical Polymerisation in the Presence of Transition Metal Complexes, Journal of the American Chemical Society 117 (1995) 5614-5615.
7. M. Kato; T. Ando; M. Kamigato; M. Sawamoto; T. Higashimura. Polymerisation of Methyl Methacrylate with the Carbon Tetrachloride/ Dichlorotris (Triphenylphosphine) Ruthenium(II) / Methylaluminum Bis(2,6-Di-Tert-Butylphenoxide) Initiating System: Possibility of Living Radical Polymerisation, Macromolecules 28 (1995) 1721-1723.

8. W. Jakubowski; B. Kirci-Denizli; R. Gil; K. Matyjaszewski. Polystyrene with Improved Chain-End Functionality and Higher Molecular Weight by ARGET ATRP, Macromolecular Chemistry and Physics 209 (2008) 32-39.
9. A. Carlmark ; E. Malmstrom. ATRP Grafting from Cellulose Fibres to Create Block Co-Polmer Grafts, Biomacromolecules 4 (2003) 1740-1745.
10. J. Lindqvist; D. Nystrom; E. Ostmark; P. Antoni; A. Carlmark ; M. Johansson; A. Hult; E. Malmstrom. Intelligent Dual-Responsive Cellulose Surfaces via Surface-Initiated ATRP, Biomacromolecules 9 (2008) 2139-2145.
11. J. Lindqvist; E. Malmstrom. Surface Modification of Natural Substrates B Atom Transfer Radical Polymerisation, Journal of Applied Polymer Science 100 (2006) 4155-4162.
12. N. Singh; Z. Chen; N. Tower; S. Wichramasinghe; N. Soice. Modification of Regenerated Cellulose Ultrafiltration Membranes by Surface Initiated Atom Transfer Radical Polymerisation, Journal of Membrane Science (2008)
13. K. Matyjaszewski; W. Jakubowski; K. Min; W. Tang; J. Huang; W. Braunaker; N. Tsarevsky. Diminishing Catalyst Concentration in Atom Transfer Radical Polymerisation with Reducing Agents, PNAS 103 (2006) 15309-15314.
14. W. Jakubowski; K. Min; K. Matyjaszewski. Activators Regenerated by Electron Transfer for Atom Transfer Radical Polymerisation of Styrene, Macromolecules 39 (2006) 39-45.
15. S. Hansson; E. Ostmark; A. Carlmark; E. Malmstrom. ARGET ATRP for Versatile Grafting of Cellulose Using Various Monomers, Applied Materials and Interfaces 1 (2009) 2651-2659.
16. A. Carlmark; E. Malmstrom. Atom Transfer Radical Polymerisation from Cellulose Fibers at Ambient Temperature, Journal of the American Chemical Society 124 (2002) 900-901.

17. H. Gulec; A. Topacli; C. Topacli; N. Albayrak; M. Mutlu. Modification of Cellulose Acetate Membrane via Low-Pressure Plasma Polymerisation for Sugar Separation Applications: Part I. Membrane Development and Characterisation, Journal of Membrane Science 350 (2010) 310-321.
18. D. Shen; Y. Huang. The Synthesis of CDA-g-PMMA Copolymers through Atom Transfer Radical Polymerisation, Polymer 45 (2004) 7091-7097.
19. Z. Zhang; S. Chen; Y. Chang; S. Jiang. Surface Grafted Sulfobetaine Polymers Via Atom Transfer Radical Polymerisation as Superlow Fouling Coatings, The Journal Of Physical Chemistry B 110 (2006) 10799-10804.
20. C. Huang; C.-Y. Tsai; R.-S. Juang; H.-C. Kao. Tailoring Surface Properties of Cellulose Acetate Membranes by Low-Pressure Plasma Processing, Journal of Applied Polymer Science 118 (2010) 3227-3235.
21. P.-S. Liu; Q. Chen; S.-S. Wu; J. Shen; S.-C. Lin. Surface Modification of Cellulose Membranes with Zwitterionic Polymers for Resistance to Protein Adsorption and Platelet Adhesion, Jounal of Membrane Science 350 (2010) 387-394.
22. U. Rodrigues-Filho; Y. Gushikem; M. Carmo Goncalves; R. Cachichi. Composite Membranes of Cellulose Acetate and Zirconium Dioxide: Preparation and Study of Physicochemical Characteristics, Chem. Mater. 8 (1996) 1375-1379.
23. S. Paterson; D. Brown; T. Chirila; I. Keen; A. Whittaker; M. Baker. The Synthesis of Water-Soluble Phema Via ARGET ATRP in Protic Media, Journal of Polymer Science: PartA: Polymer Chemistry 48 (2010) 4084-4092.
24. X.-S. Wang; S. Armes. Facile Atom Transfer Radical Polymerisation of Methoxy-Capped Oligo(Ethylene Glycol) Methacrylate in Aqueous Media at Ambient Temperature, Macromolecules 33 (2000) 6640-6647.

25. K. Robinson; M. Khan; M. de Paz Banez; X. Wang; S. Armes. Controlled Polymerisation of 2-Hydroxyethyl Methacrylate by ATRP at Ambient Temperature, Macromolecules 34 (2001) 3155-3158.
26. T. Fukuda; Y. Tsujii; K. Ohno. Grafting and Polymer Brushes on Solid Surfaces, Macromolecular Engineering 2 (2007) 1137-1178.
27. S. Hansson; E. Ostmark; A. Carlmark; E. Malmstrom. ARGET ATRP for Versatile Grafting of Cellulose Using Various Monomers, Applied Materials and Interfaces 1 (2009) 2651-2659.
28. T. von Werne; T. Pattern. Atom Transfer Radical Polymerisation from Nanoparticles: A Tool for the Preparation of Well-Defined Hybrid Nanostructures and for Understanding the Chemistry of Controlled/“Living” Radical Polymerisations from Surfaces, Journal of the American Chemical Society 123 (2001) 7497-7505.
29. R. Jeyanthi; K. Pandugranga. Collagen-Poly(Hema) Hydrogels for the Controlled Release of Anticancer Drugs—Preparation and Characterization, Journal of Bioactive and Compatible Polymers 5 (1990) 194-211.
30. J. Pyun; T. Kowalewski; K. Matyjaszewski. Synthesis of Polymer Brushes Using Atom Transfer Radical Polymerisation, Macromolecules Rapid Communications 24 (2003) 1043-1059.
31. E. Uchida; H. Iwata; Y. Ikada. Surface Structure of Poly(Ethylene Terephthalate) Film Grafted with Poly(Methacrylic Acid), Polmyer 41 (2000) 3609-3614.
32. F. Xu; J. Zha; E. Kang; K. Neoh; J. Li. Functionalization of Nyoln Membranes Via Surface-Initiated Atom-Transfer Radical Polymerisation, Langmuir 23 (2007) 8585-8592.

4 Chapter Four

The Performance and Biofouling Resistance of pHEMA-Modified Cellulose Acetate Membranes

Preface

This chapter describes the characterisation of a series of poly(2-hydroxyethyl methacrylate) (pHEMA)-modified cellulose acetate membranes (CAMs). pHEMA-CAMs were prepared to elucidate their potential as low-biofouling CAM RO membrane coating layers. Scanning electon microscopy (SEM), atomic force microscopy (AFM) and water contact angle (WCA) measurements of pristine and modified membranes were performed to measure and compare the amount of polymer deposited, the surface morphology and the hydrophilicity of the surfaces, respectively. Relationships between morphology and wettability were explored. The biofouling resistance of pHEMA-modified membranes immersed in seawater aquarium tanks was compared to pristine membranes. Based on aquaria experiments, the results showed a greater resistance to seawater microbial biofouling for pHEMA-modified CAMs with respect to pristine CAMs. Modified membranes were tested using stirred-cell to determine salt rejection and water flux values. The results revealed the optimum graft density in order to maximize biofouling resistance, whilst maintaining filtration properties relative to pristine CAM.

Some work presented in this chapter has been published in the Journal of Membrane Science, 385–386 (2011) 30–39.

4.1 Introduction

Asymmetric cellulose acetate membranes (CAMs) are commonly used in the reverse osmosis (RO) desalination of brackish waters (see Chapter One for indepth discussion). CAMs are prone to hydrolysis and have very tight pH operating requirements (between pH 4 and pH 8). However, the cellulose acetate membrane, which has largely been replaced by thin-film polyamide membrane, still seems to offer the best fouling resistance. Studies suggest that the single most important factor in preventing mineral fouling as well as fouling caused by colloidal particles is the membrane surface morphology [1]. The CAMs combination of smooth surface morphology, neutral charge and chlorine tolerance make them well-suited for high-fouling applications. However, as with all membranes, the application of CAMs is restricted to some extent due to the adsorption and subsequent growth of microorganisams at the membrane surface, a phenomenon known as biofouling [2].

In general the productivity of RO membranes during operation will be reduced due to fouling, and continued fouling conditions will lead to the decrease in the salt rejection properties of the membrane. In the initial stages of biofouling, proteins and microorganisms are attached to the membrane surface via weak physicochemical interactions [2] including hydrophobic and/or electrostatic interactions, hydrogen bonding and van der Waal's interactions [3]. Therefore it is of interest to produce membrane surfaces that minimise these interactions by surface modification of CAMs with low-fouling coatings. Such surface modification usually alters the surface chemical composition and morphology, surface topography and roughness, the hydrophilic/hydrophobic balance, as well as the surface energy and polarity.

Suitable polymeric coating materials with reduced bacterial affinity should be hydrophilic, charge-neutral, have a stable surface hydration [4-6], and be able to form coatings with a low surface roughness [2, 3]. Kochkodan *et al.* [2] compared membranes coated with hydrophilic monomers with basic, acidic and neutral properties. They showed that hydrophilicity and roughness were important for resisting fouling and that a neutral surface charge enabled higher ability to recover performance upon washing.

Chapter 3 described the surface-initiated pHEMA coating on CAMs. Briefly, 2-hydroxyethyl methacrylate (HEMA) was polymerized from the CAM surface by reacting hydroxyl groups with the ATRP initiator 2-bromoisobutyryl bromide, followed by polymeric grafting of HEMA using Atom Transfer Radical Polymerisation utilizing Activators ReGenerated by Electron Transfer (ARGET ATRP) conditions.

The focus of this study is to evaluate the effect of surface modification under various reaction conditions on the biofouling mitigation, transport properties, and hydrolysis under acidic and alkaline pH conditions. Optimised conditions produced a membrane that showed flux and salt rejection comparable to pristine CAM, as well as improved biofouling resistance. It also resisted hydrolysis and retained its salt rejecting ability across a broade range of pHs when compared to unmodified CAMs.

4.2 Results and Discussion

4.2.1 Changes in Morphology due to Membrane Modification

Since membrane surface morphology has been shown to be one of the most important factors in membrane fouling, SEM and AFM were employed to characterise the modified membranes.

4.2.1.1 SEM Analysis

Modified membrane morphology was investigated using SEM in order to determine the extent of polymer coverage, and elucidate the effect of graft density on morphology and polymer layer thickness.

A typical image of pristine CAM and low graft density modified membranes is shown in Figure 4.1 with the surface morphology on the left, and cross-section on the right. Sample labels are described in Table 3.3, page 84. Pristine CAM (a) has a smooth and featureless surface and the asymmetric structure is evident in the cross-sectional image, where the structure appears dense at the membrane surface and more open as the distance from the surface increases. CAM-g-pHEMA membranes (b) PRT30IMV1 (polymerisation reaction time 30 minutes, initial monomer volume 1 mL), (c) PRT15IMV5, and (d) PRT30IMV2 had low graft densities of 0.15 μg/cm^2, 0.46 μg/cm^2, and 0.56 μg/cm^2, respectively. From their respective SEM images no polymer is evident and the membranes closely resemble pristine CAM - the polymer layer is so thin as to be undetectable in a surface image or in a cross-sectional image.

With increasing graft density polymer starts to become evident on the membrane, with the surface morphology becoming more nodulated. Figure 4.2 shows morphology and cross-sectional images for modified membranes with higher graft densities. They are CAM-g-pHEMA (e) PRT30IMV3, (f) PRT30IMV5, (g) PRT45IMV5, and (h) PRT60IMV5, which have graft densities of 0.69 μg/cm^2, 1.17 μg/cm^2, 1.35 μg/cm^2 and 2.33 μg/cm^2, respectively.

From the cross-sectional images the nodulated nature of the polymer layer can be clearly seen, and the thickness of the layer tends to increase with increasing graft density from around 2 μm for membrane CAM-g-pHEMA (f) PRT30IMV5, to approximately 14 μm for CAM-g-pHEMA (h) PRT60IMV5. These apparent thicknesses are much larger than suggested by FTIR.

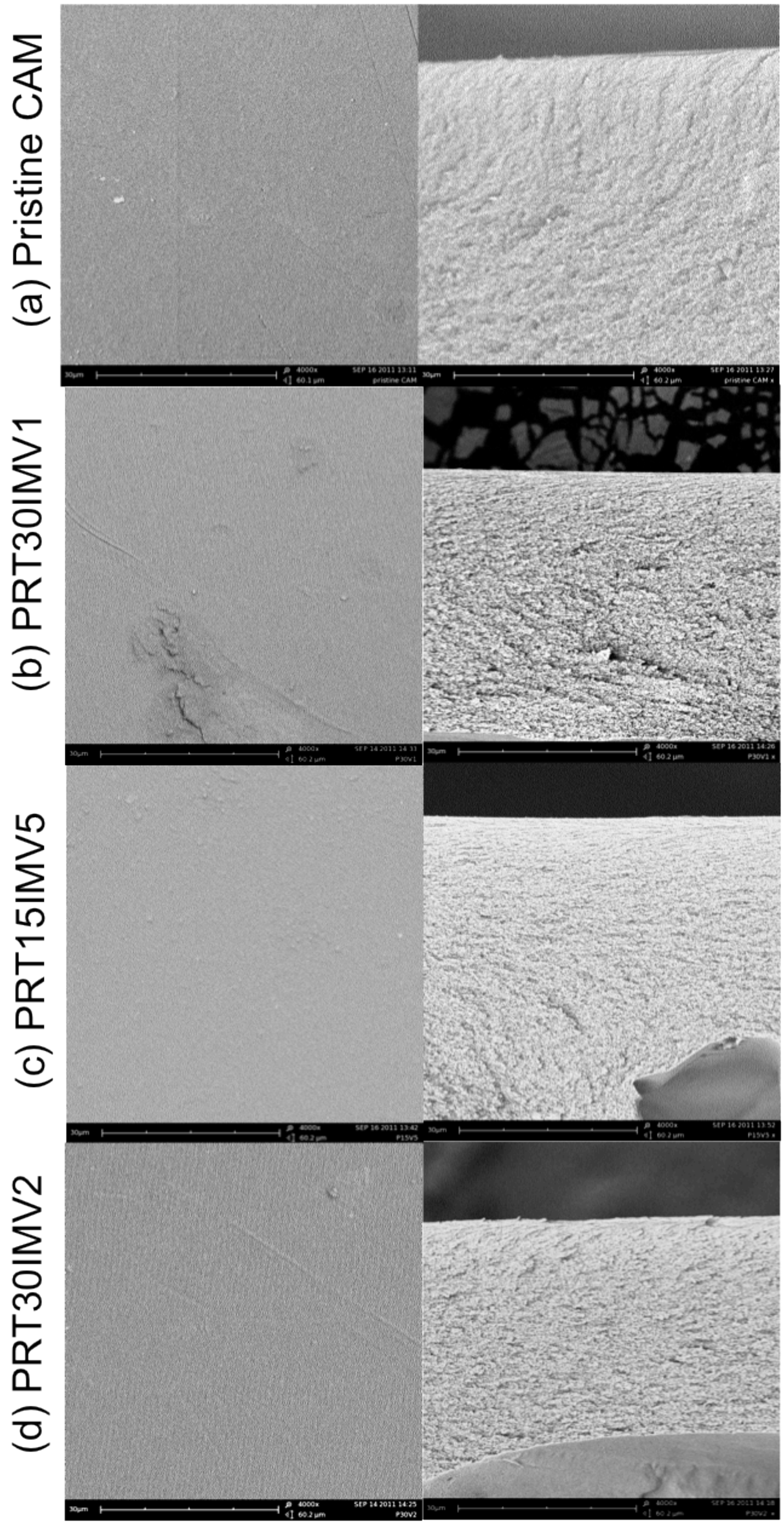

Figure 4.1. Surface morphology and cross-sectional images of (a) pristine CAM and low graft density modified membranes CAM-g-pHEMA (b) PRT30IMV1, (c) PRT15IMV5, and (d) PRT30IMV2. All images are 4000x magnification. Scale bar is 30 μm, and field height is 60.2 μm.

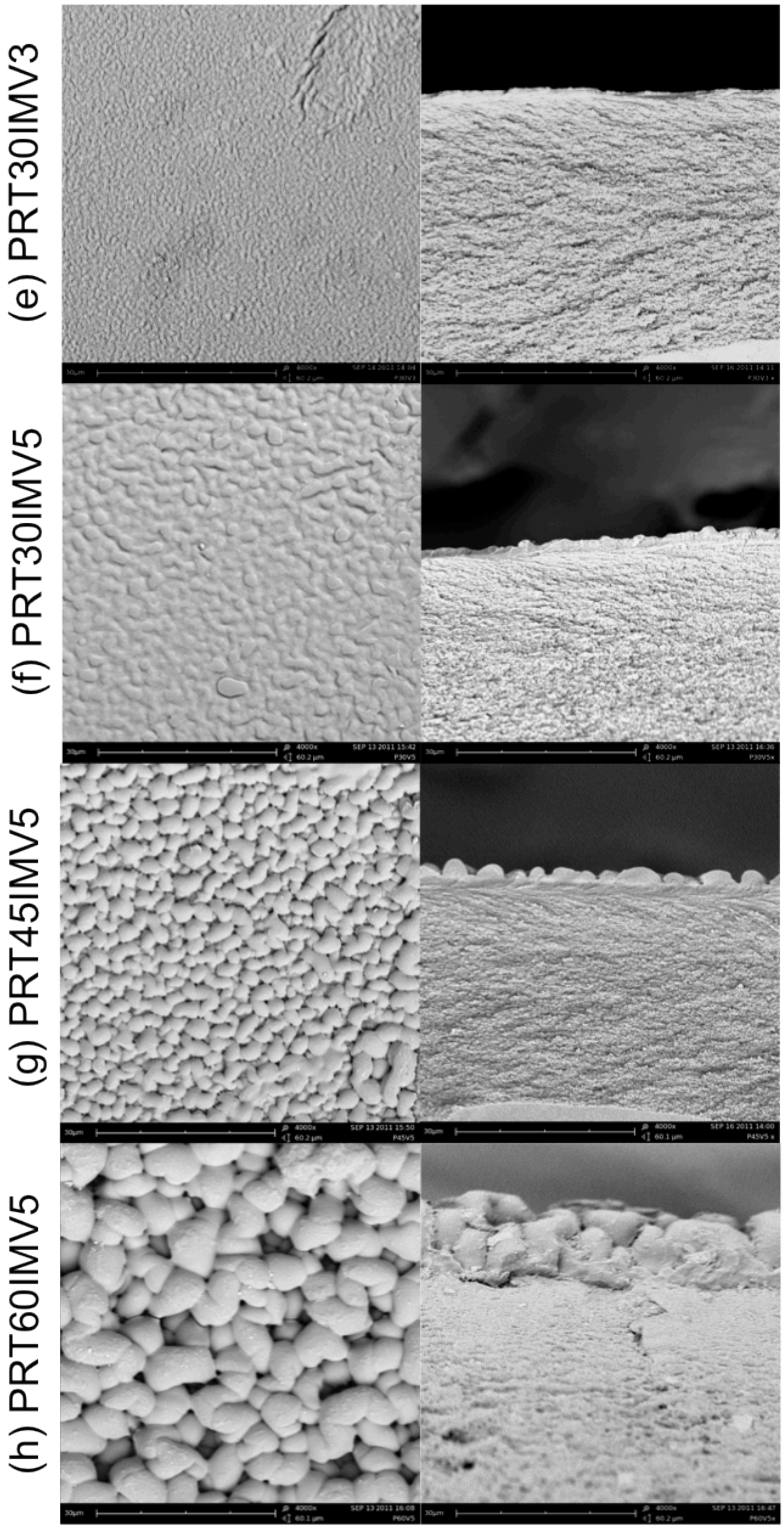

Figure 4.2. Surface morphology and cross-sectional images of high graft density modified membranes CAM-g-pHEMA (e) PRT30IMV3, (f) PRT30IMV5, (g) PRT45IMV5, and (h) PRT60IMV5. All images are 4000x magnification. Scale bar is 30 μm, and field height is 60.2 μm.

On all modified membranes the polymer appears to reside exclusively on the membrane surface, with no penetration into the membrane matrix visible. The asymmetric structure has been preserved, indicating no damage to the membrane material. All of the modified membranes appear to have continuous and homogeneous grafted phases over a long range.

The large increase in thickness between CAM-g-pHEMA (g) PRT45IMV5 and (h) PRT60IMV5 can be explained by the increase in graft density. At lower graft density the chains are spaced far apart and can lie parallel to the membrane surface, as the density increases the chains form polymer brushes and stand perpendicular to the membrane surface, resulting in a thicker polymer layer (Figure 4.3, modified from Mei *et al.* [7]). Uchida *et al.* [8] also observed an increase in grafted layer thickness with increasing graft density for surface-grafted poly(methacrylic acid). Mei *et al.* [7, 9] also observed this effect for pHEMA surface grafted from silica.

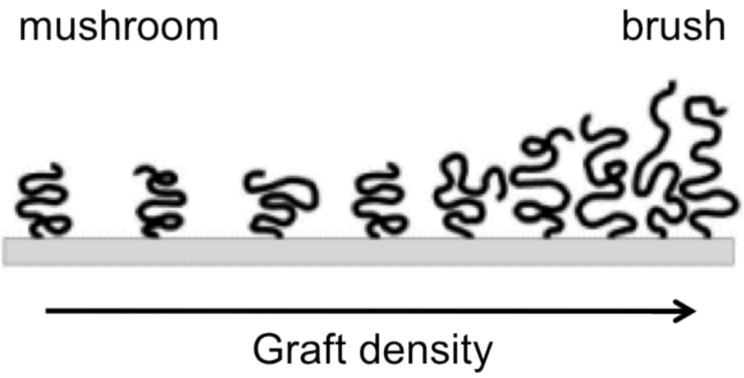

Figure 4.3: Surface-grafted polymers in the mushroom regime at low density and the brush regime at high density [7].

From analytical techniques TGA and ATR-FTIR it was shown in Chapter Three that polymer is present on the surfaces of CAM-g-pHEMA membranes with low PRTs and IMVs, even though it was not visible via SEM. It is hypothesised that these very thin polymer layers will cause less impedance to the flow of water across the membrane than the thicker polymer layers seen for longer PRTs and higher IMCs. In contrast it is expected that the increased surface roughness caused by the nodulated surface of the thicker polymer layers will affect the fouling behaviour of the modified membranes. These properties will be examined in the following sections.

4.2.1.2 AFM Analysis

AFM analysis was performed in order to quantify the roughness of the membrane surface. Previously, it has been shown that membrane surfaces become more susceptible to biofouling with increased surface roughness [2, 3]. Such roughness is attributed to the presence of ‘hills and valleys’, which increase the surface area and hence provide more binding sites for bacteria to attach to. In addition, the rougher the surface the more difficult it is to remove deposited bacteria by hydrodynamic force [2].

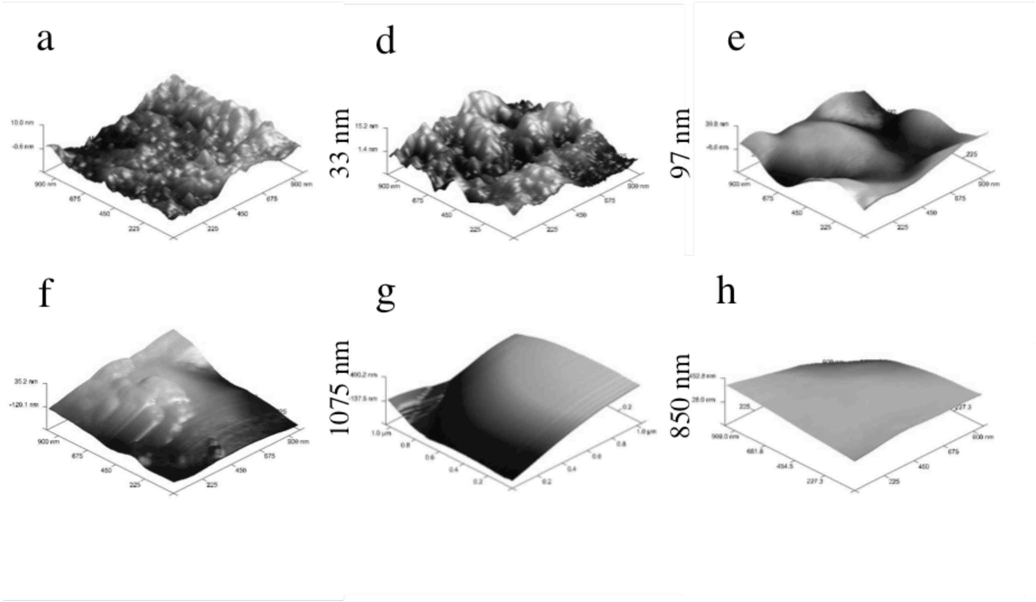

Figure 4.4. AFM image of the surfaces of (a) pristine CAM, and CAM-g-pHEMA (d) PRT30IMV2. (e) PRT30IMV3, (f) PRT30IMV5, (g) PRT45IMV5 and (h) PRT60IMV5.

Figure 4.4 represents typical AFM images of pristine CAM and CAM-g-pHEMA. Note that the x and y axes represent 1 μm, while the z axes differ for each image. Figure 4.4 (a) shows the surface of a pristine CAM membrane. Although pristine CAM appeared flat and featureless by SEM, on the scale of AFM the surface displays a relatively uniform but nodulated structure with a roughness parameter (R_a) of 2 ± 0.1 nm. The other images in Figure 4.4 represent CAM-g-PHEMA membranes pHEMA (d) PRT30IMV2. (e) PRT30IMV3, (f) PRT30IMV5, (g) PRT45IMV5 and (h) PRT60IMV5, respectively. The modified CAM-g-PHEMA surfaces show nodulated morphologies consistent with a polymeric layer. The R_a values for CAM-g-pHEMA membranes are: (c) 3 ± 0 nm, (d) 15 ± 2 nm, (f) 28 ± 7 nm, (g) 56 ± 12 nm, and (h) 56 ± 17 nm. The R_a values increase with increasing polymer and are significantly greater than the value for the pristine CAM. Kochkodan *et al*. [2] also noted a simultaneous increase of surface roughness with graft density. Although there is a large increase in surface roughness, the figures are still at the lower end of typically reported polyamide RO membrane surface roughness of approximately 50-100nm [10].

4.2.2 Wettability Studies

4.2.2.1 Contact Angles

Hydrophilicity was shown by Pasmore *et al*. [3] to be the most important factor in resisting biofouling. In order to evaluate the hydrophilicity of the modified membranes, water contact angle (WCA) measurements were carried out in air with a water droplet (static sessile drop method), and analysed using ImageJ software. Typical images are shown in Figure 4.5.

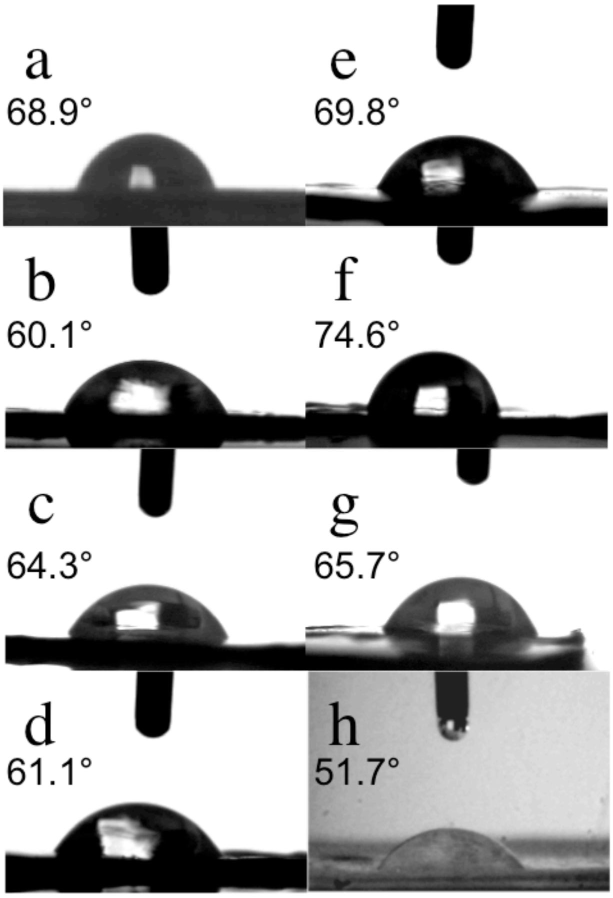

Figure 4.5. Sessile drop contact angles for (a) pristine CAM, and CAM-g-pHEMA (b) PRT30IMV1, (c) PRT15IMV5, (d) PRT30IMV2. (e) PRT30IMV3, (f) PRT30IMV5, (g) PRT45IMV5 and (h) PRT60IMV5.

Pristine CAM displayed an average WCA of 70 ± 2° (Figure 4.5 (a)). Low graft density pHEMA surfaces intially exhibit lower WCAs than pristine CAM, indicating a relatively more hydrophilic surface. At higher graft densities WCA increases to a maximum for CAM-g-pHEMA (f) PRT30IMV5, which had an average WCA of 75 ± 1° (Figure 4.5 (f)). The increase in WCA for pHEMA-coated membranes indicates a relatively less hydrophilic surface than pristine CAM.

4.2.2.2 Water Uptake

Wettability of the modified membranes was further investigated using water-uptake experiments, in which the membranes were hydrated, and the weight change due to the uptake of water was recorded. Unlike sessile drop contact angle measurements, during water uptake testing the membranes are allowed time to equilibrate in water. The water uptake study results are shown in Table 4.1.

Table 4.1. Water Uptake data for pristine CAM and CAM-g-PHEMA.

Membrane	Average % weight change
(a) pristine CAM	39.71 ± 1.23
(b) PRT30IMV1	52.52 ± 5.38
(c) PRT15IMV5	53.14 ± 2.81
(d) PRT30IMV2	35.43 ± 2.09
(e) PRT30IMV3	43.89 ± 0.44
(f) PRT30IMV5	36.06 ± 1.63
(g) PRT45IMV5	37.85 ± 3.27
(h) PRT60IMV5	37.08 ± 1.95

Interestingly, there was no clear correlation between water uptake and contact angle or graft density. Membranes (d) PRT30IMV2, (g) PRT45IMV5, and (h) PRT60IMV5, which had lower contact angles than pristine CAM (hence were more hydrophilic), yet showed less water uptake (indicating less hydrophilicity). Also, membrane (e) PRT30IMV3 showed a higher contact angle than pristine CAM, indicating less hydrophilicity, yet higher water uptake, indicating more hydrophilicity.

Holly and Refojo [11] reported that non-linear changes in hydrophilicity can be explained by the dynamic behavior of the pHEMA surface [12]. Dried membrane samples are used for WCA measurements taken in air and therefore pHEMA is in a dehydrated state where the polar side groups are buried in the bulk and the hydrophobic backbone of the polymer is oriented outwards presenting a less hydrophilic surface. However, in an aqueous environment, such as during water uptake experimetns, the situation is reversed and the polar side groups are oriented outwards. Direct structural evidence for this rearrangement was provided by Chen *et al.* [12] using sum frequency generation spectroscopy. The two scenarios are represented in Figure 4.6 (modified from Chen *et al.* [12]).

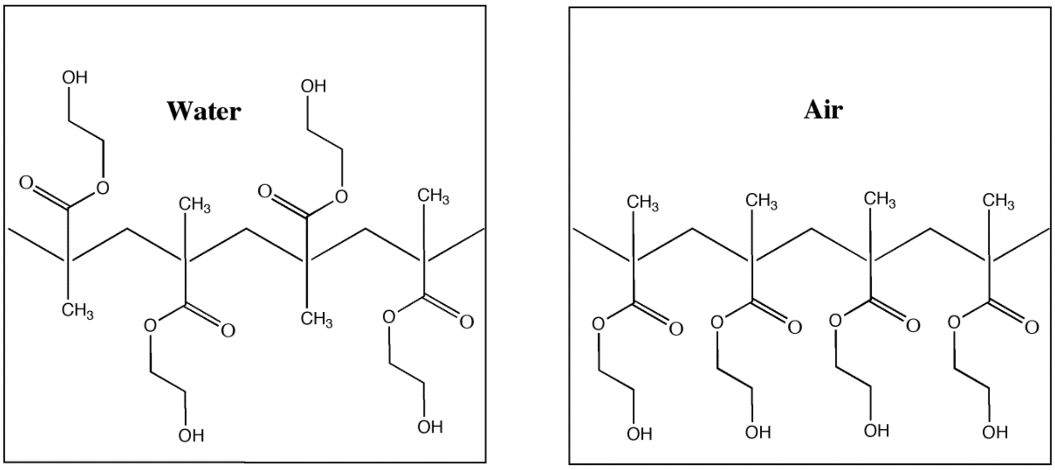

Hydrated state

Dehydrated state

Figure 4.6. Proposed model for the reorientation of polyHEMA during dehydration [12].

As pHEMA graft density increased further, WCA decreased again. In contrast to CAM-g-pHEMA (f) PRT30IMV5, CAM-g-pHEMA (h) PRT60IMV5 had an average WCA of 52 ±2 ° (Figure 4.5 (h)), indicating an increase in hydrophilicity relative to pristine CAM. This dependence of WCA on graft density was also observed by Mei *et al.* [7] who proposed that the minimum WCA occurred at the transition from partial to complete surface coverage. They proposed that intermolecular hydrogen bonding between the hydroxyethyl groups in the brush regime could be preventing reorientation.

4.2.3 Membrane Filtration Properties

Modified membranes were analysed using stirred-cell to find the effect of changing different variables on the filtration properties of the membranes. In this technique, pure water or a salt solution is passed through the membrane under pressure, approximating operation conditions. Measuring the conductivity of the feed, permeate and retentate, as well as the mass/volume of the collected permeate solution, allows the calculation of the water flux per area per unit time (represented in Figure 4.7, Figure 4.8, and Figure 4.9), and the percentage salt rejection associated with each membrane. Values are often lower than reported by the manufacturer because stirred-cell operates in dead-end filtration, and concentration polarization plays a greater role than in cross flow filtration. However, stirred-cell is a convenient technique since it requires only small membrane coupons (14 cm^2) and can be done fairly quickly, with experiments taking approximately one day per sample. Experiments were carried out using pure water (MilliQ, resistivity = 18 MΩ cm) or a sodium chloride (NaCl) solution with a concentration of 2000 ppm. Initially, the pressure applied was 15.5 bar, later this was adjusted to 26.0 bar in order to achieve greater water flux and reduce experiment times. The differences between the fluxes achieved for both pure water and NaCl solution at the two pressures for pristine CAM are shown in Figure 4.7. The increase in pressure leads to an increase in flux, as expected. It is also notable that the salt-water flux was always slightly lower than the pure water flux, due to increased osmotic pressure. Also, salt rejection increased slightly with increased pressure, from 84.7% at 15.5 bar to 87.9% at 26.0 bar. Hereafter, both water flux and salt rejection values are reported for 2000 ppm NaCl solution and 26.0 bar experimental conditions.

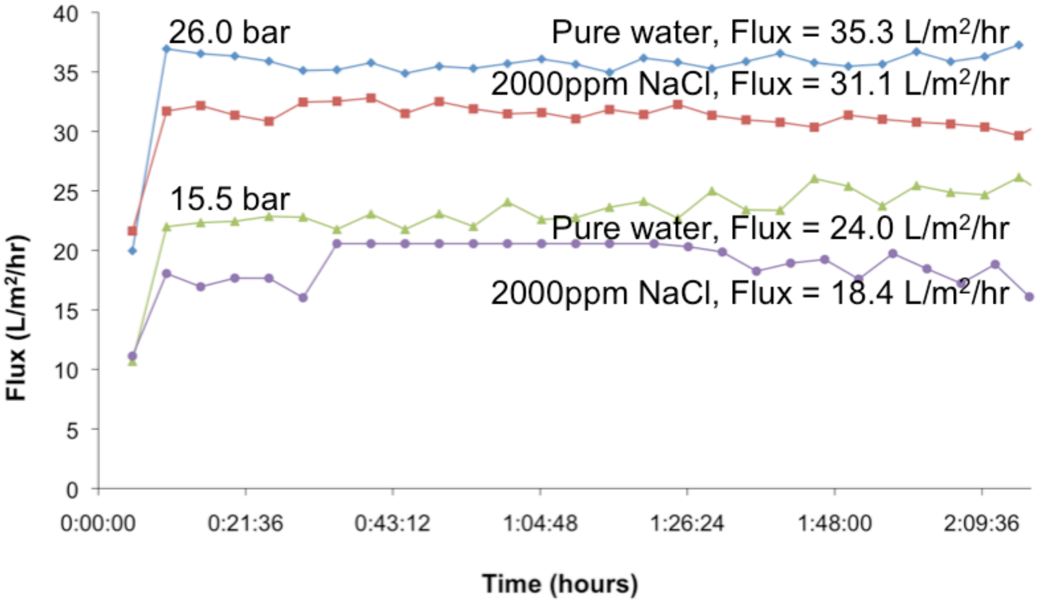

Figure 4.7. Stirred-cell results for pristine CAM with pure water and 2000 ppm NaCl solution at 15.5 bar and 26.0 bar.

4.2.3.1 Effect of polymerisation time on filtration properties

Figure 4.8 shows the stirred-cell results for membranes polymerised for various times with IMCs of 2.58 $\mathrm{molL^{-1}}$, filtering 2000 ppm NaCl solution. As discussed in Chapter Three, increasing polymerisation time represents increasing amount of polymer on the membrane surface.

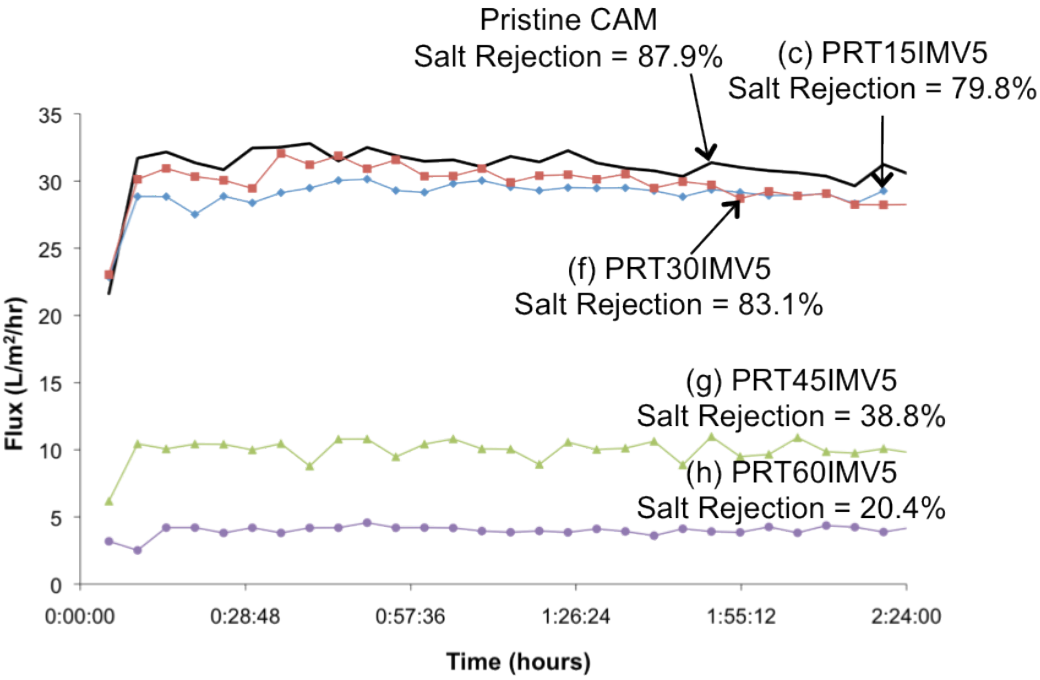

Figure 4.8: The effect of polymerisation time on CAM-g-PHEMA salt-water flux.

Pristine CAM had an average salt water flux of 33.1 $\mathrm{L/m^2/hr}$ ± 6.5%, and an average salt rejection of 87.9%. As can be seen from the data, there was minimal change in performance due to pHEMA modification for 15 mintues (5% decrease in water flux (within experimental error), and 9% decrease in NaCl rejection relative to pristine CAM), or 30 minutes (12% decrease in water flux, and 5% decrease in NaCl rejection relative to pristine CAM), indicating that a pHEMA coating can be achieved without major loss of filtration properties. However, at polymerisation times greater than 30 minutes the graft density of the polymer layer has increased such that water flux is drastically impeded by the increased hydraulic resistance. For example, modification of CAM for 60 minutes caused

83% decrease in water flux, and 77% decrease in NaCl rejection relative to pristine CAM. Flux decreases of 55 to 80% have been previously reported [13] for RO membranes modified with PEG for 10 to 60 minutes. One would expect salt rejection to increase with decreasing flux, however, the salt rejection values followed the same trend as the water flux, that is, they showed little change for short polymerisation times and decreased as the amount of polymer increased. The increase in surface roughness with increasing graft density can contribute to a decreased mass transfer coefficient and thus increased concentration polarisation [14, 15]. Another factor possibly affecting the salt rejection is the depth of polymer grafting. If polymer grafting occurred only on the membrane surface, the initial dense layer of CA should have remained the same in terms of microstructure, thereby maintaining a very good salt rejection. More likely, as the reaction time increases, the grafting goes deeper, altering the structure of the dense layer of CA.

The data suggests that polymerisation times of 30 minutes or less (corresponding to a graft density below 1.17 $\mu g/cm^2$) should be used in order to maximize water flux and salt rejection.

4.2.3.2 Effect of initial monomer volume on filtration properties

The effect on the filtration properties of varying the initial monomer volume for a given polymerisation reaction time was also investigated. Once again, increasing monomer volume corresponds to increasing polymer coverage.

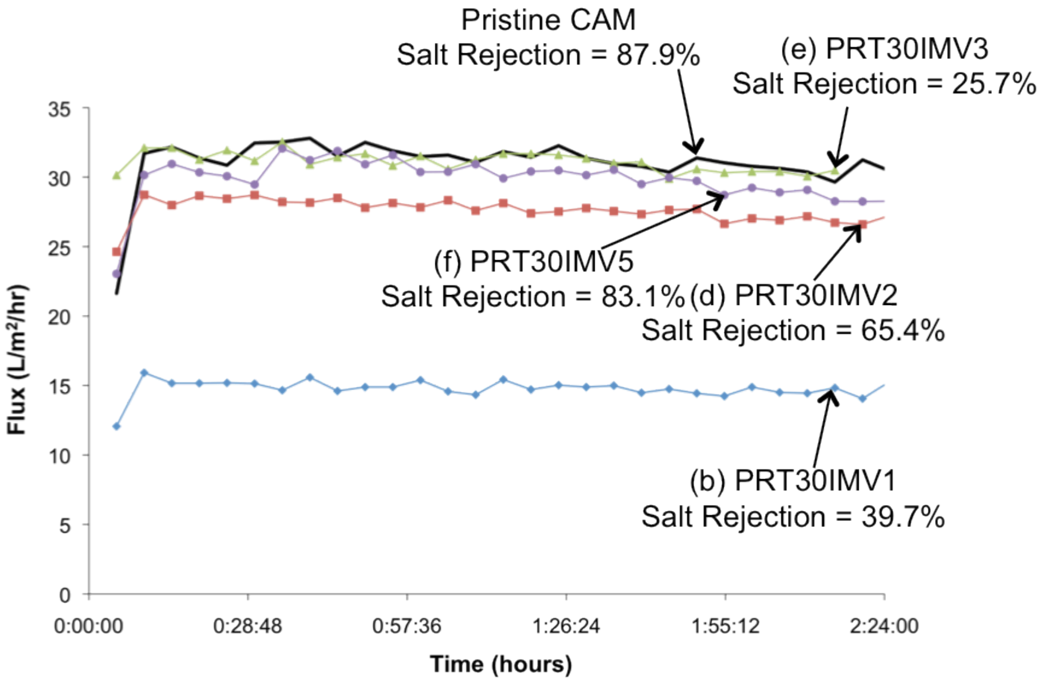

Figure 4.9. The effect of monomer concentration on CAM-g-PHEMA salt water flux.

When varying the IMV, it is evident from the data presented in Figure 4.9, that the higher volumes of monomer give filtration properties in line with the commercial CAM, whereas the lower volumes showed decreased flux and salt rejection. There is a slight reduction in flux values between IMV 3 mL and 5 mL, perhaps suggesting that the latter has enough polymer present to start to hinder water flux. Notably, again the salt rejection values follow the same trend as the flux values, both increase with monomer volume, with the exception of membrane (e) PRT30IMV3. This membrane had excellent water flux, however the salt rejection was consistently low, despite being tested several times. These results indicate that an IMV of at least 2 mL (corresponding to an initial monomer concentraion of 1.03 molL^{-1}, and a graft density of at least 0.56 μg/cm^2) is necessary to maximize flux and salt rejection.

The stirred-cell results are summarized in Table 4.2, page 115. Taking all the data into account, the optimal graft density for maintaining water flux, relative to pristine CAM, is between 0.46 μg/cm^2 and 1.17 μg/cm^2.

4.2.4 Changes in Hydrolysis Due to Membrane Modification

Due to their susceptibility to pH dependant hydrolysis, CAMs have a recommended operating range between pH 4 and pH 8. The removal of acetyl groups from the polymer backbone leads to changes in membrane crystallinity, molecular weight and water content, which in turn affects membrane performance [16, 17].

The degree of acetylation is known to be inversely proportional to the permeability of the membrane to water and salt. As discussed in Chapter One, a high degree of acetylation leads to high salt rejection and low flux, a low degree of acetylation leads to low salt rejection and high flux. This has been attributed to decreased crystallinity of the polymer with decreased acetyl content, meaning that more free water is present in the membrane and is available to transport more salt [16].

In order to determine the effect of the membrane modification on the effective pH range of the CAMs, pieces of pristine CAM and membrane (f) CAM-g-pHEMA PRT30IMV5 were soaked for 24 hours in pH buffers outside of the recommended pH range (pH 2.2 and 9.0). They were then used to perform stirred-cell and ATR-FTIR in order to analyse the effect different pHs had on degree of acetylation and membrane filtration performance.

The ATR-FTIR spectrum comparing the soaked membranes to pristine CAM and completely hydrolysed CAM is shown in Figure 4.10.

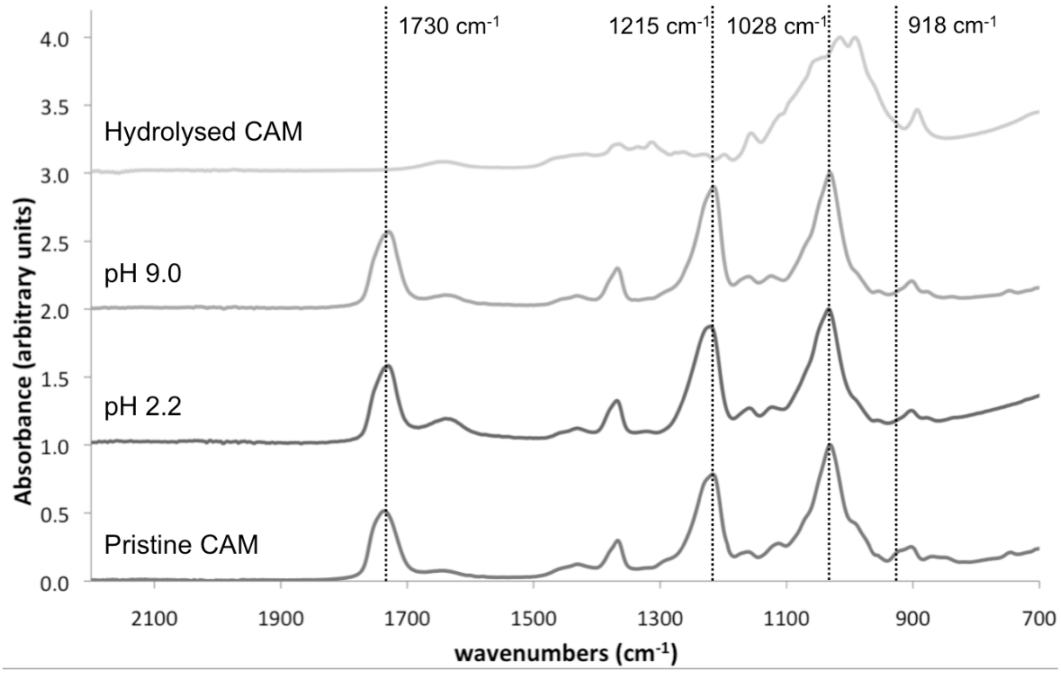

Figure 4.10. ATR-FTIR in the range 700 cm^{-1} to 2200 cm^{-1}, comparing pristine CAM soaked in different pH buffers to unsoaked CAM and completely hydrolysed CAM.

Expected changes upon hydrolysis of cellulose acetate include decreases in the peaks at 1730 cm^{-1}, 1215 cm^{-1}, 1028 cm^{-1} and 918 cm^{-1} [18-20]. These correspond to the carboxylate C=O stretch, and the carboxylate C-O stetching and two bending modes, respectively. After hydrolysation of pristine CAM with 0.5M NaOH for 4 hours, the ATR-FTIR spectrum (labelled hydrolysed CAM) resembles that of cellulose [19, 21], indicating that deacetylation is complete. The spectra for the CAM-g-pHEMA membranes soaked at pH 2.2 and pH 9.0 resemble pristine CAM, not hydrolysed CAM, suggesting that the coated membranes have been protected from hydrolytic deterioration. Although very little deacetylation appears to have occured, the effect on the filtration properties was significant.

The stirred-cell results for salt rejection versus pH are shown in Figure 4.11. The data shown are relative salt rejections compared to an unsoaked control of either pristine CAM or CAM-g-PHEMA. The alkaline pH had a greater effect than the acidic pH on the salt rejection of both samples. Compared to an unsoaked control, pristine CAM suffered a loss of around 12% of its salt rejection ability after being soaked at pH 2.2, and a massive loss of approximately 75% of salt rejection ability after being soaked at pH 9.0. In contrast, CAM-g-PHEMA suffered only minor loss of salt rejecting ability relative to unsoaked CAM-g-PHEMA, less than 1% at pH 2.2, and only 5% at pH 9.0. The modified membrane was able to retain its salt rejecting ability across a broad pH range.

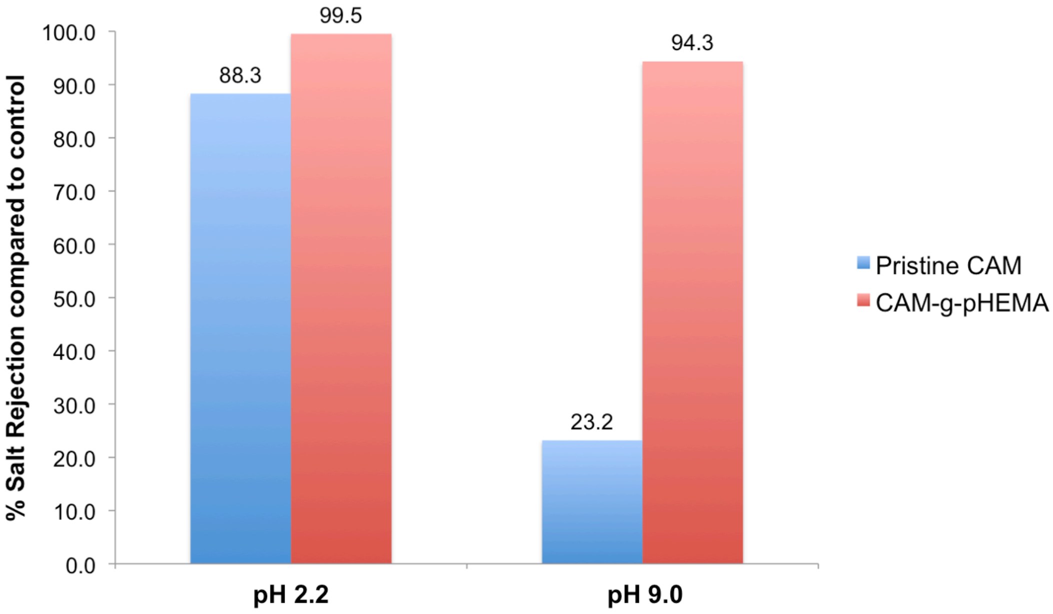

Figure 4.11. Relative salt rejection for membranes after exposure to extreme pH.

4.2.5 Biofouling Resistance

Coated and pristine membranes were tested for biological fouling resistance by immersion in a natural seawater aquarium with a salinity of 35,000 ppm. The advantage of this method is the exposure of the membrane to “real-world” ecological conditions, giving a more realistic indication of how fouling may occur during operation. One of the disadvantages, compared to testing with model solutions in the stirred-cell, is that it is not possible to avoid fouling on the back side of the RO membranes. This could of course influence the results, and was taken into account by comparing all results to a control that had been exposed to the same conditions. After three weeks, the fouled membranes were removed from the aquarium, chemically fixed and analysed with SEM. Microbial abundance for each sample was determined by counting the number of microbes on each of 27 images – 3 images for each of 3 areas on each of 3 replicate samples. The data is presented as number of cells and is the mean calculated from 27 randomly selected areas per sample.

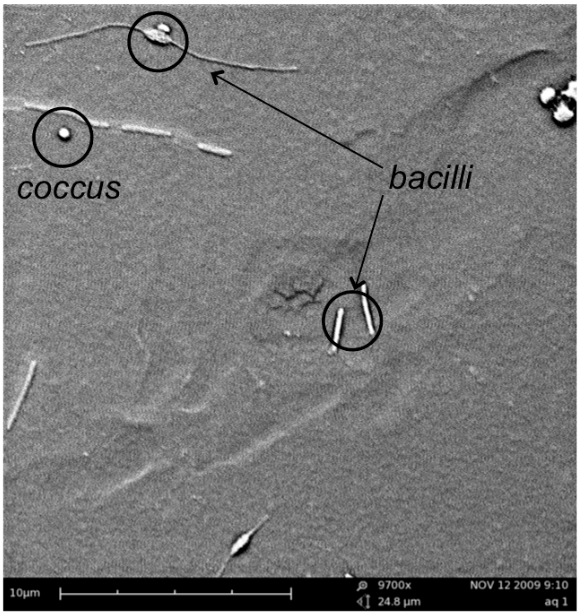

Figure 4.12: Bacterial varieties commonly observed during static aquarium testing, shown here on the surface of pristine CAM. Scale bar is 10 µm.

Although detailed identification of the bacterial species present was not undertaken, three general bacterial types were generally observed: spherical *coccus*, rod-shaped *bacillus* (most likely *Pseudomonas aeruginosa*, which is found in almost all natural waters [3]) and another rod-shaped variety with long filaments extending from each end of the rod. These three bacterial types (shown on a pristine CAM surface in Figure 4.12) were seen on all samples to differing degrees, and for membranes that had been fouled for a long time, larger organisms such as algae and diatoms were also sometimes observed.

Figure 4.13 (a) shows typical SEM images for pristine CAM, after exposure to the seawater aquarium. The average number of cells per image was 33.0. Figure 4.13 (b) – (h) represent membranes with increasing graft density, biofouling data is listed in Table 4.2, page 115. The results are reported as percent change in the average number of cells relative to the control for the relevant experiment.

All CAM-g-pHEMA membranes showed an improvement in biofouling resistance relative to pristine CAM, that is, they had fewer average cells per image. One anomaly in the data is membrane CAM-g-pHEMA (c) PRT15IMV5, which actually had 18% more cells on average than the pristine CAM control. This was possibly due to inconsistent polymer coverage, leaving hydrophobic initiator exposed in the areas studied. However, the data for this membrane does overlap with the control within experimental error.

At higher graft densities the biofouling resistance is improved relative to the control. The results show that the greatest benefit to antifouling properties is achieved at grafting densities of 0.56 to 0.69 μg/cm^2, which gave a 67% and 55% relative reduction in the average number of cells, respectively. Mei *et al.* [9] tested fibronectin absorption on a polymer grafting density gradient and observed the protein absorption to be lowest where the polymer was in the brush regime. Therefore it was expected that the biofouling would be the lowest at the highest graft density, however, above a graft density of 0.69 μg/cm^2 the average number of cells rose again slightly, although was still lower than for the control. The decline in biofouling resistance at the highest graft densities is probably due to an increase in surface roughness with the thicker polymeric coating.

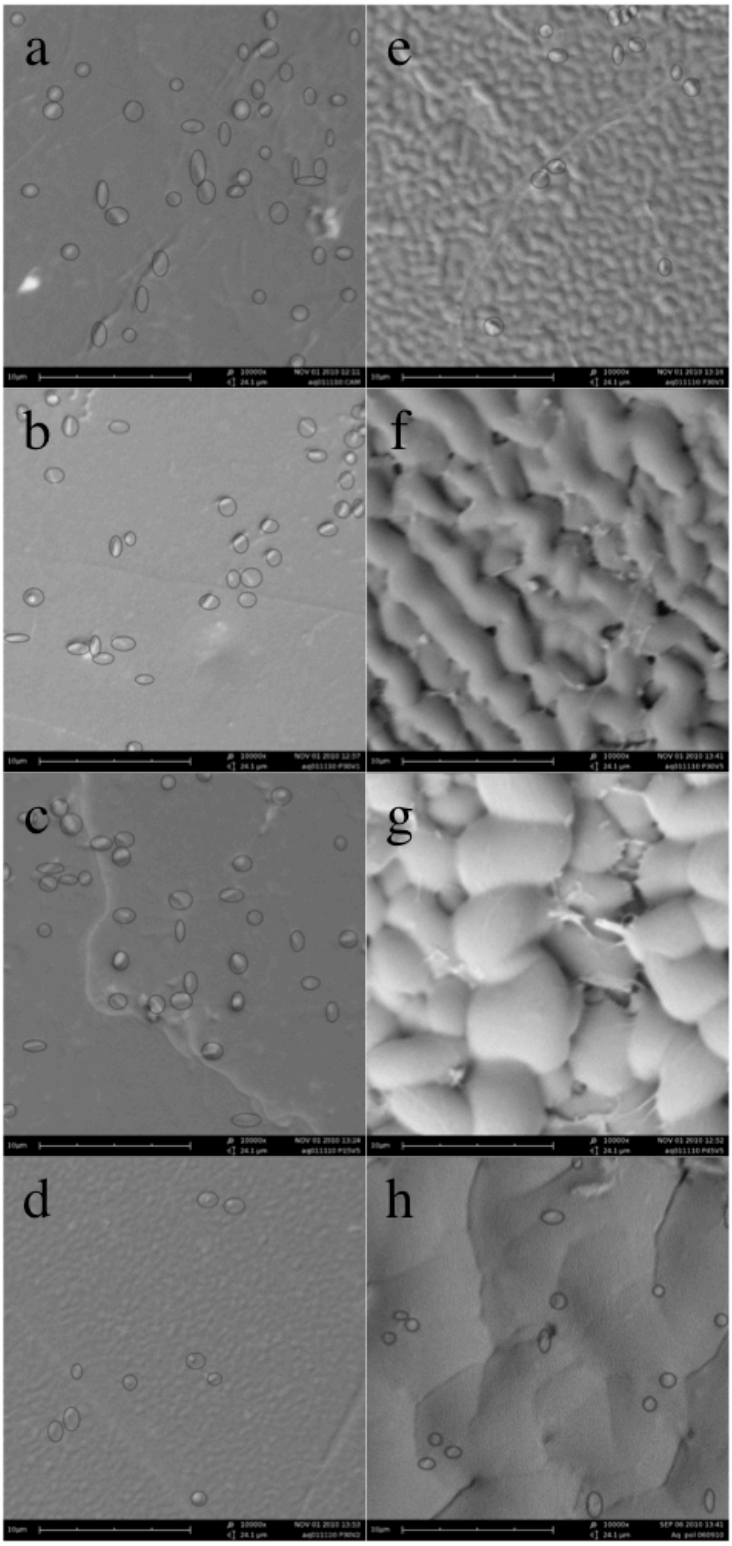

Figure 4.13. Typical SEM images after static aquarium biofouling tests for (a) pristine CAM, and CAM-g-pHEMA with increasing graft density (b) PRT30IMV1, (c) PRT15IMV5, (d) PRT30IMV2, (e) PRT30IMV3, (f) PRT30IMV5, (g) PRT45IMV5, and (h) PRT60IMV5. All images are 10000x magnification. Scale bars are 10 μm, and field height is 24.1 μm. Counted cells are circled.

Pasmore *et al.* [3] found that micro-scale roughness had less effect than hydrophilicity for fouling by *Pseudomonas aeruginosa*. However, since (h) PRT60IMV5 is more hydrophilic and has greater roughness than (f) PRT30IMV5, yet exhibits slightly less biofouling reduction, these results seem to indicate a greater dependence of biofouling propensity on roughness than hydrophilicity. This agrees with the observations of Vrijenhoek *et al.* [22] who reported that physical roughness of the membrane surface was the most important parameter for fouling of reverse osmosis and nanofiltration membranes.

The 'best' membrane in terms of biofouling reduction is the one with the lowest cell count, i.e. membrane (d) PRT30IMV2. However, comparing the fouling data to water flux and salt rejection results, it can be seen that while this membrane had a satisfactory water flux, the salt rejection of 65.4% is significantly lower than for pristine CAM. The membrane which is best able to retain salt rejection and water flux, whilst still showing improved resistance to biofouling is membrane (f) PRT30IMV5, which has flux and salt rejection comparable to pristine CAM, and also shows a 27% reduction in biofouling. The graft density of this membrane was 1.17 $\mu g/cm^2$.

Table 4.2. Summary of characterisation results of pristine CAM and CAM-g-pHEMA membranes with increasing graft density.

Membrane	**Graft Density ($\mu g/cm^2$)**	**Contact Angle (°)**	**Water Uptake (% change)**	**Roughness (nm)**	**Water Flux ($L/m^2/hr$)**	**Salt Rejection (%)**	**# Cells (% change)**
(a) pristine CAM	0	68.9	40	2	33.1	87.9	0
(b) PRT30IMV1	0.15	60.1	53	-	14.6	39.7	-21
(c) PRT15IMV5	0.46	64.3	53	-	31.6	79.8	18
(d) PRT30IMV2	0.56	61.1	35	3	27.2	65.4	-67
(e) PRT30IMV3	0.69	69.8	44	15	31.1	25.7	-55
(f) PRT30IMV5	1.17	74.6	36	28	29.2	83.1	-27
(g) PRT45IMV5	1.35	65.7	38	56	10.7	38.8	-27
(h) PRT60IMV5	2.33	51.7	37	56	5.8	20.4	-25

4.3 Conclusion

Modified membranes were imaged using SEM and the morphology confirms other characterisation results. Namely, the polymer layer becomes thicker and more nodulated with increasing graft density. Modified membranes were tested by AFM for surface roughness, and were shown to increase in roughness with increasing graft density. Water contact angles were measured and showed evidence for the reorientation of the pHEMA chains from wet to dry and depending on graft density. CAM-g-pHEMA membranes have an operating range between pH 2.2 and pH 9.0 compared to pristine CAMs which have an operating range between pH 4 and pH 8. Hydrolysis had little effect on modified membrane filtration properties when soaked at pHs outside the recommended range for pristine CAM.

Based on aquaria experiments, the pHEMA modified CA membranes showed a greater resistance to seawater microbial biofouling with respect to pristine CA membranes. In the case of the low graft density pHEMA-modified membranes, this has been achieved without significant loss of function in terms of water flux and salt rejection.

From this study it has been possible to determine the optimal reaction conditions to obtain a pHEMA-modified membrane, which is able to resist biofouling in a static aquarium test, whilst still maintaining transport properties comparable to pristine CAM.

References

1. M. Hashino; T. Katagiri; N. Kubota; Y. Ohmukai; T. Maruyama; H. Matsuyama. Effect of Membrane Surface Morphology on Membrane Fouling with Sodium Alginate, Journal of Membrane Science 366 (2011) 258-265.
2. V. Kochkodan; N. Hilal; V. Goncharuk; L. Al-Khatib; T. Levadna. Effect of the Surface Modification of Polymer Membranes on Their Microbiological Fouling, Colloid Journal 68 (2006) 267-273.
3. M. Pasmore; P. Todd; S. Smith; D. Baker; J. Silverstein; D. Coons; C. Bowmn. Effects of Untlrafiltration Membrane Surface Properties on Pseudonmonas Aeruginosa Biofilm Initiation for the Purpose of Rerducing Biofouling, Journal of Membrane Science 194 (2001) 15-32.
4. E. Ostuni; R. Chapman; R. Homlin; S. Takayama; G. Whitesides. A Survey of Structure-Property Relationships of Surfaces That Resist the Adsorption of Protein, Langmuir 17 (2001) 5605-5620.
5. R. Holmlin; X. Chen; R. Chapman; S. Takayama; G. Whitesides. Zwitterionic Sams That Resist Nonspecific Adsorption of Protein from Aqueous Buffer, Langmuir 17 (2001) 2841-2850.
6. A. Rosenhahn; S. Schilp; H.J. Kreuzer; M. Grunze. The Role Of "Inert" Surface Chemistry in Marine Biofouling Prevention, PCCP 12 (2010) 4275-4286.
7. Y. Mei; T. Wu; C. Xu; K.J. Langenbach; J.T. Elliott; B.D. Vogt; K.L. Beers; E.J. Amis; N.R. Washburn. Tuning Cell Adhesion on Gradient Poly(2-Hydroxyethyl Methacrylate)-Grafted Surfaces, Langmuir 21 (2005) 12309-12314.
8. E. Uchida; H. Iwata; Y. Ikada. Surface Structure of Poly(Ethylene Terephthalate) Film Grafted with Poly(Methacrylic Acid), Polmyer 41 (2000) 3609-3614.

9. Y. Mei; T. Wu; C. Xu; K.J. Langenbach; J.T. Elliott; B.D. Vogt; K.L. Beers; E.J. Amis; N.R. Washburn. Combinatorial Studies of the Effect of Polymer Grafting Density on Protein Absorption and Cell Adhesion, Polymer Preprints 46 (2005) 13-14.
10. E. Van Wagner; A. Sagle; M. Sharma; Y.-H. La; B. Freeman. Surface Modification of Commercial Polyamide Desalination Membranes Using Poly(Ethylene Glycol) Diglycidyl Ether to Enhance Membrane Fouling Resistance, Journal of Membrane Science 367 (2011) 273-287.
11. F. Holly; M. Refojo. Wettability of Hydrogels I. Poly(2-Hydroxyethyl Methacrylate), Journal of Biomedical Materials Research, Part A. 9 (1975) 315-326.
12. Q. Chen; D. Zhang; G. Somorjai; C. Bertozzi. Probing the Surface Structural Rearrangement of Hydrogels by Sum-Frequency Generation Spectroscopy, Journal of the American Chemical Society 121 (1999) 446-447.
13. B. McCloskey; H. Park; H. Ju; B. Rowe; D. Miller; B. Chun; K. Kin; B. Freeman. Influence of Polydopamine Deposition Conditions on Pure Water Fux and Foulant Adhesion Resistance of Reverse Osmosis, Ultrafiltration, and Microfiltration Membranes, Polymer 51 (2010) 3472-3485.
14. T. Matsuura. Progress in Membane Science and Technology for Seawater Desalination - a Review, Desalination 134 (2001) 47-54.
15. A. Schafer; A. Fane; T. Waite. Nanofiltration of Natural Organic Matter: Removal, Fouling and the Influence of Multivalent Ions, Desalination 118 (1998) 109-122.
16. S. McCray; V. Vilker; K. Nobe. Reverse Osmosis Cellulose Acetate Membranes II. Dependance of Transport Properties on Acteyl Content, Journal of Membrane Science 59 (1991) 317-330.

17. S. McCray; V. Vilker; K. Nobe. Reverse Osmosis Cellulose Acetate Membranes I, Rate of Hydrolysis, Journal of Membrane Science 59 (1991) 305-316.
18. H. Liu; Y. Hsieh. Ultrafine Fibrous Cellulose Membranes from Electrospinning of Cellulose Acetate, Journal of Applied Polymer Science 40 (2002) 2119-2129.
19. K. Pandey. A Study of Chemical Structure of Soft and Hardwood and Wood Polymers by FTIR Spectroscopy, Journal of Applied Polymer Science 71 (1999) 1969-1975.
20. Y. Chen; X. Xiong; G. Yang; L. Zhang; S. Lei; H. Liang. Characterisation of Regenerated Cellulose Membranes Hydrolysed from Cellulose Acetate, Chinese Journal of Polymer Science 20 (2002) 369-375.
21. W. Shurong; L. Qian; L. Zhongyang; W. Lihua; C. Kefa. Mechanism Study on Cellulose Pyrolysis Using Thermogravimetric Analysis Coupled with Infrared Spectroscopy, Frontiers of Energy Power Engineering China 1 (2007) 413-419.
22. E. Vrijenhoek; S. Hong; M. Elimelech. Influence of Membrane Surface Properties on Initial Rate of Colloidal Fouling of Reverse Osmosis and Nanofiltration Membranes, Journal of Membrane Science 188 (2001) 115-128.

5 Chapter Five

A study into the effect of POSS nanoparticles on cellulose acetate membranes

Preface

This chapter investigates the effect of polyhedral oligomeric silsesquioxane (POSS) nanoparticle inclusion in cellulose acetate (CA) membranes. The synthesis and characterisation of a novel CA-anchored nanoparticle additive (CA-POSS) is described. Membranes were fabricated with no additive, or either POSS or CA-POSS as an additive at different weight percent loadings. Nanoparticle dispersion, agglomeration, sedimentation and leaching were investigated using scanning electron microscopy. Dynamic mechanical analysis was used to investigate the mechanical strength of the nanocomposite membranes. The effect of nanoparticle inclusion on the filtration properties and compaction behaviour of the membranes was also investigated. Compared to the CA control, nanocomposite membranes exhibited superior flux and compaction resistance, and decreased salt rejection and mechanical strength.

Work presented in this chapter has been published in the Journal of Membrane Science, 431 (2013) 62-71.

5.1 Introduction

Mixed-matrix membranes (MMMs) are an emerging technology whereby the membrane morphology consists of an organic polymer (bulk phase) and homogeneously dispersed inorganic particles [1]. MMMs for gas separation are a type of membrane material displaying significant improvement in separation properties when compared to original polymeric membranes [1], however, such membranes have rarely been applied for desalination applications. To date, inorganic particles incorporated into desalination membranes have included such fillers as zeolite [2, 3], titanium oxide [4], and carbon nanotubes [5]. Jeong *et al.* [2] reported the fabrication of zeolite-polyamide nanocomposite reverse osmosis membranes. When compared to conventional polyamide RO membranes, zeolite (NaA type) modified membranes demonstrated improved water permeability, which was attributed to the preferential flow of water molecules through super-hydrophilic pores contained within the zeolite nanoparticles. Moreover, Yang *et al.* [4] prepared polysulfone/TiO_2 organic-inorganic composite, ultrafiltration membranes, which demonstrated excellent water permeability, hydrophilicity and good anti-fouling ability. Similar properties were found in the preparation of cellulose acetate/TiO_2 membranes, as well as increasing macrovoid sublayer formation with increasing nanoparticle weight percent [6]. In addition, the enhancements of mechanical properties, bursting strength and breaking strength were observed at 2 wt% TiO_2 filler concentration, when compared to unmodified polysulfone membranes [4].

Recently, Pendergast *et al.* [7] showed that polysulfone nanocomposite materials, prepared from amorphous non-porous silica and crystalline microporous zeolite nanoparticles, better resisted compaction due to improved mechanical integrity. However, an optimum balance between membrane flux and salt rejection was not achieved, and SEM images revealed aggregates of nanoparticles within the polymer matrix, which may weaken the porous polymeric material. Arthanareeswaran *et al.* [8] investigated the effect of silica particles on cellulose acetate blend ultrafiltration membranes with respect to compaction, pure water flux, percent water content and porosity with increasing SiO_2 weight percent from 10 to 40% by weight. The fumed silica powders had an average primary particle size of 0.014 mm, and agitation of the polymer/SiO_2/DMF solution was required for at least 24 hours in order to obtain a relatively homogeneous dispersion of the silica particles in the CA solution. Mechanical and compaction properties of the 10 wt% CA/SiO_2 blend membranes increased relative to the unmodified CA membranes, however, these properties declined with the addition of inorganic particles above 10 wt% to the casting solution. Furthermore, SEM investigation of the morphological topography of the membranes revealed SiO_2 aggregates precipitated onto the surface as well as increased porosity.

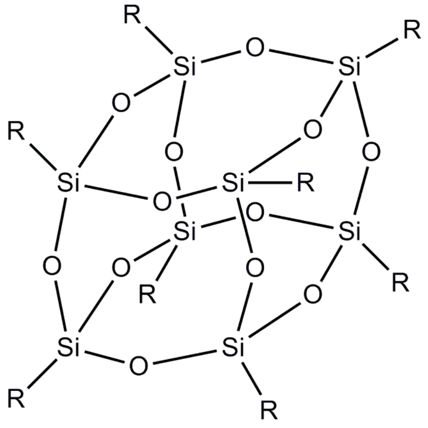

Figure 5.1. The Si-O cage structure of POSS nanoparticles [10].

Polymer-silica hybrid nanocomposite materials are a class of material that displays excellent mechanical properties, such as high chemical and thermal stability, large surface area and good compatibility with the environment [9]. In particular, POSS (Figure 5.1) is one of the many inorganic nanophases being studied for development of hybrid organic-inorganic nanocomposites. POSS are often referred to as the smallest particles of silica possible, however, unlike silica, each molecule contains organic substituents, which can be specially designed to be non-reactive or reactive [10]. POSS molecules possess a well-defined core and exterior surface affording a high surface-area-to-volume ratio, and as a nanofiller their surface areas are up to 400% more than conventional microfilled composites, which is advantageous because this leads to property amplification [11]. In addition, the bulky POSS unit causes regions of local, high free volume in the solid state [12]. This property is particularly desirable for membrane separation materials as any intrinsically high free volume increases the solubility selectivity of the membrane material in the separation process, whilst at the same time reducing the importance of diffusivity selectivity, thus increasing the overall separation efficiency [13].

Bleha *et al.* [14] investigated the effects of different POSS functionalities on the crystallinity of chitosan films. They found that the POSS could interact with the chitosan hydrophilically and cause chain conformation changes, likely to be important due to the large difference in volume between the POSS and the chitosan. Tanaka *et al.* [15] also studied octa-substituted POSS molecules with different functionalities as thermal and mechanical reinforcements for polystyrene, PMMA and ethylene (vinyl acetate). They also reported changes in polymer chain mobility caused by hydrophilic interactions between the POSS and the polymer chains. Xie *et al.* [16] prepared cellulose organic-inorganic hybrids by chemically incorporating POSS nanoparticles into the cellulose matrix. The results showed that POSS nanoparticles were homogeneously dispersed at the nanometer scale within the cellulose matrix.

The aim of the work presented in this chapter was to investigate the effect of POSS nanoparticles on cellulose acetate membranes with respect to dispersion, compaction and flux properties. To this end, POSS nanoparticles were blended into the CA membranes according to two different methods, i.e. (1) the direct blending of unmodified POSS nanoparticles into the CA casting solution and (2) covalent modification of POSS nanoparticles with CA homopolymer chains prior to inclusion in the CA casting solution. It was hypothesized that by covalently linking the POSS nanoparticles pendant to the CA homopolymers the nanoparticles would be anchored within the polymer matrix, thus reducing precipitation and/or sedimentation of the nanoparticles. Further it would allow for a homogeneous dispersion of the nanoparticles within the CA matrix, and inhibit or reduce surface migration of the POSS nanoparticles.

Modified CA polymers with pendant POSS groups (CA-POSS) have been prepared by chemical modification of commercially available CA with POSS nanoparticles; covalently coupled via isocyanate linking groups. The stable carbamate-cellulose acetate linkage formed is strongly resistant to both acid and alkaline hydrolysis [17]. The chemical composition of CA-POSS has been confirmed by ^{1}H NMR and ATR-FTIR spectroscopies, and the thermal properties investigated using thermogravimetric analysis (TGA).

CA-POSS and POSS were then tested as the additive in nanocomposite CA membranes, prepared via the phase inversion method [18]. The effects of varying the concentration of CA-POSS and POSS in the casting solution on the morphology and performance of CA membranes were investigated. SEM studies were done to investigate the morphology of the nanocomposite membranes. The compaction behaviour and permeation characteristics of the prepared membranes were evaluated using stirred-cell filtration of 2000 ppm NaCl solution. The changes in membrane morphology due to compaction were determined using dynamic mechanical analysis (DMA), and by analysing SEM cross-sectional images.

5.2 Results and Discussion

5.2.1 The synthesis of CA-POSS Additive

The POSS-modified cellulose acetate (CA-POSS) was synthesised via a two-step reaction as shown in Firgure 5.2. The first step was the formation of isocyanate-functionalised POSS. The POSS nanoparticle used in this study was aminopropyl isobutyl POSS. It has unreactive isopropyl groups on seven of the cage corners, and a reactive aminopropyl group on the eighth corner. Since there is only one reactive functionality, cross-linking is not possible and the POSS nanoparticles will exist as pendants on the CA chain. The toluene-2,4-diisocyanate (TDI) molecule has two isocyanate groups, each of which can react with a hydroxyl group to form a carbamate linkage. TDI is an asymmetric molecule and its two isocyanate groups have different reactivities. Due to steric hindrance within the molecule, the para-position reacts preferentially with the amine group of aminopropylisobutyl POSS [19]. In the second step the ortho-isocyanate of TDI was reacted, using a tin catalyst, with the hydroxyl groups on the CA backbone to form CA-POSS. The ratios were selected such that each CA chain had approximately four pendant POSS groups on average.

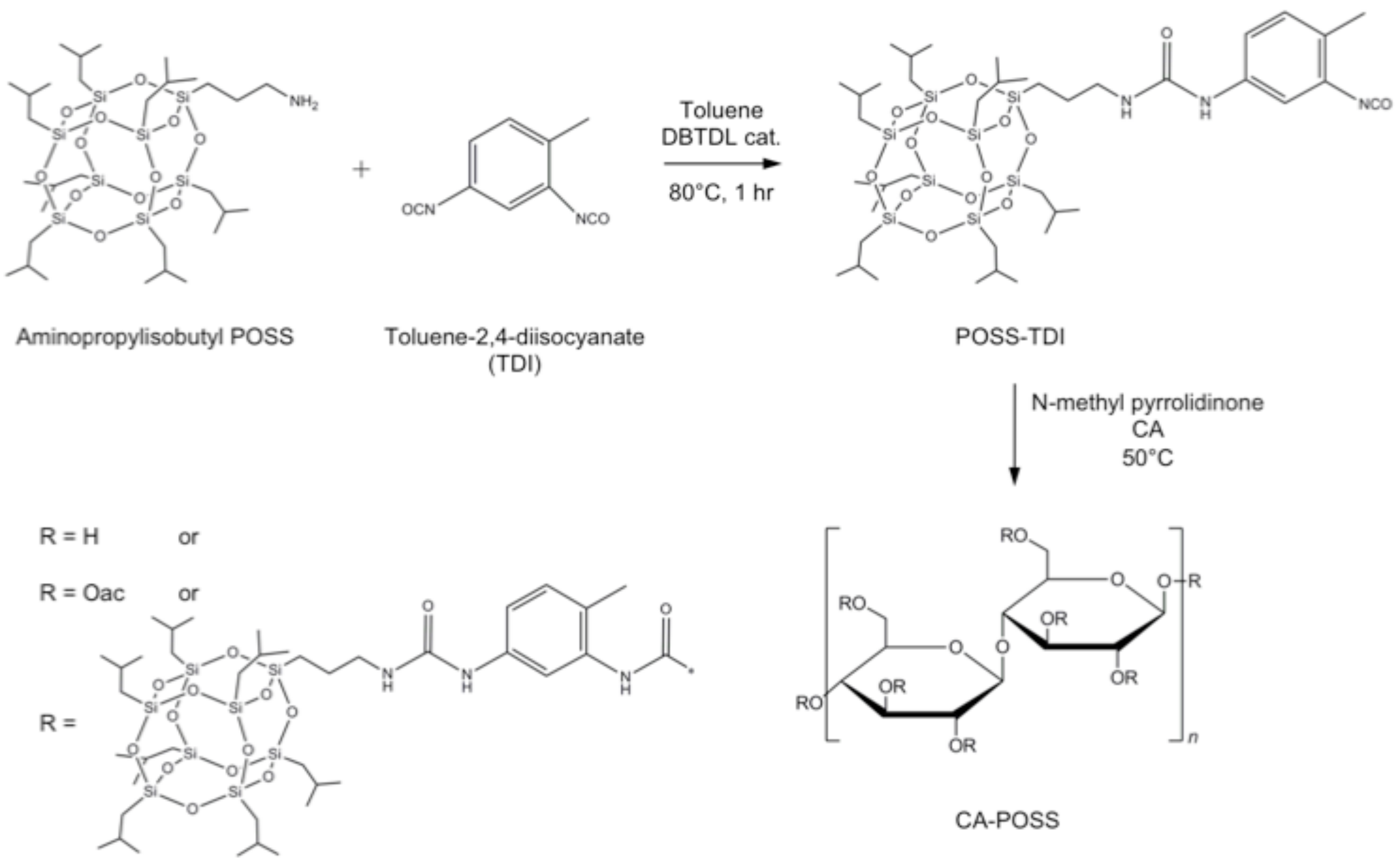

Figure 5.2. Synthetic method for preparation of CA-POSS

5.2.2 CA-POSS Characterisation

5.2.2.1 ATR-FTIR Analysis

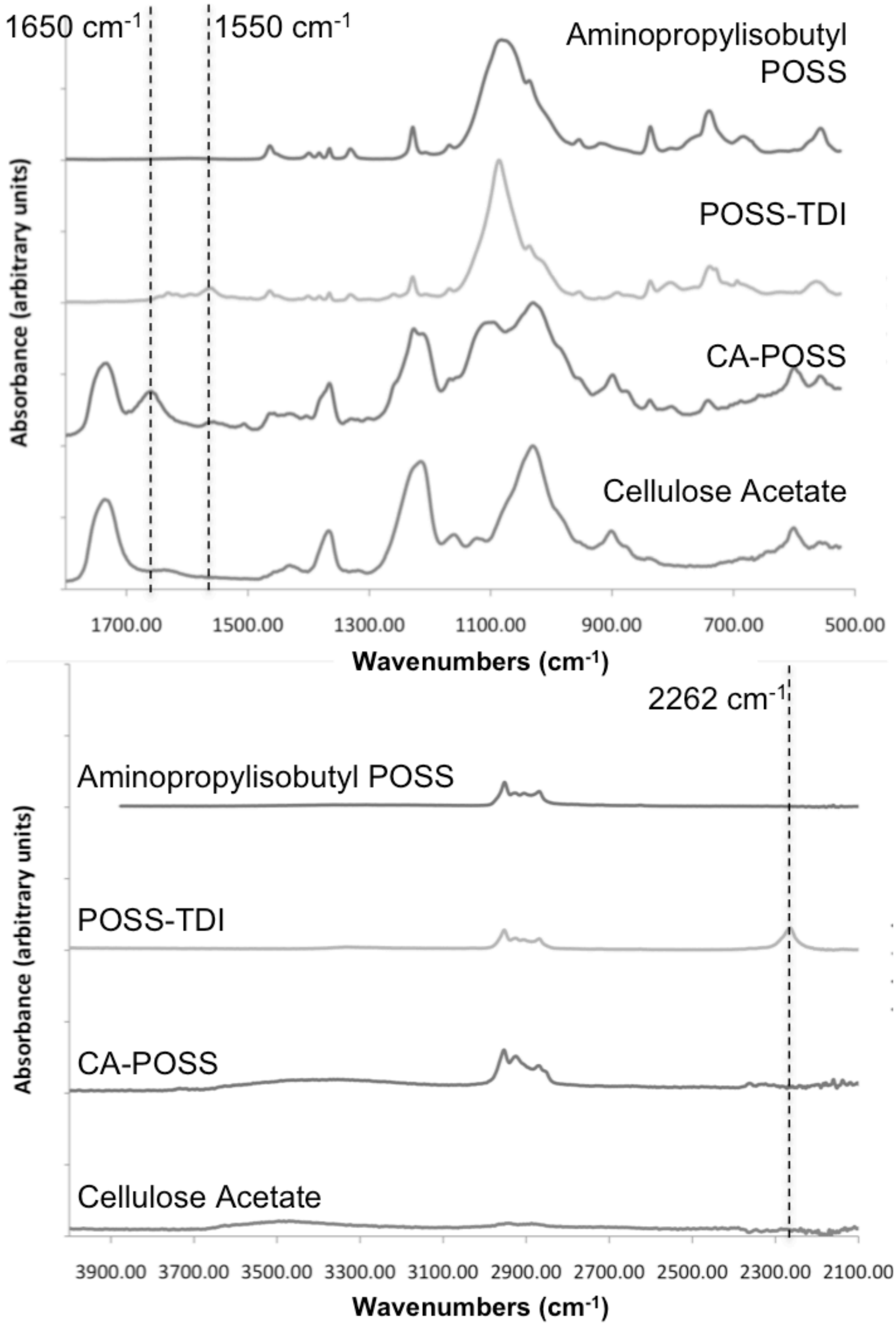

Figure 5.2. Absorbance spectra of aminopropylisobutyl POSS, POSS-TDI, CA-POSS and cellulose acetate in the range 500 to 1800 cm^{-1} (top), and 2100 to 4000 cm^{-1} (bottom).

The CA-POSS synthesis reaction was followed using ATR-FTIR. Figure 5.2 shows the spectra for POSS, POSS-TDI, CA-POSS and CA.

The ATR-FTIR spectrum of CA displays characteristic cellulosic peaks at 3484cm^{-1} (-OH stretching), 2944cm^{-1} and 2886cm^{-1} (asymmetric and symmetric C-H stretching, respectively), 1730cm^{-1} (C=O stretching), 1215cm^{-1} (carboxylate C-O stretch), 1161cm^{-1} (asymmetric stretching of the C-O-C bridge), and 1028cm^{-1} (stretching of pyranose ring C-O-C). Characteristic peaks for aminopropylisobutyl POSS are observed at 2800 - 2950 cm^{-1} (C-H bond vibration), ~1230 cm^{-1} (Si-C bonds), and ~1072 cm^{-1} (Si-O-Si cage structure) [20, 21]. In the spectrum of POSS-TDI, the appearance of a peak for the N-H bend at ~1550 cm^{-1} from the urea linkage formed between POSS and TDI, and the characteristic band for the isocyanate group (N=C=O) observed at ~2262 cm^{-1} indicate the completion of the POSS-TDI reaction [22, 23]. After the reaction of the POSS-TDI with cellulose acetate, the spectrum of CA-POSS retains much of the character of cellulose acetate, but notably has characteristic peaks at 2800 - 2950 cm^{-1} and ~1085 cm^{-1}, which are assigned for POSS. Also, the isocyanate peak from POSS-TDI (~2262 cm^{-}) is now absent, having been converted into a carbamate linkage (~1650 cm^{-1}), thus confirming the covalent attachment of POSS to CA via TDI. The peak assignmentss for some important bands are summarised in Table 5.1.

Table 5.1. Spectral band assignments comparing POSS, POSS-TDI and CA-POSS.

Peak Assignment	POSS	POSS-TDI	CA-POSS
POSS Si-C	1230	1230	1230
POSS Si-O-Si	1072	1080	1085
Urea linkage N-H bend	-	1550	1550
Isocyanate N=C=O	-	2262	-
Carbamate linkage C=O	-	-	1650

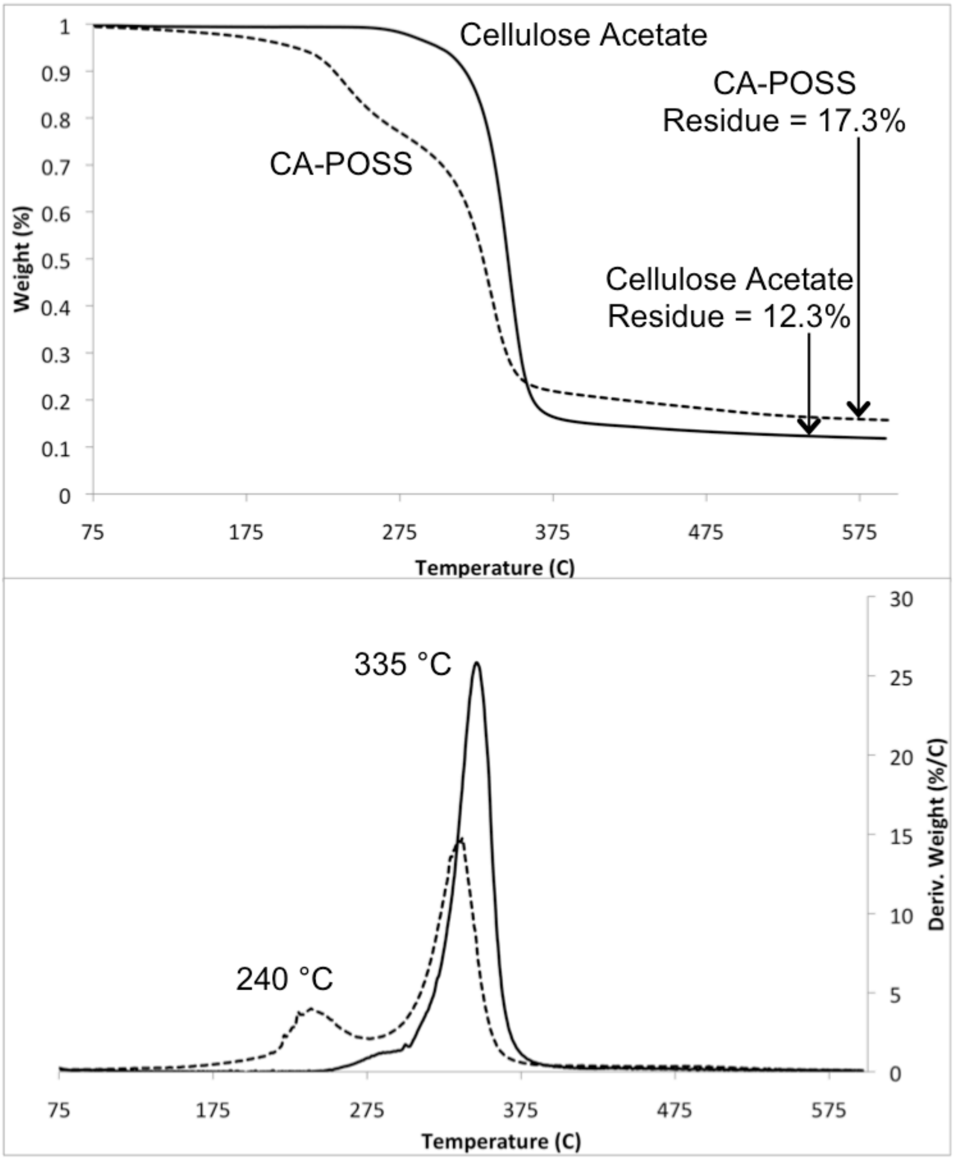

Figure 5.3. TGA and DTG thermograms of cellulose acetate and CA-POSS.

5.2.2.2 *Thermal Analysis*

CA-POSS was also characterised using thermogravimetric analysis. Figure 5.3 shows the TGA and DTG (first derivative) thermograms of cellulose acetate powder and CA-POSS over the temperature range of 75-600°C. After the loss of solvents, the cellulose acetate loses 83.6% of its weight in a single step between 250 and 400°C, and has 12.3% residue at 500°C. In contrast, the CA-POSS displays a two-step degradation mechanism, the first weight loss at ~240°C

(23.5%) is due to the cleavage of the carbamate linkage between the POSS and the cellulose acetate. The second weight loss is at ~335°C, and is due to the cellulose acetate. CA-POSS has 17.3% residue at 500°C. The difference in residues between CA and CA-POSS indicates that CA-POSS contains ~5 wt% POSS, which is comparable to the 8 wt% POSS content predicted from calculations.

5.2.3 Nanocomposite Membrane Casting

Cellulose acetate membranes were made via the phase inversion method, as described in Chapter 1 (page 14).

Since there are many variables that effect membrane casting, only three were varied for this study: the additive used (unmodified POSS, anchored CA-POSS or none), the composition of the casting solution, and the substrate onto which the membrane was cast. The casting conditions are summarised in Table 5.2. Membranes were cast onto non-woven Hollytex substrate on a glass plate using a doctors blade with the height set at 250 μm. The solvent was allowed to evaporate for 90 seconds before the membranes were immersed in the quenching bath for 90 minutes at 0°C. Next they were annealed at 90°C for 10 minutes. After annealing the membranes were either stored in water until used in the stirred-cell, or dried by exchanging solvents with isopropanol, then hexane, then drying in air.

Table 5.2. Nanocomposite membrane casting variables and conditions.

Casting Variable	**Fixed**	**Changing**
Polymer	CA (39.8 wt%, Mw 30,000)	
Solvents	Methanol	
Additives	Formamide	None/POSS/CA-POSS
Casting solution composition		Additive:CA:MeOH:Formamide xg : 5-xg : 11.5mL : 5.3mL
Quench medium	Water (0°C) 90 minutes	
Annealing Bath	Water (90°C) 10 minutes	
Casting atmosphere	Laboratory conditions	
Evaporation time	90 seconds	
Casting thickness	250 μm	
Casting speed	By hand	
Membrane support material		Glass/Hollytex
Drying conditions	Isopropanol, n-hexane, air	

To investigate the effect of the CA-POSS as a nanofiller, cellulose acetate membranes (CAMs) were cast from the solutions shown in Table 5.3. For all compositions 11.5 mL of acetone as the solvent, and 5.3 mL of formamide as the swelling agent were used. The concentration of cellulose acetate was varied according to the amount of filler used, so that the total mass added was 5.0 g. The additive was either POSS or CA-POSS at 0.5, 1.0 or 5.0 weight % loading. For example, 5.0 weight % of POSS is equivalent to 0.025 g, therefore 4.975 g of cellulose acetate was used.

Table 5.3. Membrane casting solution formulations.

Additive	**Additive (g)**	**wt% POSS**	**CA (g)**	**Acetone (mL)**	**Formamide (mL)**
none	0	0	5	11.5	5.3
CA-POSS	0.41	1	4.59	11.5	5.3
CA-POSS	2.07	5	2.93	11.5	5.3
CA-POSS	0.205	0.5	4.795	11.5	5.3
POSS	0.05	1	4.95	11.5	5.3
POSS	0.25	5	4.75	11.5	5.3
POSS	0.025	0.5	4.975	11.5	5.3

Membranes are labelled according to their additive and weight % loading, for example POSS 5.0 wt% represents the membrnae with the unmodified POSS additive at a loading of 5.0 weight percent. Particle dispersion in the cast membranes was investigated using FTIR and EDAX.

5.2.4 Particle Dispersion in CA Membranes

5.2.4.1 ATR-FTIR Analysis

ATR-FTIR analysis was performed to confirm the presence of POSS in the nanocomposite membranes, and to compare different POSS loadings. Figure 5.4 shows the spectra for an unmodified CA control membrane, CA-POSS additive and a nanocomposite membrane in the range 900-1500 cm^{-1}. For clarity, the data for only one nanocomposite (CA-POSS 5.0 wt%) is shown.

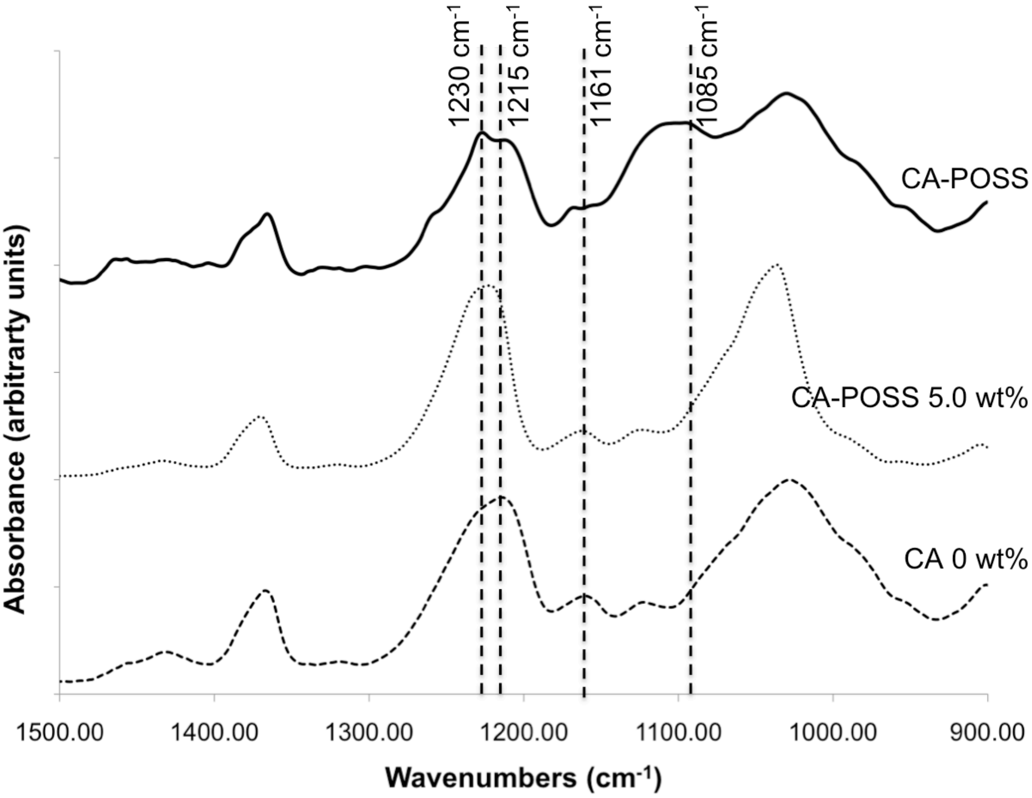

Figure 5.4. ATR-FTIR of CA control membrane, CA-POSS additive and nanocomposite containing 5wt% CA-POSS.

The spectra of the CA membrane and the POSS-containing membrane are almost identical, which is to be expected given the low loading of POSS. However, differences can be seen in the relative intenisites of the peaks for CA compared to POSS. For example, in the CA-POSS spectrum there is a peak at 1230 cm^{-1} that corresponds to the Si-C peak of POSS, in the nanocomposite spectrum of CA-POSS 5 wt% the intensity of this peak has increased relative to the CA C-O peak at 1215 cm^{-1}.

Table 5.4 shows the nanocomposite membrane relative peak intensities for bands contributed by POSS and CA. For the CA-POSS nanocomposites, the ratio of 1161 cm^{-1} (CA C-O-C) to 1085 cm^{-1} (POSS Si-O-Si) decreases with increasing POSS loading, from 0.81, to 0.80 to 0.58 at 0.5 wt%, 1.0 wt% and 5.0 wt%, respectively. This is also true for the ratio of 1215 cm^{-1} (CA C-O) to 1230 cm^{-1}

(POSS Si-C), which decreases from 1.08, to 1.04, to 1.03 as the CA-POSS loading increases from 0.5 to 1.0 to 5.0 wt%, respectively. This confirms the presence of POSS within the nanocomposites. For the POSS composites the ratio for both 1161 cm^{-1} (CA C-O-C) to 1085 cm^{-1} (POSS Si-O-Si) and 1215 cm^{-1} (CA C-O) to 1230 cm^{-1} (POSS Si-C) actually increases slightly from 0.5 wt% loading to 1.0 wt% loading before decreasing again for 5.0 wt% loading.

Table 5.4. Relative peak intensities for nanocomposite membranes.

Membrane	Weight % additive	Ratio 1161/1085	Ratio 1215/1230
CA	0	0.84	1.08
CA-POSS	0.5	0.81	1.08
CA-POSS	1.0	0.80	1.04
CA-POSS	5.0	0.58	1.03
POSS	0.5	0.75	1.10
POSS	1.0	0.85	1.11
POSS	5.0	0.60	1.02

The reason for the apparent inconsistency is not evident from the FTIR data, but leaching and agglomeration were investigated as possible causes by using SEM coupled with Energy Dispersive X-ray Microanalysis (EDAX) of the membrane surfaces to further investigate particle dispersion in the cast membranes.

5.2.4.2 SEM and EDAX Analysis

SEM was used to image the composite membranes and EDAX was used to compare the height of the carbon peak (CK) to the height of the silicon peak (SiK) to gauge how the Si content varied relative to the C content. EDAX was performed by focussing the electron beam onto a small area from which x-rays were generated. The size of the beam was similar for each area examined.

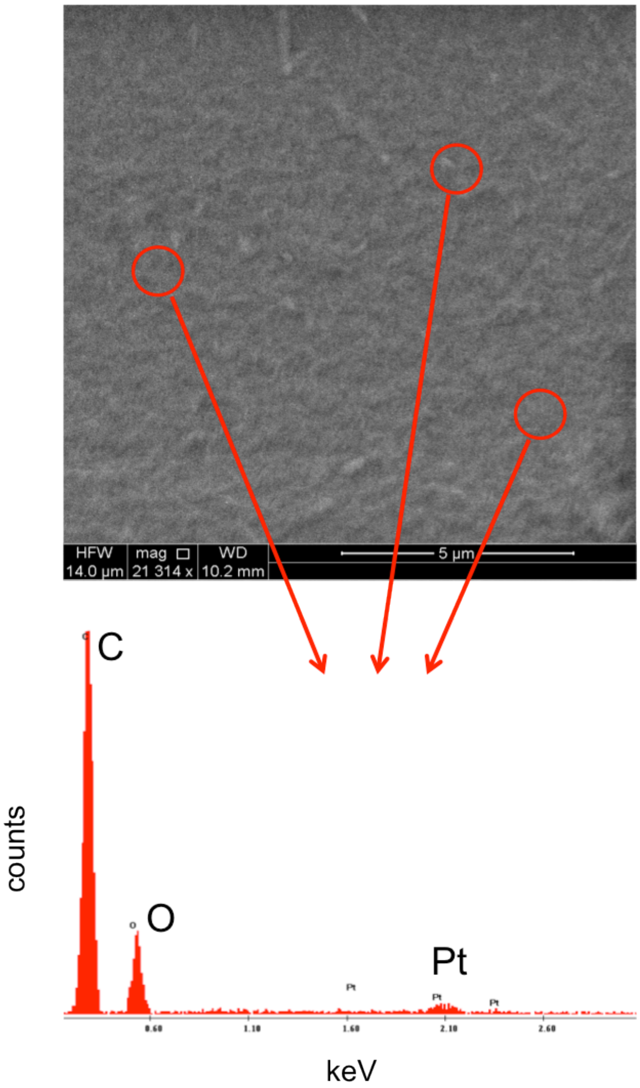

Figure 5.5. SEM and EDAX results for different areas on cast CA.

Figure 5.5 shows a typical SEM image for the CA control membrane (scale bar is 5 µm). The membrane surface was nodulated uniformly across the entire membrane surface with no apparent phase differences. Three areas (circled) were chosen at random for analysis by EDAX. The spectra obtained contained only the expected carbon (~0.28 keV), oxygen (~0.5 keV), and platinum (~2.1 keV, from the sputter coating applied to the membrane for SEM analysis). Since the CA matrix contains no silicon, no silicon was observed as expected.

Figure 5.6 shows a typical SEM image for the POSS 1wt% nanocomposite membrane (scale bar is 5 µm). Most of the membrane appears to be relatively uniform, however there were some examples of crystals sitting on the membrane surface, and some lighter regions within the membrane material, ranging in size from 1.0 to 2.0 µm. Three areas (circled) were chosen for analysis by EDAX. All three areas showed the presence of carbon (~0.28 keV), oxygen (~0.5 keV), from the polymer matrix, and platinum (~2.1 keV) due to sputter coating. The crystal sitting on the surface appears to be salt because it also exhibits a sodium peak at ~1.0 keV, most likely an artefact from the casting process. The lighter regions contained a peak at ~1.7 keV, corresponding to silicon. No silicon was observed outside of the lighter regions, indicating agglomeration of the POSS nanoparticles within the lighter regions.

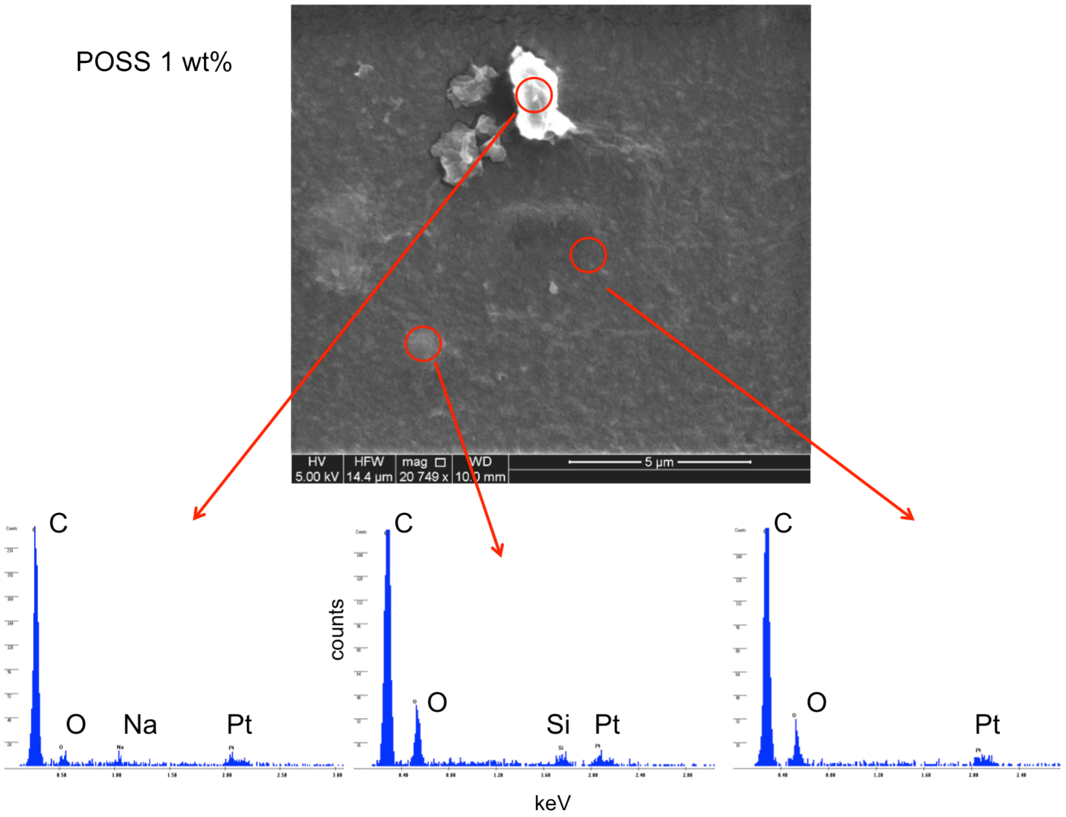

Figure 5.6. SEM and EDAX results for different areas on the cast POSS 1wt% nanocomposite membrane.

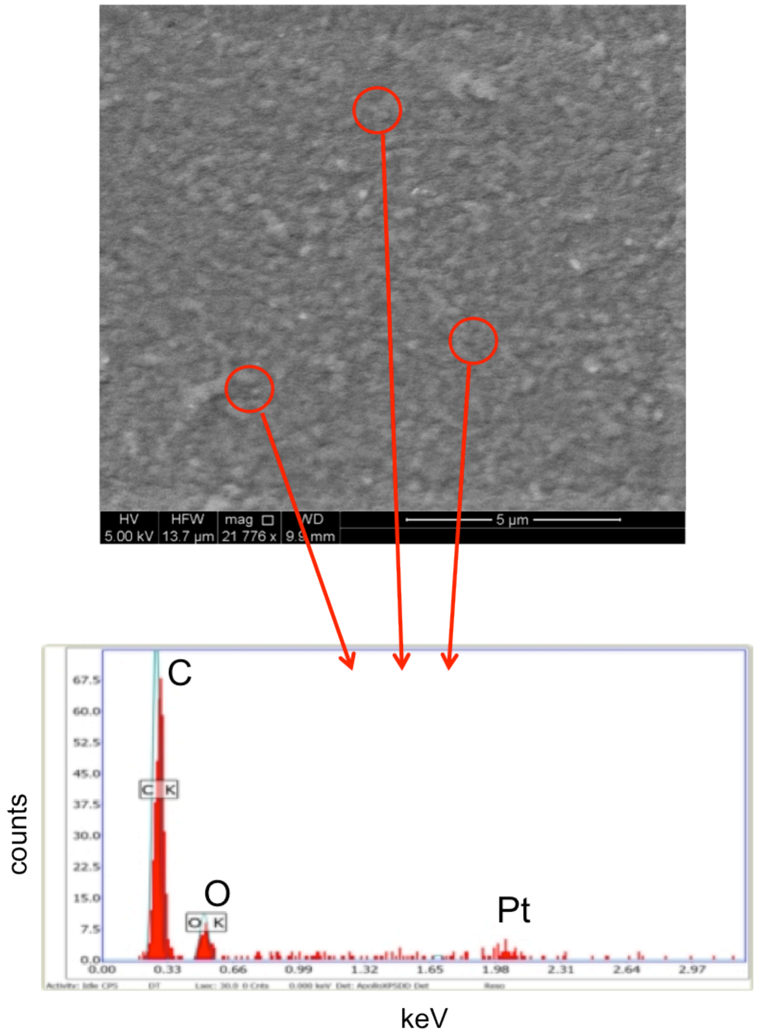

Figure 5.7. SEM and EDAX results for different areas on the cast CA-POSS 1wt% nanocomposite membrane.

Figure 5.7 shows a typical SEM image for the CA-POSS 1wt% nanocomposite membrane (scale bar is 5 μm). This membrane had a consistent texture across the surface of the membrane. No lighter areas were observed as in the POSS nanocomposite. Three random areas (circled) were analysed by EDAX, and gave essentially the same spectrum, containing carbon (~0.28 keV), oxygen (~0.5 keV), and platinum (~2.1 keV), but no silicon was observed. In the absence of accumulation of POSS the Si concentration is below the detectable threshold. Thus indicating that the covalent attachment of POSS to cellulose acetate before membrane casting helps to reduce POSS aggregation at the membrane surface, and results in good dispersion of the nanoparticles throughout the membrane compared to the unmodified POSS nanoparticle additive.

5.2.5 Changes in RO membrane flux and rejection due to compaction

The cast membranes were tested for salt rejection and water flux using stirred-cell apparatus operating in dead-end flow conditions. They were initially compacted for several hours using MIlliQ water under 1000 KPa of pressure, then flux and salt rejection data was collected for 2000 ppm NaCl solution under 1000 KPa of pressure.

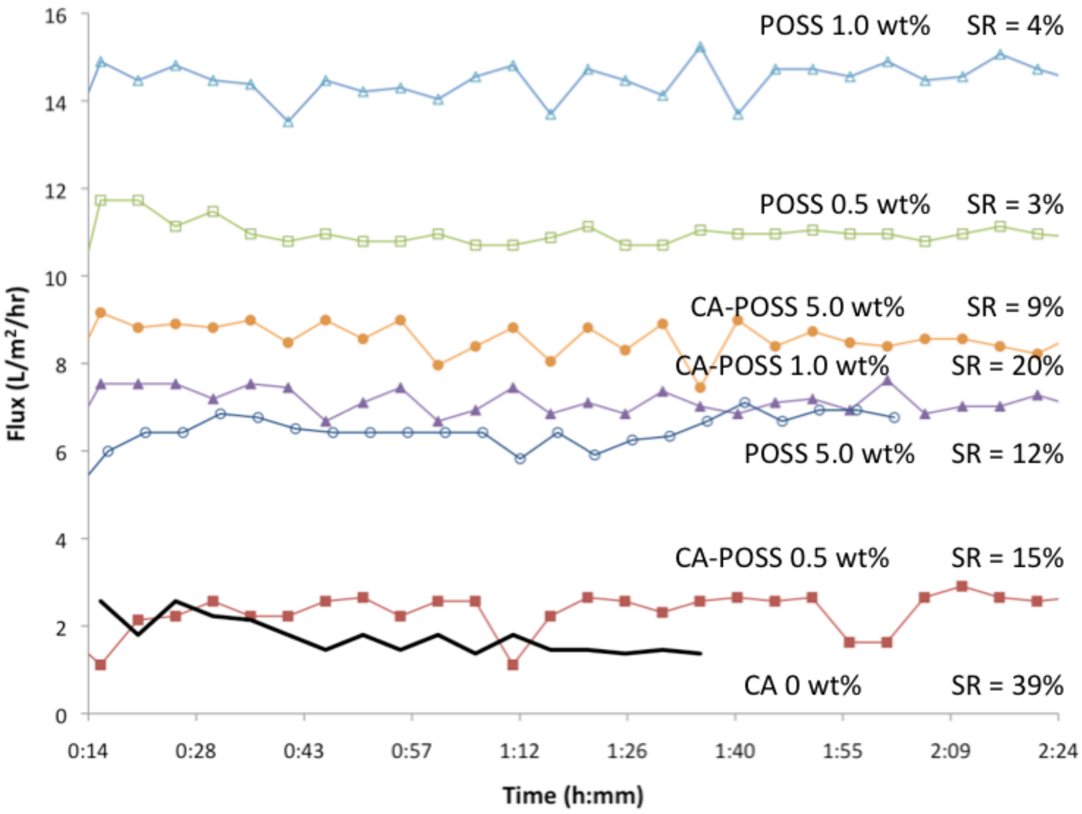

Figure 5.8. Stirred-cell data showing 2000 ppm NaCl solution flux over time for cast membranes with varying amounts of incorporated nanoparticles.

The results shown in Figure 5.8 reveal that all nanocomposite membranes had increased flux, relative to an unmodified cellulose acetate control membrane, with the exception of CA-POSS 0.5 wt%, which has approximately the same flux.

For the anchored additive CA-POSS, the flux increased with increasing nanoparticle loading, from 2.2 L/m^2/hr for 0.5 wt%, to 6.8 L/m^2/hr for 1.0 wt% and 8.3 L/m^2/hr for 5.0 wt%. Meanwhile the salt rejection initially increased, and then decreased with increasing nanoparticle loading, from 15% at for 0.5 wt%, to 20% for 1.0 wt% and 9% for 5.0 wt%. For the unanchored POSS particle the flux initially increased with nanoparticle loading, from 10.6 L/m^2/hr for 0.5 wt% to 13.8 L/m^2/hr for 1.0 wt%. However, as the loading increased to 5.0 wt% the flux decreased again to 5.7 L/m^2/hr. The salt rejection was roughly the same for 0.5 wt% and 1.0 wt% loadings of POSS (3% and 4%, respectively), and increased to 12% at 5.0 wt% loading.

Pendergast *et al.* [7] also saw increased flux for nanocomposite-polysulfone membranes, and attributed this to enhanced mechanical strength imparted by the nanoparticles. In this case, however, the salt rejection was also decreased roughly inversely proportional to flux increase, leading to the hypothesis that the nanoparticles are acting to open pores in the membrane structure, increasing the flux of both water and salt.

5.2.6 Changes in membrane morphology due to compaction

The effect of compaction on the morphology of the nanocomposite membranes was investigated using SEM to image cross-sections of the membranes pre-compaction (as-cast) and post compaction at 1000 KPa in the stirred-cell. The samples were prepared by snapping in liquid nitrogen, and mounting between two plates before platinum coating and imaging. Thicknesses reported are the mean of at least five measurements taken at random areas of the membrane sample.

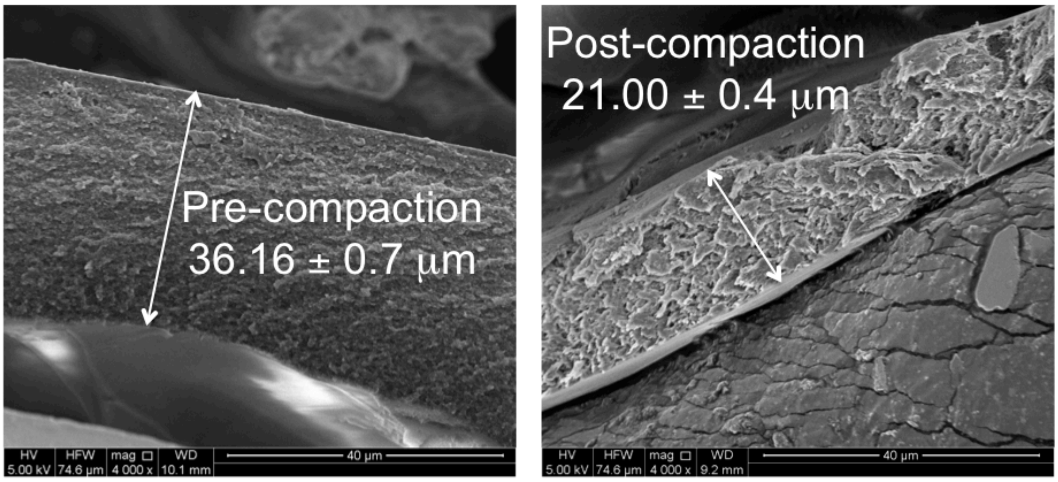

Figure 5.9. Cross-sectional SEM images of unmodified CA membrane before and after compaction at 1000 KPa. Scale bar is 40μm.

For the unmodified CA control membrane the pre-compaction thickness was 36.16 ± 0.7 μm. After compaction the thickness was 21.00 ± 0.4 μ, representing a 42% decrease in membrane thickness (Figure 5.9). The nanocomposite membrane CA-POSS 0.5 wt% had pre-compaction and post-compaction thicknesses of 28.66 ± 0.3 μm, and 28.63 ± 1.6 μm, respectively, representing just a 0.1% decrease in membrane thickness (Figure 5.10).

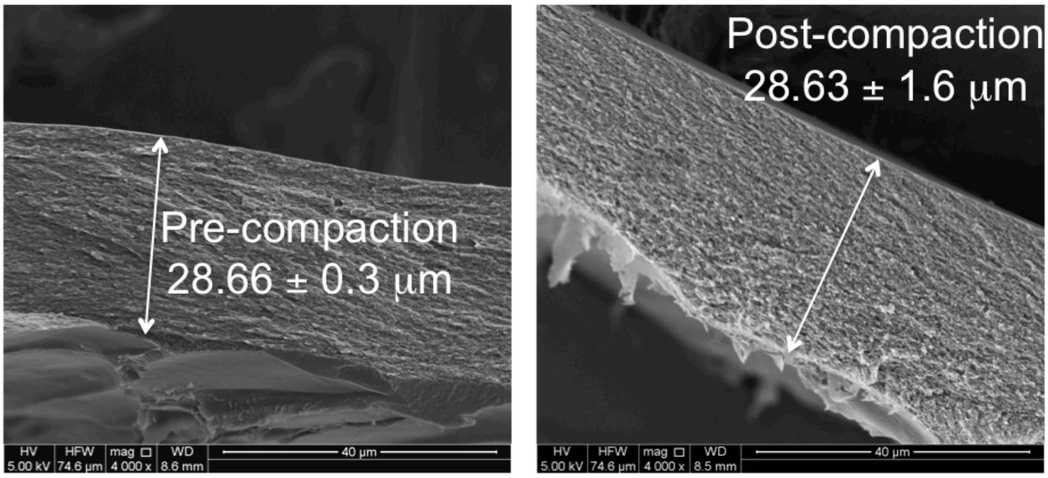

Figure 5.10. Cross-sectional SEM images of nanocomposite membrane CA-POSS 0.5 wt% before and after compaction at 1000 KPa. Scale bar is 40μm.

The compaction data for all of the cast membranes is represented in Table 5.5. All of the nanocomposite membranes underwent less compaction than the unmodified CA control membrane, except for CA-POSS 5.0 wt%. Additionally, each of the additives displayed increasing compaction with increasing nanoparticle wt% inclusion. The CA-POSS nanocomposite membranes increased from 0.1 % change in thickness for 0.5 wt% loading, to 25% change in thickness for 1.0 wt% loading, and 62% change in thickness for 5.0 wt% loading. Similarly, the POSS additive nanocomposite membranes showed increased % change in thickness as the nanopoarticle loading increased, from -11%, to 25%, to 34%, for 0.5, 1.0 and 5.0 wt% loading, respectively.

Table 5.5. Compaction data for nanocomposite membranes.

Membrane	Weight % Additive	Precompaction Thickness (μm)	Post-compaction Thickness (μm)	% Change in Thickness
CA	0	36.16 ± 0.7	21.00 ± 0.4	42
CA-POSS	0.5	28.66 ± 0.3	28.63 ± 1.6	0.1
CA-POSS	1.0	48.06 ± 0.5	36.26 ± 1.2	25
CA-POSS	5.0	46.10 ± 1.3	17.63 ± 0.7	62
POSS	0.5	28.60 ± 1.4	31.63 ± 0.3	-11
POSS	1.0	41.24 ± 0.6	30.76 ± 0.8	25
POSS	5.0	67.69 ± 1.5	44.64 ± 0.5	34

The thickness data presented here should be considered semi-quantitative at best, because there is variation in thickness across a membrane, and also the thickness can sometimes be distorted during the process of snapping the membranes for imaging. This is the most likely reason for the slight increase in thickness observed after compaction for the nanocomposite POSS 0.5 wt%. Pendergast *et al*. [7] also observed some increases in nanocomposite membrane thickness after compaction in polysulfone membranes, and attributed this to local variations in imaging.

POSS particles are not apparent in any of the images, and it was not possible to perform EDAX in cross-section due to the extremely low counts. Therefore, it was not possible to determine the location or dispersion of the POSS nanoparticles.

5.2.7 Nanocomposite Mechanical Strength

Dynamic mechanical analysis (DMA) was used in order to gauge the effect of the nanoparticles on the mechanical properties of the nanocomposite membranes. The storage modulus E’ gives an indication of the stiffness of the material, it is plotted as a function of temperature for the POSS and CA-POSS nanocomposites and a CA control in Figure 5.11 and Figure 5.12 , respectively.

The CA control displays a decreasing storage modulus with increasing temperature, with a transition from the higher storage modulus glassy state, to a lower storage modulus rubbery state around 80 - 120°C. Other groups have reported increased storage modulus with increasing nanoparticle loading [24]. In this case, all nanocomposite membranes, except for POSS 1.0 wt%, showed a decrease in storage modulus, relative to the CA control. The inclusion of nanoparticles appears to be having a plasticising effect because the modulus in the glassy region is reduced, and the transition to the rubbery region occurs at lower temperatures [25].

Plasticisation occurs when there is a reduction in the interaction between neighbouring polymer chains, leading to more chain mobility [26]. The result is a decrease in membrane stiffness and Tg, an increase in permeability, and a loss of selectivity [26]. Plasticisation rather than pore-opening could be an explanation for the stirred-cell results of the composite membranes.

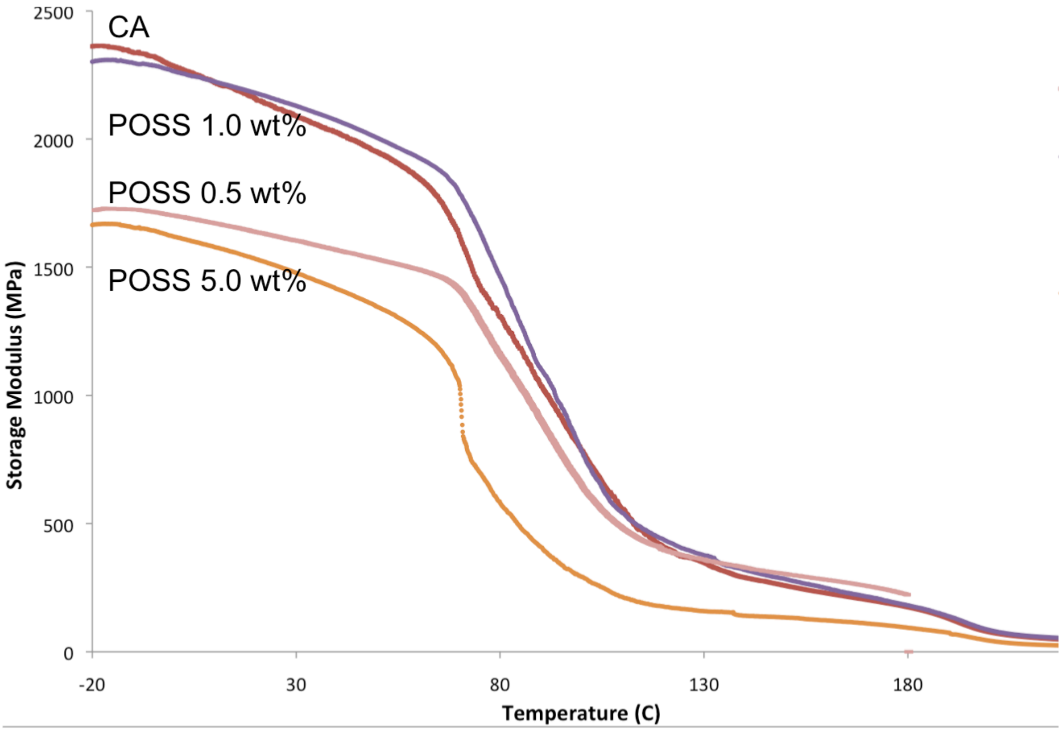

Figure 5.11. Storage modulus for POSS composites and CA control.

As shown in Figure 5.11, the storage modulus for POSS 1.0 wt% starts slightly below CA but is more stable as the temperature increases, indicating that the POSS additive is acting to stiffen the membrane matrix. POSS 0.5 wt% also has a more stable storage modulus, while POSS 5.0 wt% decreases quickly. Kopesky *et al*. [27] reported similar results to those seen for the POSS composites, when forming POSS composites with PMMA. At the lowest loading the modulus was slightly lower than for an unmodified control membrane, they attributed this to the small fraction of molecularly dispersed POSS. As the loading increased they saw an increase in modulus due to the dominance of phase-separated crystallites with small diameter. Finally, the modulus was decreased at the highest loadings, as larger POSS crystallites significantly weakened the material. The current data follows the same pattern.

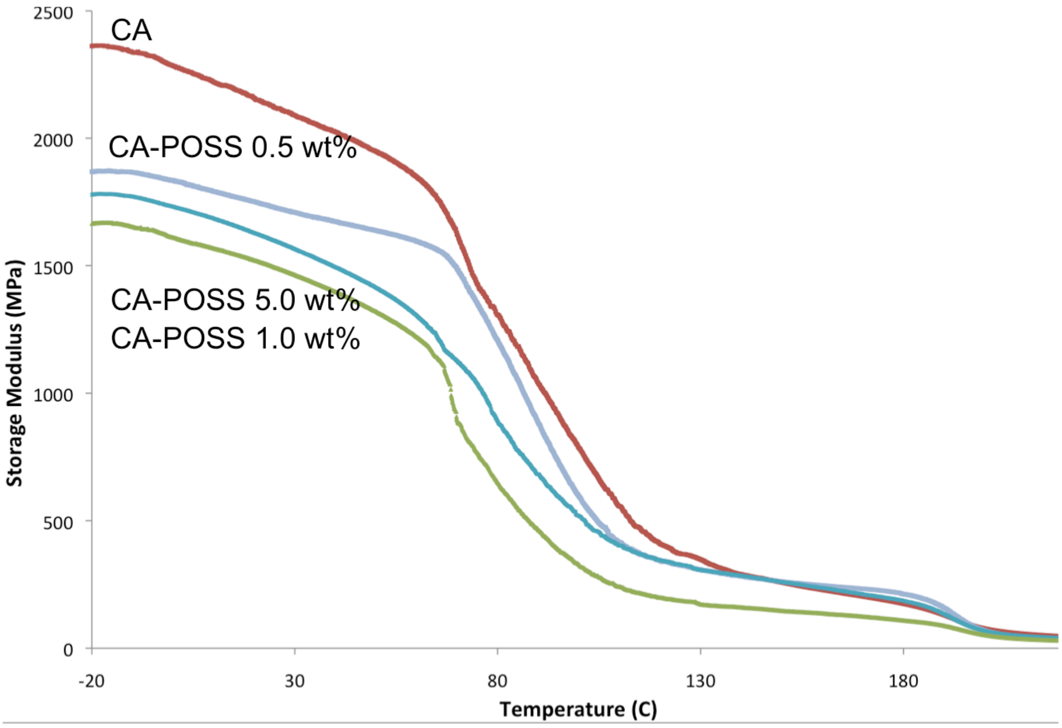

Figure 5.12. Storage modulus for CA-POSS nanocomposites and CA control.

For the CA-POSS nanocomposites (Figure 5.12) the 0.5 wt% loading showed a stiffening effect, with increased storage modulus stability compared to the CA control. Storage modulus for nanoparticle loadings of 1.0 wt% and 5.0 wt% decrease at a similar rate to the control. When Hartmann-Thompson *et al*. [28] made sulfonated polyphenylsulfone nanocomposites containing POSS functionalised with sulfonic acid groups, mixed sulfonic acid and alkyl groups, and phosphonic acid groups, they also observed a reduction in mechanical strength, relative to a control.

5.3 Conclusions

Nanocomposite membranes were cast with 0.5, 1.0 or 5.0 weight % of either POSS or anchored CA-POSS as additives. The anchored CA-POSS additive showed better dispersion than POSS as evidenced by FTIR and XPS. All nanocomposite membranes showed increased water flux; relative to an unmodified CA control membrane. Salt rejection values suggested a pore-opening effect. DMA showed a decrease in storage modulus for most nanocomposite membranes, indicating a plasticisation effect. Membrane compaction was mitigated at loadings of 0.5 wt% for both POSS and CA-POSS additives. Overall, anchoring the POSS had a greater effect on dispersion of CA-POSS compared to POSS nanofiller, than filtration and mechanical properties.

References

1. T. Chung; L. Jiang; Y. Li; S. Kulprathipanja. Mixed Matrix Membranes (MMMs) Comprising Organic Polymers with Dispersed Inorganic Fillers for Gas Separation, Progress in Polymer Science 32 (2007) 483-507.
2. B.-H. Jeong; E. Hoek; Y. Yan; A. Subramani; X. Huang; G. Hurwitz; A. Ghosh; A. Jawor. Interfacial Polymerisation of Thin Film Nanocomposites: A New Concept for Reverse Osmosis Membranes, Journal of Membrane Science - Rapid Communication 294 (2007) 1-7.
3. L. Li; J. Dong; T. Nenoff; R. Lee. Desalination by Reverse Osmosis Using MFI Zeolite Membranes, Journal of Membrane Science 243 (2004) 401-404.
4. Y. Yang; H. Zhang; P. Wang; Q. Zheng; J. Li. The Influence of Nano-Sized TiO_2 Fillers on the Morphologies and Properties of PSF UF Membrane, Journal of Membrane Science 288 (2007) 231-238.
5. J. Holt; H. Park; Y. Wang; M. Staderman; A. Artyukhin; C. Grigoropoulos; A. Noy; O. Bakajin. Fast Mass Transport through Sub–2-Nanometer Carbon Nanotubes, Science 312 (2006)
6. R. Abedini; S. Mousavi; R. Aminzadeh. A Novel Cellulose Acetate (CA) Membrane Using TiO_2 Nanoparticles: Preparation, Characterization and Permeation Study, Desalination 277 (2011) 40-45.
7. M. Pendergast; J. Nygaard; A. Ghosh; E. Hoek. Using Nanocomposite Materials Technology to Understand and Control Reverse Osmosis Membrane Compaction, Desalination 261 (2010) 255-263.
8. G. Arthanareeswaran; T. Sriyamuna Devi; M. Raajenthiren. Effect of Silica Particles on Cellulose Acetate Blend Ultrafiltration Membranes: Part I, Separation and Purification Technology 64 (2008) 38-47.
9. H. Takahashi; B. Li; T. Sasaki; C. Miyazaki; T. Kajino; S. Inagaki. Catalytic Activity in Organic Solvents and Stability of Immobilized

Enzymes Depend on the Pore Size and Surface Characteristics of Mesoporous Silica, Chemistry of Materials 12 (2000) 3301-3305.

10. D. Cordes; P. Lickiss; F. Rataboul. Recent Developments in the Chemistry of Cubic Polyhedral Oligosilsesquioxanes, Chemical Reviews 110 (2010) 2081-2173.
11. R. Kannan; H. Salacinski; M. Odlyha; P. Butler; A. Seifalian. The Degradative Resistance of Polyhedral Oligomeric Silsesquioxane Nanocore Integrated Polyurethanes: An in Vitro Study, Biomaterials 27 (2006) 1971-1979.
12. M. Tsai; W. Whang. Dynamic Mechanical Properties of Polyimide/ Poly(Silsesquioxane)-Like Hybrid Films, Journal of Applied Polymer Science 81 (2001) 2500-2516.
13. R. Bouma; A. Checchetti; G. Chidichimo; E. Drioli. Permeation through a Heterogeneous Membrane: The Effect of the Dispersed Phase, Journal of Membrane Science 128 (1997) 141-149.
14. M. Bleha; G. Tishchenko; Z. Pientka; J. Brus. Effect of POSS Functionality on Morphology of Thin Hybrid Chitosan Films, Designed Monomers and Polymers 7 (2004) 25-43.
15. K. Tanaka; S. Adachi; Y. Chujo. Structure-Property Relationship of Octa-Substituted Poss in Thermal and Mechanical Reinforcements of Conventional Polymers, Journal of Polymer Science: Part A: Polymer Chemistry 47 (2009) 5690-5697.
16. K. Xie; Y. Zhang; Y. Yu. Preparation and Characterization of Cellulose Hybrids Grafted with the Polyhedral Oligomeric Silsesquioxanes (POSS), Carbohydrate Polymers 77 (2009) 858-862.
17. W. Hearon; G. Hiatt; C. Fordyce. Carbamates of Cellulose and Celllulose Acetate. II. Stability toward Hydrolysis, Journal of the American Chemical Society 65 (1943) 833-836.

18. S. Nunes; K. Peinemann, *Membrane Technology in the Chemical Industry*. 2nd ed.; Wiley-VCH.
19. D. Simons; R. Arnold. Relative Reactivity of the Isocyanate Groups in Toluene-2,4-Diisocyanate, Journal of the American Chemical Society 78 (1956) 1658-1659.
20. J. Zhou; Y. Zhao; K. Yu; X. Zhou; X. Xie. Synthesis, Thermal Stability and Photoresponsive Behaviors of Azobenzene-Tethered Polyhedral Oligomeric Silsesquioxanes, New Journal of Chemistry 35 (2011) 2781-2792.
21. D. Yei; S. Kuo; Y. Su; F. Chang. Enhanced Thermal Properties of PS Nanocomposites Formed from Inorganic POSS-Treated Montmorillonite, Polymer 45 (2004) 2633-2640.
22. C. Jose. Infrared Spectra of Substituted Ureas—I. Alkyl Ureas, Spectrochimica Acta Part A: Molecular Spectroscopy 25 (1969) 111-118.
23. J. Girones; M. Pimenta; F. Vilaseca; C. A.; P. Mutje; A. Curvelo. Blocked Isocyanates as Coupling Agents for Cellulose-Based Composites, Carbohydrate Polymers 68 (2007) 537-543.
24. J. Jordan; K. Jacob; T. R.; M. Sharaf; I. Jasiuk. Experimental Trends in Polymer Nanocomposites—a Review, Materials Science and Engineering A 393 (2005) 1-11.
25. E. Kopesky; T. Haddad; G. McKinley; R. Cohen. Miscibility and Viscoelastic Properties of Acrylic Polyhedral Oligomeric Silsesquioxane–Poly(Methyl Methacrylate) Blends, Polymer 46 (2005) 4743-4752.
26. A. Ismail; W. lorna. Penetrant-Induced Plasticization Phenomenon in Glassy Polymers for Gas Separation Membrane, Separation and Purification Technology 27 (2002) 173-194.
27. E. Kopesky; G. McKinley; R. Cohen. Toughened Poly(Methyl Methacrylate) Nanocomposites by Incorporating Polyhedral Oligomeric Silsesquioxanes, Polymer 47 (2006) 299-309.

28. C. Hartmann-Thompson; A. Merrington; P. Carver; D. Keeley; J. Rousseau; D. Hucul; K. Bruza; L. Thomas; S. Keinath; R. Nowak; D. Katona; P. Santurri. Proton-Conducting Polyhedral Oligosilsesquioxane Nanoadditives for Sulfonated Polyphenylsulfone Hydrogen Fuel Cell Proton Exchange Membranes, Journal of Applied Polymer Science 110 (2008) 958-974.

6 Conclusions and Recommendations

In this thesis cellulose acetate reverse osmosis membranes have been modified using two techniques: polymeric membrane surface modification; and the incorporation of nanoparticles. This chapter summarises the main conclusions drawn from this research and offers recommendations and suggestions for future work where appropriate.

The aims of this thesis were to develop cellulose acetate (CA) reverse osmosis (RO) membranes with reduced biofouling, increased energy efficiency and extended lifetime by investigations in two areas of membrane modification: polymeric surface modification and incorporation of nanoparticles. Seven key objectives were outlined in Chapter One. Here, the conclusions for each one are discussed, and recommendations proposed.

The first area of research was membrane surface modification via polymeric grafting.

6.1 Surface modification of CA RO membrane using commercially attractive radical polymerisation techniques.

A detailed study of the modification of CA membrane surfaces with pHEMA was undertaken. In the first step, the membrane -OH groups were substituted with known ATRP initiator BiBBr, as confirmed by FTIR and XPS data. TEA and BiBBr needed to be injected simultaneously to maintain pH, and reaction times beyond 3 hours gave no further product.

In the second part of the reaction pHEMA chains were successfully grafted from the surface of commercially available cellulose acetate reverse osmosis membranes using surface-initiated ARGET ATRP. The polymerization conditions were designed to create an industrially attractive process, by using low ppm levels of copper catalyst, half the amount of methanol solvent, and environmentally friendly reducing agent ascorbic acid. Sacrificial initiator was not employed since it leads to excess polymer adhering to the membrane surface, even in the absence of surface initiator. A new TGA DTG peak was observed at 410 °C for modified membranes, corresponding to pHEMA degradation.

6.2 Optimisation of reaction conditions to achieve a range of polymer graft-densities.

Reaction kinetics and FTIR confirmed the livingness of the polymerisation reaction, showing increasing polymer graft density with increasing reaction times and increasing monomer concentrations. This was the first time pHEMA had been grafted from cellulose acetate using ARGET ATRP.

Modified membranes were imaged using SEM and the morphology confirmed results from other characterisation techniques. Namely, the polymer layer became thicker and more nodulated with increasing graft density. Modified membranes were tested by AFM for surface roughness and were shown to increase in roughness with increasing graft density. Water contact angle (WCA) measurements showed evidence for the reorientation of the pHEMA chains from wet to dry and depending on graft density. WCA increased with increasing graft density, indicating that the pHEMA chains had rearranged upon drying to expose the hydrophobic backbone. Once the graft density was such that the pHEMA chains were in a brush conformation, chain rearrangement was no longer possible and the hydrophilic end groups remained oriented outwards, leading to a lower WCA.

The outcome of this body of work was the synthesis of a series of membranes with different graft densities, ranging from 0-2.33 $\mu g/cm^2$, and suitable for testing for properties including hydrophilicity, surface roughness and biofouling resistance.

6.3 Biofouling resistance tests that more closely imitate actual fouling conditions.

Placing membrane samples in natural seawater for a period of several weeks was the approach used for Biofouling testing. The advantage of this technique was the use of natural seawater microbes, and a complete system including nutrients and other NOM. Biofouling was quantified by counting bacteria cells on the membrane surface using a technique described in the experimental section. This technique was found to be an appropriate way to compare membranes for their relative biofouling resistance capacity, as well as a direct and visual way to gain an understanding of the extent of biofouling incurred.

6.4 Characterisation of the modified membranes to determine ideal outcome: prevention of biofouling of the membrane whilst maintaining water flux and salt rejection properties.

Polymer layer thickness and surface roughness both increased with increasing graft density. The hydrophilicity results were more complex, and suggested rearrangement of the pHEMA chains on drying. Modified membranes were resistant to hydrolytic degradation in the pH range 2.2 to 9.0 compared to unmodified CA membranes which have an operating pH range from 4.0 to 8.0. In addition the modified membranes retained their filtration properties at pHs outside the normal operating range for CA.

Based on aquaria experiments, the pHEMA modified CA membranes showed a greater resistance to seawater microbial biofouling with respect to pristine CA membranes. In the case of the low graft density pHEMA-modified membranes, this was achieved without significant loss of function in terms of water flux and salt rejection. Roughness was found to be more important than hydrophilicity for indicating biofouling resistance.

The "best" membrane was membrane CAM-g-pHEMA (f) PRT30IMV5, which had flux and salt rejection comparable to pristine CAM, and also showed a 27% reduction in biofouling. This membrane had a graft density of 1.17 $\mu g/cm^2$, which was achieved by reaction of the membrane with initiator for 3 hours, followed by polymerisation under ARGET ATRP conditions for 30 minutes in the presence of 5 mL of HEMA monomer.

The second area of research was a study on the effect of nanoparticles inclusion in the membrane casting solution.

6.5 Synthesis of CA-anchored nanoparticles.

Anchored POSS additive was synthesised via a two-step reaction. The first step was the reaction of aminopropylisobutyl POSS with the para-isocyanate of TDI to form POSS-TDI. This step was confirmed by the presence of urea and isocyanate peaks in ATR-FTIR. In the second step the ortho-isocyanate of TDI was reacted with the hydroxyl groups on the CA backbone to form CA-POSS. The ratios were selected such that each CA chain had approximately four pendant POSS groups on average. The synthesis was confirmed using ATR-FTIR by the disappearance of the isocyanate peak, and the appearance of a carbamate linkage. TGA data further confirmed the synthesis, with a new weight loss event due to the cleavage of the carbamate linkage.

6.6 Inclusion of anchored and unanchored nanoparticles in the CA matrix at different weight % to determine the effect of anchoring the nanoparticles on their dispersion in the membrane matrix.

Nanocomposite membranes were cast with 0.5, 1.0 or 5.0 weight % of either POSS or anchored CA-POSS as additives, using a technique described in the experimental section. The ratio of key peaks in the FTIR spectra confirmed the presence of POSS in the nanocomposite membranes. The anchored CA-POSS additive showed better dispersion than POSS as evidenced by XPS and EDAX. SEM images of both CA-POSS nanocomposite membranes were homogeneous and EDAX did not detect the presence of Si, indicating good dispersion of the POSS nanoparticles. In contrast, the POSS nanocomposite membranes showed areas on the scale of 1-2 µm where Si was detected by EDAX, indicating agglomeration of the unanchored nanoparticles.

6.7 Investigation of the effect of nanoparticle inclusion on the filtration properties and mechanical strength of the membranes.

All nanocomposite membranes showed increased water flux, relative to an unmodified CA control membrane, although they also displayed decreased salt rejection. At low nanoparticle loadings compaction was mitigated. Compaction increased with increasing nanoparticle loading, but was mitigated at loadings of 0.5 wt% for both POSS and CA-POSS additives. DMA showed a decrease in storage modulus for all nanocomposite membranes, indicating a plasticisation effect. Overall, despite anchored POSS having no clear advantage over unanchored POSS for filtration properties, dispersion in the CA matrix was improved and compaction was reduced at low loadings of CA-POSS.

6.8 Recommendations:

ARGET ATRP is an effective method for the covalent modification of CA membrane surfaces. Carefully selected conditions can lead to a graft density where surface morphology and chemical properties are in balance to provide biofouling resistance whilst not inhibiting water flux and salt rejection. For pHEMA, graft density should be targeted around 1.17 $\mu g/cm^2$ to achieve this.

Although other polymers could be investigated, conditions would have to be optimised for each new monomer.

Anchoring of POSS nanoparticles with compatible polymer chains can promote dispersion in the polymer matrix. For the CA-POSS additive with a CA to POSS ratio 4:1, the lowest loadings (0.5 wt%) were optimal for mitigating membrane compaction. Future work in this area could involve investigating different ratios of POSS to CA in CA-POSS.